2015

Effect of beam strength on seismic performance of two-story X-braced frames

Pinar Toru Seker
Iowa State University

Effect of beam strength on seismic performance of Two-story X-braced frames

by

Pinar Toru Seker

A thesis submitted to the graduate faculty

in partial fulfillment of the requirements for the degree of

MASTER OF SCIENCE

Major: Civil Engineering (Structural Engineering)

Program of Study Committee:
Jay Shen, Major Professor
Fouad Fanous
Halil Ceylan

Iowa State University

Ames, Iowa

2015

DEDICATION

"When you go through a hard period,

When everything seems to oppose you

When you feel you cannot even bear one more minute,

Never give up!

Because it is the time and place that the course will divert!"

Rumi.

TABLE OF CONTENTS

NOMENCLATURE

AISC	American Institute of Steel Construction
ASCE	American Society of Civil Engineers
CBF	Concentrically Braced Frame
DL	Dead Load
ELF	Equivalent Lateral Force
FN	Fault Normal
FP	Fault Parallel
GM	Ground Motion
GMG	Ground Motion Group
HSS	Hollow Structural Section
LL	Live Load
OCBF	Ordinary Concentrically Braced Frame
SCBF	Special Concentrically Braced Frame
TSXBF	Two-Story X-Braced Frames

ACKNOWLEDGMENTS

First and foremost, I would like to thank my advisor and my teacher Dr. Shen.

Dr. Shen, you are a great teacher and I learned a lot from you. This work would not have been possible without your support, encouragement and great mentorship.

Your frequent insights and patience with me are always appreciated. I feel very lucky and thankful that I had a chance to work with you. On top of everything, I should thank you not only for being a great teacher but also treating me like family.

I would like to thank my committee members, Dr. Fanous and Dr. Ceylan, for their guidance and support throughout the course of this research.

I want to also thank Dr. Akbas for supporting me from the very beginning. In addition, I would like to thank Dr. Wen for helping me a lot.

I wish to thank my father Tuhal, mother Guler and brother Tugrul, mother in-law Yasemin, father in-law Zekai and my sister Oylum, who have brought great joy to my life.

Finally, I owe much my friend, my husband and my colleague Onur. Without your love, help and understanding I would not have completed this work.

ABSTRACT

Two-story X-braced frames (TSXBFs), which are the frames having the bracing configurations V- and inverted V-braces in alternate stories creating an X-configuration over two stories have become one of the most commonly used Special Concentrically Braced Frames (SCBFs) in areas with high seismicity. The primary reason that makes TSXBFs attractive to the industry is that the brace-intersected girders of TSXBFs are much lighter than that of the CBFs with the other bracing configurations.

According to the current AISC Seismic Provisions, the brace-intersected beams in TSXBFs can be designed considering only the first-mode loading pattern, which reduces the vertical unbalanced loads acting on the brace-intersected girders of TSXBFs as well as the size of the brace-intersected beams substantially. Even though seismic behavior of CBFs has been extensively studied in general, a little work has been done on seismic behavior of the brace-intersected beams in TSXBFs.

The purpose of this study is to present the seismic demand on the brace-intersected beams and its impact on seismic performance of TSXBFs. For this purpose, five 6-story TSXBFs and one 6-story CBF with inverted-V bracing are designed and subjected to twenty recorded earthquake ground motions. The results of non-linear time history analyses are presented and discussed in terms of brace ductility, beam ductility and story drift ratio in order to evaluate seismic response of TSXBFs.

The study concludes that brace-intersected beams in the TSXBFs with weak beams tend to experience vertical inelastic deformations within beam spans when the structures undergo 2% or larger story drift ratio response and the ductility demand on the braces might increase

significantly when the vertical inelastic deformation at the brace-intercepting point of the beam takes place. Also, yielding of the brace-intersected beams lead the beams to deform vertically within their spans, which would result in much more complicated deformation patterns than the first-mode mechanism anticipated by AISC. Furthermore, it is found that even mid-rise frames studied in this work were affected by higher modes. Future work should therefore aim to investigate the impact of the beam responses on brace ductility response as well as overall seismic response of high-rise TSXBFs.

CHAPTER I

INTRODUCTION

1.1 Introduction

Concentrically braced frames (CBFs) have received much attention in recent years due to their large initial stiffness and relatively simple construction. CBFs are lateral load resisting systems, which the members are subjected to primarily to axial forces [1] and all beams and braces of the system meet at one point. CBFs are considered that they have less ductility due to their high strength and are commonly used lateral load resisting systems by structural engineers throughout the world. There are several brace configurations of CBFs that have been used by structural engineers such as, V-type, inverted V-type, X-type etc. as shown in Figure 1.1.

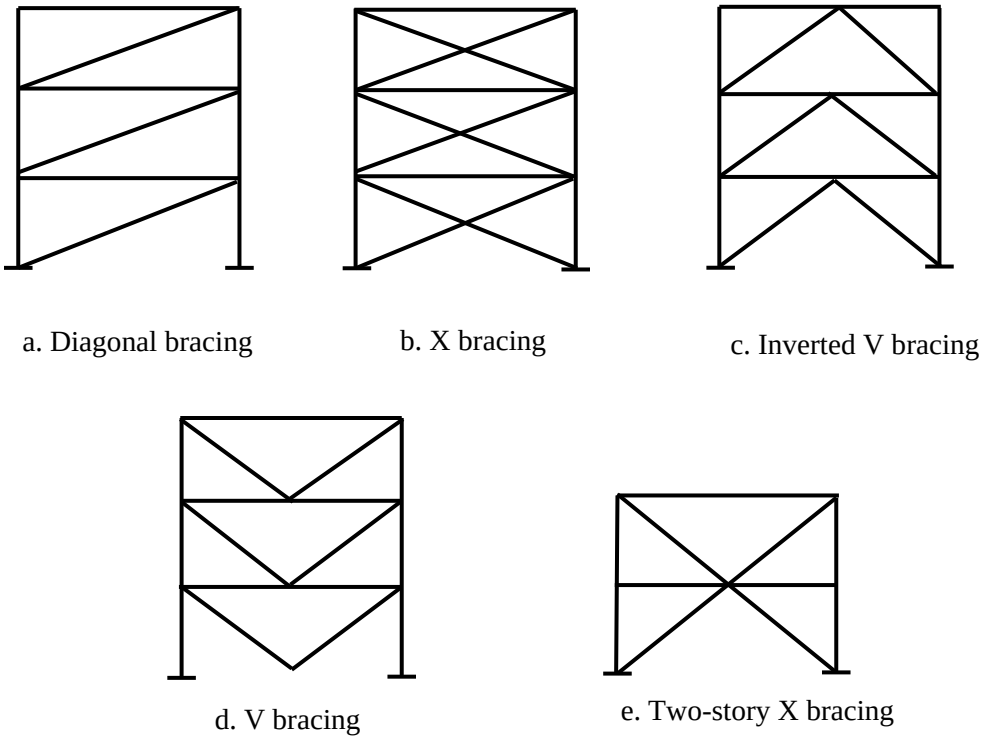

Figure 1.1. Typical configurations of concentrically braced frames (CBFs)

CBFs are categorized as ordinary concentrically braced frames (OCBFs) or special concentrically braced frames (SCBFs) in ASCE 7 (2010) [1] based on their inelastic energy dissipation capacities. OCBFs designed in accordance with the Seismic Provisions for Structural Steel Buildings (2010) [2] are expected to provide limited inelastic deformation capacity in their members and connections. On the other hand, SCBFs are expected to provide significant inelastic deformation capacity primarily through buckling and yielding of the braces [2] while their columns and girders are expected to remain elastic. Therefore, girders and columns of SCBFs are designed based on the capacity design approach using the unbalanced forces owing to the difference between the expected tension force and expected buckling or post-buckling force of the braces in tension and compression, respectively. The current AISC Seismic Provisions [2] anticipates that braces in all stories buckles or yields simultaneously with the first-mode loading pattern for the design of girders and columns. Due to the unbalanced vertical forces, the braces impose very large demands on the girders of inverted-V type CBFs. Thus, the girder size of inverted V type CBFs, which are one of the most popular type of CBFs in seismic regions are often deep and heavy sections.

Two-story X-braced frames (TSXBFs), which are combination of V-type and inverted V-type CBFs have become one of the most commonly used Special Concentrically Braced Frames (SCBFs) in areas with high seismicity. The primary reason that makes TSXBFs more attractive to design engineers than the other types (e.g. Inverted V or V brace configurations) is that the brace-intersected girders of TSXBFs are much lighter than that of the CBFs with the other bracing configurations. According to AISC 341 (2010) [2], TSXBFs can be designed with post-elastic behavior consistent with the expected behavior of V-braced SCBFs. Since the current AISC Seismic Provisions considers only the first-mode loading pattern for seismic design of

SCBFs (shown in Fig. 1.2), the vertical unbalanced loads acting on the brace-intersected girders of TSXBFs can be substantially reduced compared to CBFs with V and inverted-V bracing configurations. As can be interpreted from the Figure 1.2, AISC 341 (2010) and the examples provided in AISC Seismic Design Manual [3] encourage engineers to design the brace-intersected girders with the assumption that the braces above and below the brace-intersected beam reach their expected tension and compression capacities (buckling or post-buckling) at the same time. As a result of the anticipated braced-frame mechanism, seismic loads acting on the brace-intersected girders may be zero by choosing the same brace sizes for the stories above and below the girder. However, this doubtful first mode assumption anticipated by AISC [2] would be an issue that needs to be addressed when TSXBFs subjected to severe earthquake ground motions due to complicated deformation patterns in inelastic stage.

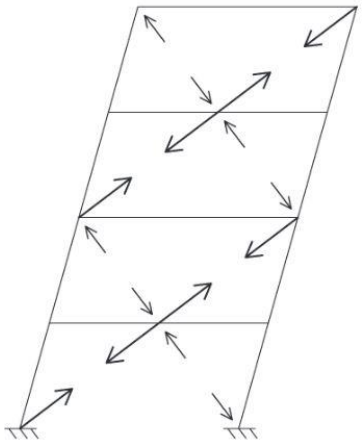

Figure 1.2 Anticipated braced-frame mechanism [2]

Few studies have demonstrated the problem of using story drift ratio alone as an indicator of damage or seismic hazard level as well as significant consequences of neglecting possible deformation patterns due to higher mode effects in the design of the brace-intersected beams in TSXBFs. Shen et al. indicated that the braces above and below the brace-intersected girders of TSXBFs might impose very large seismic demands on the brace-intersected girders and therefore

the girders might yield during an earthquake ground motion [4]. Moreover, their study addressed that using story drift ratio as a damage indicator would not be adequate for the seismic performance evaluation of TSXBFs, since the deformation demands on the braces can be affected by both horizontal and vertical translations of the brace-intersected girder.

The purpose of this study is to present the seismic demand on the brace-intersected beams and its impact on seismic performance of TSXBFs. For this purpose, brace ductility, beam ductility and story drift ratio responses are investigated through an ensemble of non-linear time history analyses in order to evaluate seismic response of TSXBFs.

1.2 Design of SCBFs based on AISC 341-10 [2]

According to AISC 341 (2010) [2], SCBFs are designed to dissipate the input energy mainly through the inelastic deformation of the braces, since the braces are designed based on the design base shear force, which is equal to elastic base shear force divided by the response modification factor ($V_{design}=V_{elastic}/R$ where R=6 for SCBFs). Based on the capacity design approach, AISC requires that design of the members of lateral force resisting system other than braces (e.g. girders) shall remain elastic. Thus, the required strength of the structural members of lateral force resisting system other than braces and their connections should be determined based on the expected capacity of the bracing member. Section F2.3 of AISC 341 (2010) [2] requires two structural analysis cases for design of the girders and three analysis cases for design of the columns in SCBFs. Structural analysis cases for the girders and columns are shown in Fig. 1.3. Note that the given brace forces are based on the assumption that braces in all stories buckles or yields simultaneously with the first-mode loading pattern. The required strength of beams shall be taken as larger of the forces determined from the following two analyses:

(i) An analysis in which all braces are assumed to resist forces corresponding to their expected strength in compression or in tension.

(ii) An analysis in which all braces in tension are assumed to resist forces corresponding to their expected strength and all braces in compression are assumed resist their post-buckling strength.

In addition to the two analysis cases, AISC requires an additional structural analysis case for determination of required column strength by removing all braces in compression. In this case, the applied load should be determined using load combinations including the amplified seismic loads, $\Omega_0 F$, where Ω_0 is overstrength factor.

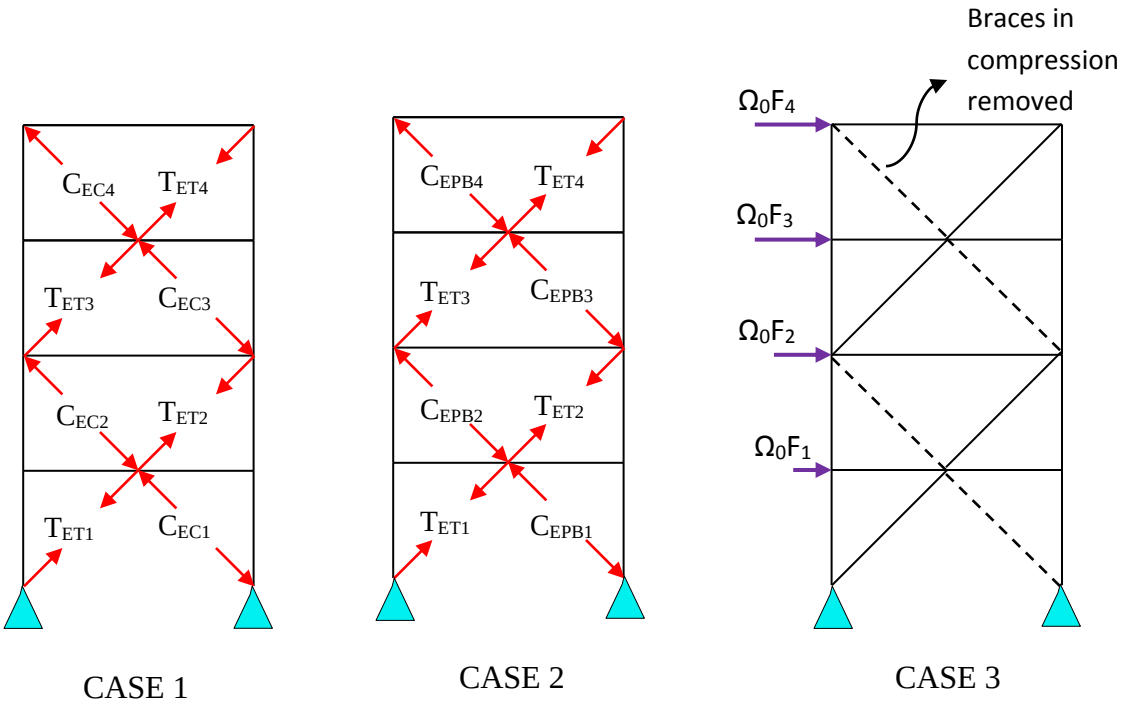

Fig. 1.3. Structural Analysis Cases for Girders and Columns

The expected brace strength in tension (T_{ET}) is $R_y F_y A_g$ and the expected brace strength in compression (C_{EC}) is permitted to be taken as the lesser of $R_y F_y A_g$ and $1.14 F_{cre} A_g$ [2], where F_y= Specified minimum yielding stress of steel, F_{cre}= Critical stress calculated using the expected

yield stress, R_y=Ratio of expected yield stress to the specified minimum yield stress and A_g=Gross area. The expected post-buckling strength (C_{EPB}) shall be taken as 0.3 times the expected strength in compression.

Typical cyclic behavior of a bracing member is shown in Fig. 1.4 [5]. The envelope of the tension and compression behaviors is indicated with red as simplified model in the figure. Expected tension, expected buckling and expected post-buckling strengths are obtained from the envelope of the cyclic response of a brace for the analysis cases, as shown in Fig. 1.5.

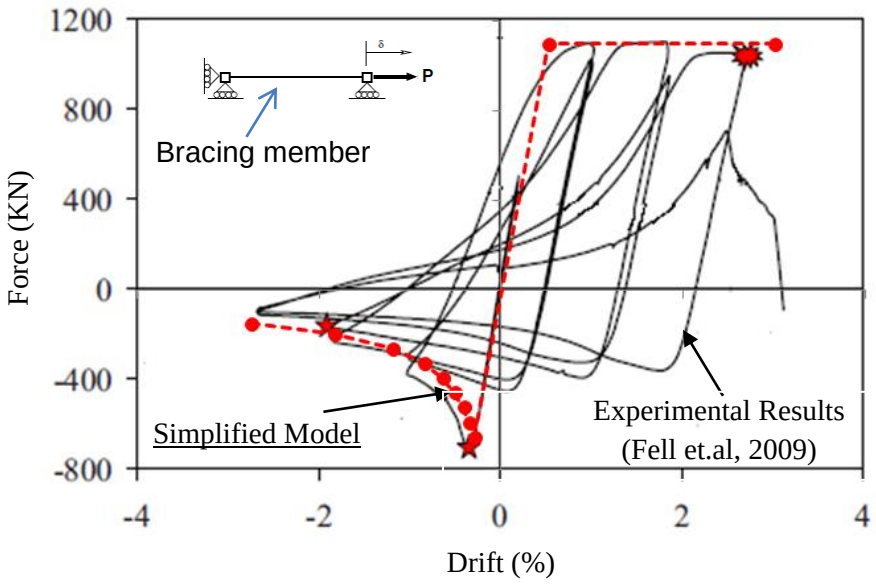

Fig. 1.4 Typical hysteretic behavior of a steel bracing member [5]

The purpose of the analysis cases is to obtain the worst case possible for beam design in order to make sure that beams remain elastic during an earthquake excitation. Thus, the size of the brace-intersected beams should be determined based on the two analysis cases whichever results a deeper and heavier beam section. The first structural analysis case considers that all braces in tension and compression reach their expected tension and buckling loads, respectively. The second analysis case, on the other hand, considers that all braces in compression reach their expected post-buckling strength while all braces in tension reach their expected tension capacity.

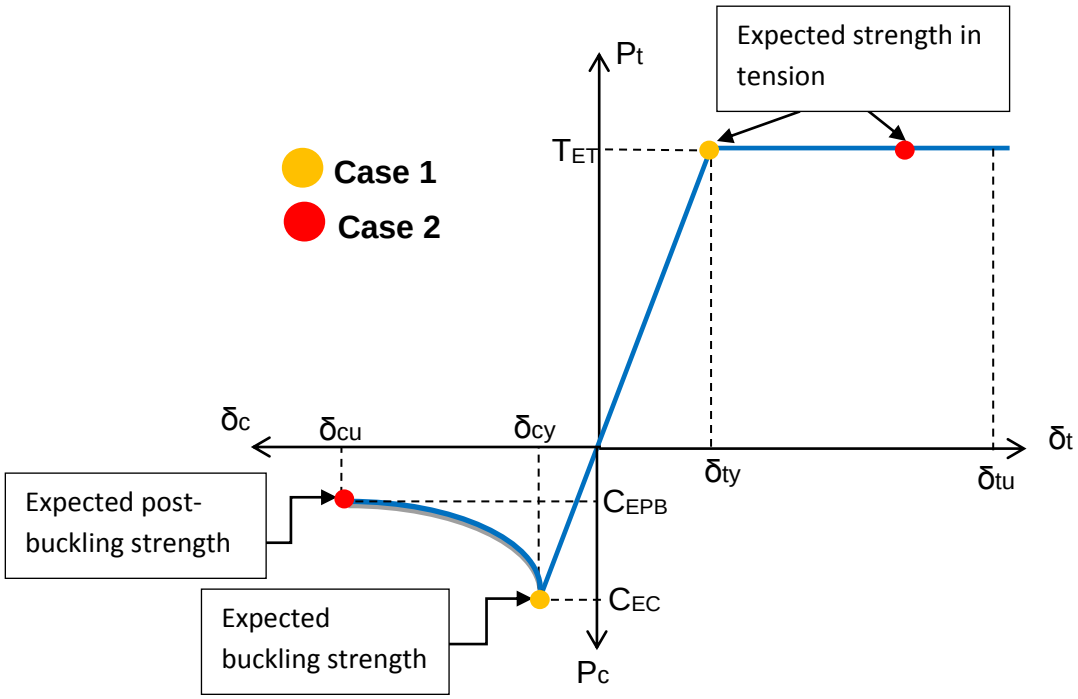

Fig. 1.5. Illustration of expected tension, buckling and post buckling strengths of a bracing member

Fracture life of a bracing member, which is the controlling limit state of the overall behavior of a CBF is affected by several parameters, such as the slenderness ratio of the member, the width-to-thickness ratio, the loading history (i.e. near field and far field loading histories), the number of cycles etc. [5, 6, 7]. With an attempt to improve the fracture life of braces in SCBFs, AISC requires that braces shall satisfy the requirement of Section D1.1 of AISC 341 (2010) for highly ductile members and braces shall have a slenderness ratio less than 200 [2].

Section Requirement: Highly ductile $\lambda \le \lambda_{hd}$ [AISC 341-10 F2.5a]

Slenderness Requirement: $\frac{KL}{r} \le 200$ [AISC 341-10 F2.5b]

In addition to the section requirement for braces, columns and beams of a SCBF shall satisfy the requirement of Section D1.1 of AISC 341 (2010) for highly ductile members and moderately ductile members, respectively [2].

1.3 Literature Review

Owing to the unexpected damage in special steel moment frames (SMFs) during the 1994 Northridge earthquake, engineers tended to use CBFs as seismic force resisting systems, which is simpler and more economical [8]. Since concentrically braced frames have been received much attraction by engineers after the 1994 Northridge earthquake, the number of studies on CBFs increased substantially in the last decades. The studies on CBFs can be divided into three groups.

First group of studies on CBFs conducted on the effect of connections, especially gusset plate connections, on the performance of braces and overall structure. A detailed literature review of the past studies on the influence of gusset plates as well as connections on performance of CBFs have been presented by Astaneh Asl [9]. Stoakes and Fahnestock [10] carried out a finite element based analytical study in order to investigate the behavior of beam-to-column connections together with gusset plates under cyclic load. Their analysis results indicated that "increasing beam depth and angle thickness and adding a supplemental seat angle, all increased the stiffness and strength of the connection while maintaining deformation capacity" [10]. In a recent study, Yoo et al. [11] have conducted a series of static pushover analyses and finite element simulations to examine the effect of gusset plate design on seismic performance of the two-story X-braced frames, which were designed with three different beam sizes. Their conclusion was that gusset plate, floor slab and stiffener designs have a significant impact on overall structural performance [11]. In a study represented by Hsiao et al. [12] focused on modeling issues as well as developing a modeling approach for beams and columns to represent the inelastic behavior of gusset plates. They concluded that an accurate modeling of a frame to

evaluate post-buckling response requires not only an accurate brace model but also an accurate modeling approach for gusset plate connections [12].

Second group of studies on CBFs focused on the impact of brace behavior on CBFs. Bracing members of CBFs are subjected to cyclic loading under an earthquake excitation. Hence, during a seismic action, the braces are subjected to tension and compression repeatedly. One of the earliest study on inelastic buckling of steel struts was published by Black et al. [13]. An experimental work was performed and post buckling behavior of twenty four brace specimens were presented in their study. In order to understand the inelastic behavior of a CBF, researchers focused on the cyclic behavior of single bracing members with different slenderness and compactness ratios under various loading histories, such as near-field, far-field and standard cyclic loading protocols [5, 6, 7]. A detailed survey of past experimental studies on the inelastic response of steel bracing members can be found the paper published by Tremblay [6].

The objective of the third group of studies was to evaluate the overall performance of CBFs. However, the purpose of this study is to present seismic response of the brace-intersected beams and the interaction between the responses of the beams and the other members. Therefore, the studies which have been summarized in this group are solely related to TSXBFs. Unfortunately, even though TSXBFs are popular in the industry, the current Seismic Provisions [2] only refers to one study. Seismic behavior of concentrically braced frames with variety of bracing configurations including zipper and two-story X-braces was investigated by Khatib et al. [14]. They concluded that "it is possible to design two-story X-braced and zipper frames with post-elastic behavior that is superior to the expected behavior of V-braced SCBF by proportioning elements to single-story mechanisms" [2]. One of the recent studies conducted by Shen et al. [4] has pointed out that instead of using story drift ratio alone as a damage indicator,

both vertical and horizontal displacements in the middle of the brace-intersected girders should be taken into account for seismic performance evaluation of TSXBFs. Combination of the horizontal and the vertical displacements of the frames with weak girders would increase ductility demands on braces and beam-to-column connections substantially even when the structure experience a story drift ratio of 2%.

CHAPTER II

STRUCTURAL MODELS AND EARTHQUAKE GROUND MOTIONS

2.1 Description of Buildings

Special concentrically braced frames (SCBFs) used in this study were designed based on the seismic design requirements for SCBFs stipulated in ASCE 7 (2010) and AISC 341 (2010). Plan and elevation of the studied 6-story buildings are given in Fig. 2.1. The 6-story buildings have plan dimensions of 150 ft x 150 ft with a typical story height of 13 ft and consist of five-bay frames in two orthogonal directions spaced at 30 ft. The seismic force resisting frames (braced frames) are arranged on the perimeter in both orthogonal directions. Beam-to-column connections of the frames along the lines other than the perimeter of the building plan are shear connections. Therefore, the frames other than the perimeter frames are only responsible for carrying gravity loads (gravity frames) and their lateral resistance is neglected. The columns are assumed to be pinned at the ground level. The floor system, which is composed of 3-1/2 in. concrete slab on the metal deck, is connected to the girders by shear studs welded to the top flange of the girders and cast in concrete decking.

The seismic force resisting systems were designed for gravity and seismic loads with a dead load of 80 psf and live load of 50 psf for both the floors and roof. The gravity loads acting on each structural member were determined based on the tributary areas. The office buildings were designed for a site in Los Angeles where site class is D, S_S is 2.0g and S_1 is 1.0g. The perimeter frames of the buildings in the direction of the design earthquake were designed using a response modification factor of R= 6. The ASCE 7 (2010) design base shears for the 6-story frames were found to be 2,400 kips using the approximate period equation specified in ASCE 7 (2010). Each frame on the perimeter of 6-story buildings are composed of two identical braced

bays. Thus, the braced frames of 6-story buildings were designed for 1/4 of the total base shear. Equivalent lateral force (ELF) procedure is used for the distribution of the total base shear along the building height.

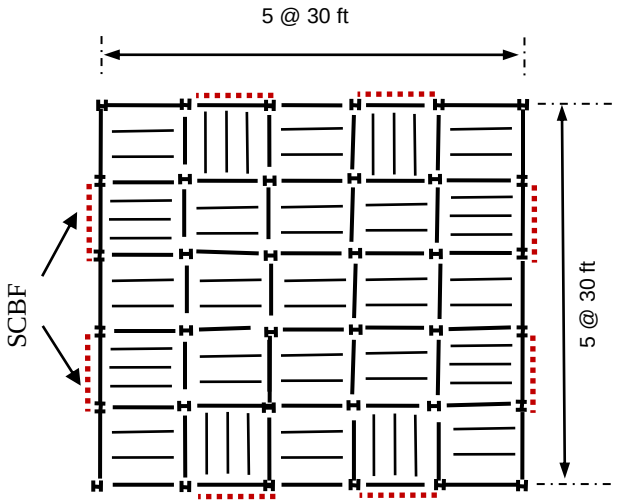

a. Typical floor plan with locations of SCBF Frames

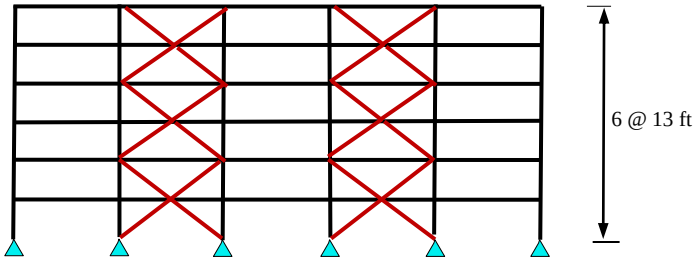

b. Elevation for frames having two-story X bracing configuration

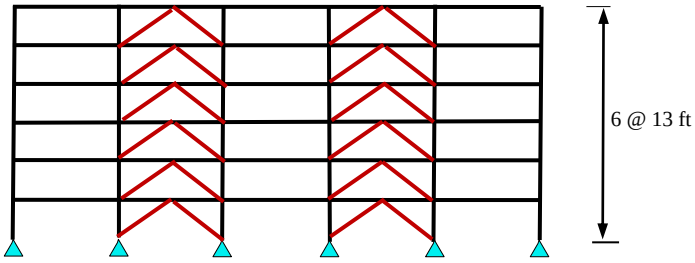

c. Elevation for frames having chevron bracing configurations

Fig. 2.1. Plan and elevation of the studied 6-story steel braced frames

The brace sections were selected considering the strength, slenderness and compactness (width-to-thickness ratio) requirements specified in AISC 341 (2010) [2]. Basic load combinations given in ASCE 7 (2010) [1] were used for the strength design. The design of the brace sections were governed by the seismic load combination: $(1.2+0.2S_{DS})$ DL$+\rho Q_E+0.5$LL with the redundancy factor of 1.30. In order to keep the capacity of the braces as close as possible to the required strength, either round or square hollow sections (HSS) were used, as indicated in Table 2.1. The brace sizes were changed every two stories and all braces satisfy the slenderness requirement as well as the width-to-thickness ratio requirement for highly ductile members [2]. The slenderness (KL/r) and the width-to-thickness ratio (D/t or b/t) of all braces are given in Table 2.1.

The columns and beams of the gravity frames as well as the columns and beams in unbraced bays of the braced frames were designed only for gravity loads. On the other hand, the columns in braced bays were designed based on the previously mentioned three structural analysis cases (see Section 1.2). The required strength of the columns in the braced bays were governed by the analysis case 3, which is an additional case for determination of required column strength. In this case, the seismic loads were amplified with an overstrength factor of 2.0 [1] and applied to the structure when all braces in compression were removed. Additionally, all columns in the braced bays meet the width-to-thickness ($b/2t_f$ and h/t_w) ratio requirement for highly ductile members [2].

In order to investigate the impact of the inelastic behavior of beams on seismic performance of the structures, a total of 6 frames were designed to have different brace-intersected beam sizes as well as capacities for 6-story buildings. Thus, as indicated in Table 2.1, the brace and column sizes in the braced bays and the design of the gravity frames were identical

for Frames A through F while the sizes of the brace-intersected beams were different. Frame A through E are the frames having the bracing configurations V- and inverted V-braces in alternate stories creating an X-configuration over two stories (Fig. 2.1b). The frame having inverted V type bracing configuration (Frame F) is designed in accordance with the requirements of AISC 341 (2010) to make a comparison between TSXBFs and inverted V type braced frames (Fig. 2.1c).

According to Section C-F2.2 of AISC 341 (2010) [2], TSXBFs can be designed with post-elastic behavior consistent with the expected behavior of V-braced SCBF. Hence, the brace-intersected beams of TSXBFs were designed based on the aforementioned two analysis cases. Fig. 2.2a and Fig. 2.2b illustrate the braced-frame mechanism anticipated by AISC 341 (2010) [2] and the free body diagram of story i. Figs. 2.2c and 2.2d show moment and axial force diagram of the beam due to the unbalanced forces. The brace-intersected beams of each TSXBF were designed based on the contribution of the V braces above (C_{i+1} and T_{i+1}), which reduces the unbalanced forces and therefore the brace-intersected beam sizes.

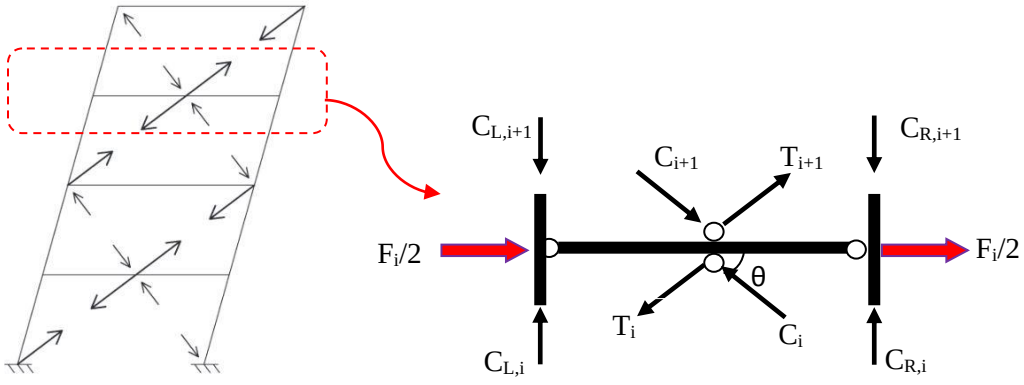

a. Anticipated braced-frame mechanism [2]

b. Free Body Diagram of story i

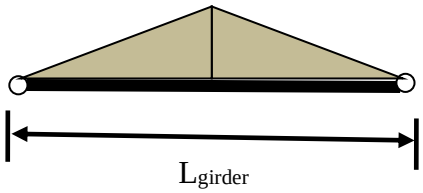

c. Moment Diagram

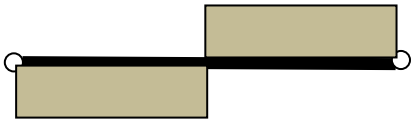

d. Axial Force Diagram

Fig. 2.2. Structural analysis of the brace-intersected girders in TSXBFs

Table 2.1. Member Sizes of the 6 – Story Braced Frames

Level	Braces	Columns in Braced Bay	Beams in Braced Bay						Gravity Columns			Gravity Beams
			Type A (0%) Frame	Type B (25%) Frame	Type C (50%) Frame	Type D (75%) Frame	Type E (100%) Frame	Type F (Inverted-V) Frame	Interior	Exterior	Corner	
6	HSS8.625×0.500 (KL/r = 82, D/t = 18.5)	W 12×65	W18×65					W30×235	W10×39	W10×33	W10×33	W21×44
5			W30×235	W27×194	W24×146	W18×97	W16×57					
4	HSS10.000×0.625 (KL/r = 71, D/t = 17.2)	W 12×136	W18×106					W33×291	W10×68	W10×39	W10×33	
3			W33×291	W27×258	W24×192	W21×111	W16×57					
2	HSS9×9×⅝ (KL/r = 70, b/t = 12.5, h/t = 12.5)	W 12×252	W18×130					W33×354	W10×100	W10×49	W10×33	
1			W33×354	W30×292	W27×217	W21×132	W16×57					

Notes: (1) The selection of brace members considers the following two considerations: (a) Either Round or Rectangle HSS is used to keep the brace design strength as close as to the required strength as possible; and (b) Round HSS has priority; (2) Highly ductile members are used for braces and columns.

TSXBFs (Frame A through E) used in this study were designed with the following assumptions:

- Frame A: The brace-intersected beams were designed without considering the contribution of the upper story braces, which means the V braces above did not exist (0% of C_{i+1} and T_{i+1}). Thus, the brace-intersected beam sizes of Frame A were the strongest and identical with the brace-intersected beam sizes of the frame with inverted V bracing configuration (Frame F).
- Frame B: The brace-intersected beams were designed considering 25% of the expected strength of the V braces above (25% of C_{i+1} and T_{i+1}).
- Frame C: The brace-intersected beams were designed considering 50% of the expected strength of the V braces above (50% of C_{i+1} and T_{i+1}).
- Frame D: The brace-intersected beams were designed considering 75% of the expected strength of the V braces above (75% of C_{i+1} and T_{i+1}).
- Frame E: The brace-intersected beams were designed following the current design provisions of AISC 341-10 [2] (100% of the expected strength of the V braces above). Thus, the brace-intersected beam sizes of Frame E were the weakest.

2.2 Finite Element Modeling

Complete analyses in this study were performed using two dimensional inelastic dynamic analysis program RUAMOKO 2D [15]. Inelastic dynamic behavior of a CBF is predominantly governed by hysteretic behavior of bracing members, which dissipate the greatest amount of the input energy during a severe earthquake ground motion. Therefore, it is crucial to simulate the actual behavior of a bracing member in the physical test. In order to evaluate capability of RUAMOKO 2D in terms of simulating post-buckling behavior of a column

member, two specimens tested by Fell et al. [5] and Nip et al. [16] were simulated. REMENNIKOV steel brace option of RUAMOKO 2D was used to simulate inelastic buckling behavior of the single braces. Note that REMENNIKOV steel brace option represents the out-of buckling option [15]. Table 2.2 presents the detailed information on the simulated test specimens. First specimen simulated in this study was tested by Nip et al. [16]. The total length and the boundary conditions of the specimen, the cross-section properties and the loading history are shown in Figure 2.3. Experimental and simulation results are compared in Figure 2.4. It seems that the experimental and simulation results are in good agreement.

Table 2.2. Properties of the tested specimens [5, 16]

Specimen	Conducted by	Section	L(mm)	F_y (Mpa)	KL/r
1	Nip et al. [15]	HSS 40^{mm}x40^{mm}x3^{mm}	2050	478	42
2	Fell et al. [5]	HSS 101.6^{mm}x101.6^{mm}x6.4^{mm}	2985	460	77

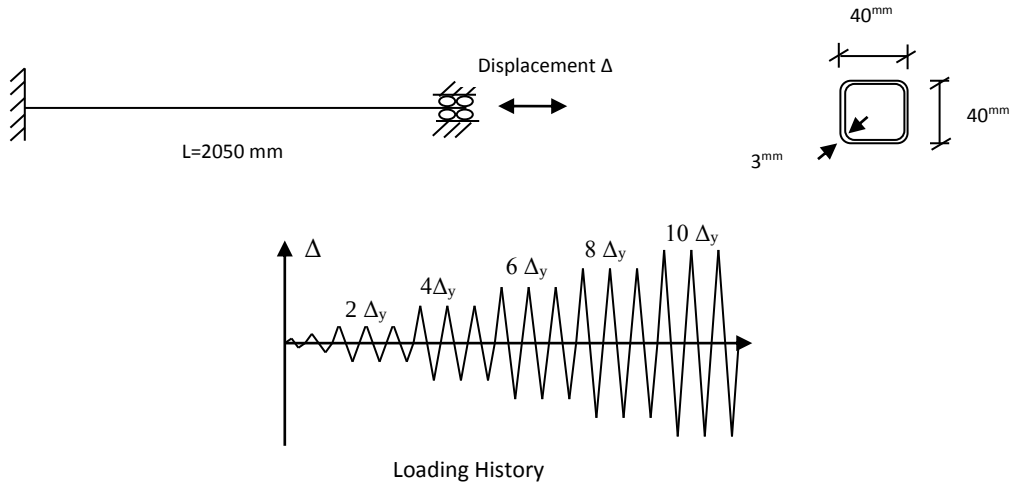

Figure 2.3. Brace specimen and loading history used in the experiment

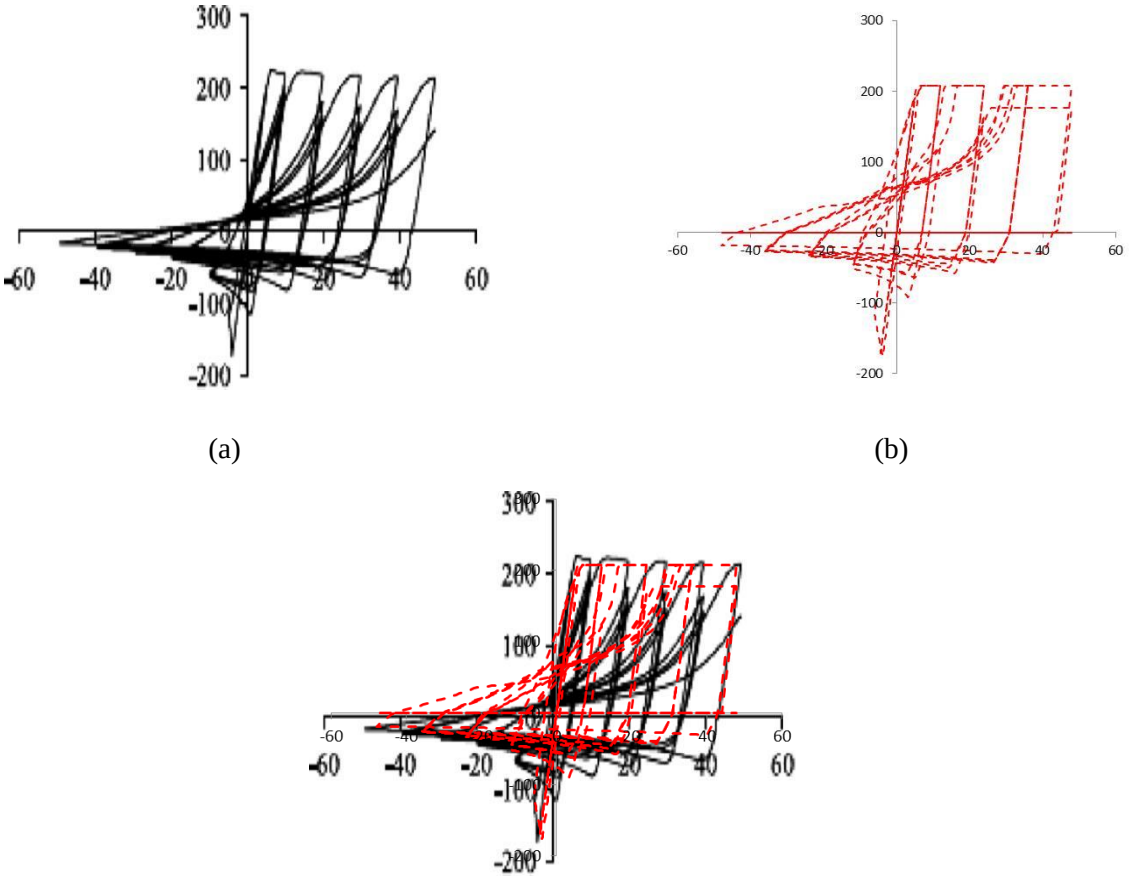

(a) (b)

(c)

Figure 2.4. Experimental and simulation results of the specimen tested by Nip et al. [16] (a) Experimental result, (b) simulation result by RUAMOKO, (c) experimental result and simulation results

Second specimen test that simulated in this study was performed by Fell et al. [5]. Since the slenderness ratio is one of the most influential parameter on post-buckling behavior of a column member, it is reasoned that there remains a need for another simulation using a specimen with a larger slenderness ratio. Thus, a recently tested square hollow section with a slenderness ratio of 77, which falls into the slenderness range of a practical bracing member has been chosen for the second simulation. Figure 2.5 shows the specimen configuration and the loading history used in the experiment conducted by Fell et al. [5]. Figure 2.6 plots the comparison between the experimental and simulation results. It appears that the experimental and simulation results are in satisfactory agreement.

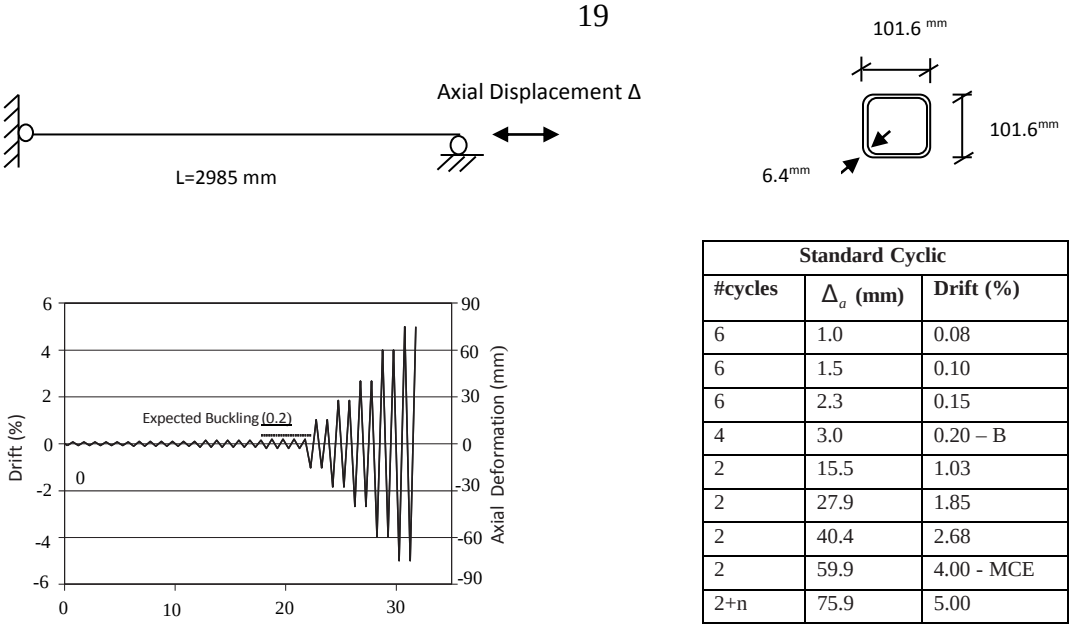

Standard Cyclic		
#cycles	**Δ_a (mm)**	**Drift (%)**
6	1.0	0.08
6	1.5	0.10
6	2.3	0.15
4	3.0	0.20 – B
2	15.5	1.03
2	27.9	1.85
2	40.4	2.68
2	59.9	4.00 - MCE
2+n	75.9	5.00

Figure 2.5. Brace specimen and loading history used in the experiment conducted by Fell et al. [5]

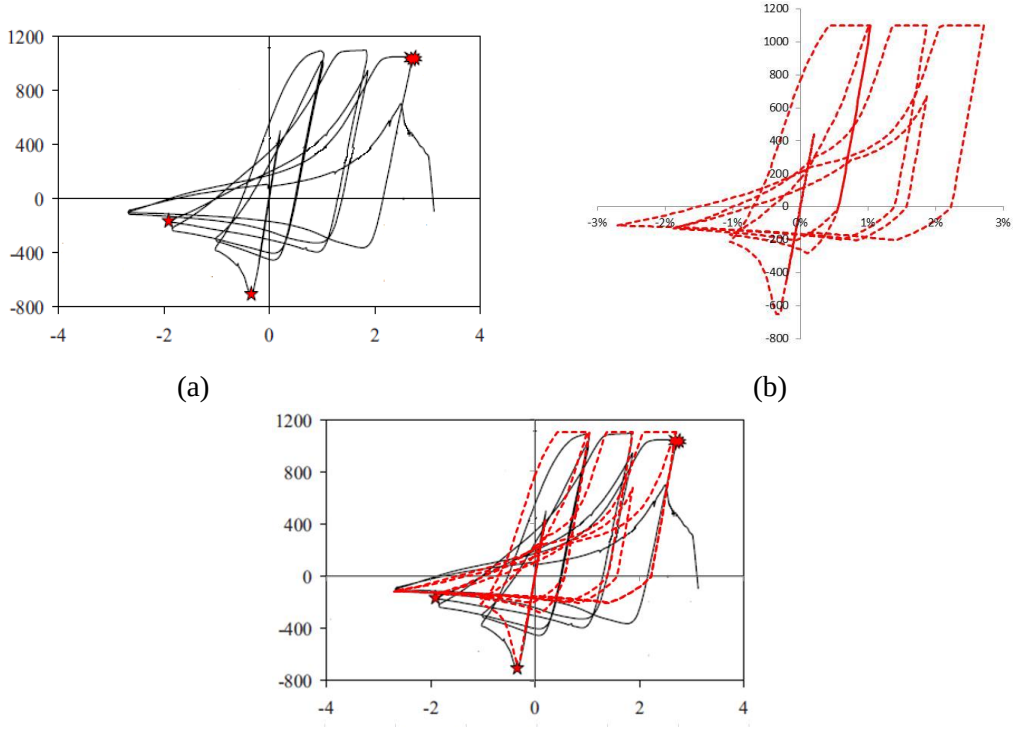

Figure 2.6. Experimental and simulation results of the specimen tested by Fell et al. (a) Experimental result, (b) simulation result by RUAMOKO, (c) experimental result and simulation results[1]

The results provide convincing evident that the single brace element in RUAMOKO 2D gives the impression of being well to simulate inelastic behavior of braces in terms of tension

yielding, compression buckling as well as strength and stiffness deterioration due to post-buckling. It is also validated that REMENNIKOV steel brace model is capable of simulating hysteretic behavior of braces fairly accurate with variety of slenderness ratios.

2.3 Analytical Model of Frames

Figure 2.7 represents the analytical modeling of two-story X-braced frames. Columns were modeled by beam-column element in RUAMOKO 2D. Beam-column element in RUAMOKO 2D is capable of representing the axial force-bending moment interaction (P-M interaction) stipulated in AISC 360 (2010) [17]. Axial force-bending moment interaction curves were employed to the structural members of the frame by defining the P-M interaction curves. Beams were modeled with two different elements. The brace-intersected beams were modeled as beam-column elements and therefore P-M interaction of beams were adopted based on equations H1-1a and H1-1b of AISC 360 (2010) [17]. On the other hand, simple beam/column elements were assigned to the beams that are not intersected by braces (e.g. second story beam). P-Δ effect was considered by introducing leaning columns attached with rigid beams to the frames. An extremely large modulus of elasticity value was adopted for rigid links for the purpose of eliminating axial deformations of the rigid links. All beam-to-column connections were modeled as pin connections. The masses were assigned to the joints of the leaning columns at every story level. The fundamental periods of vibration of the frames are given in Table 2.3. The periods of vibration did not differ considerably for each frame.

Table 2.3. Fundamental periods of the frames

FRAME	A	B	C	D	E	F

Periods (sec.)	0.72	0.72	0.72	0.72	0.72	0.70

In order to take the possible deformations of shear studs in inelastic stage into consideration, floor system was assumed to be flexible. Therefore, no floor constraints were assigned to the joints. The load combination 1.05 DL+0.25 LL was used for the gravity loads acting on leaning columns to represent the gravity frames. It should be noted that time step size of the analysis has a significant impact on the results. Hence, a small time step size of 0.0001 s was used to capture satisfactory results.

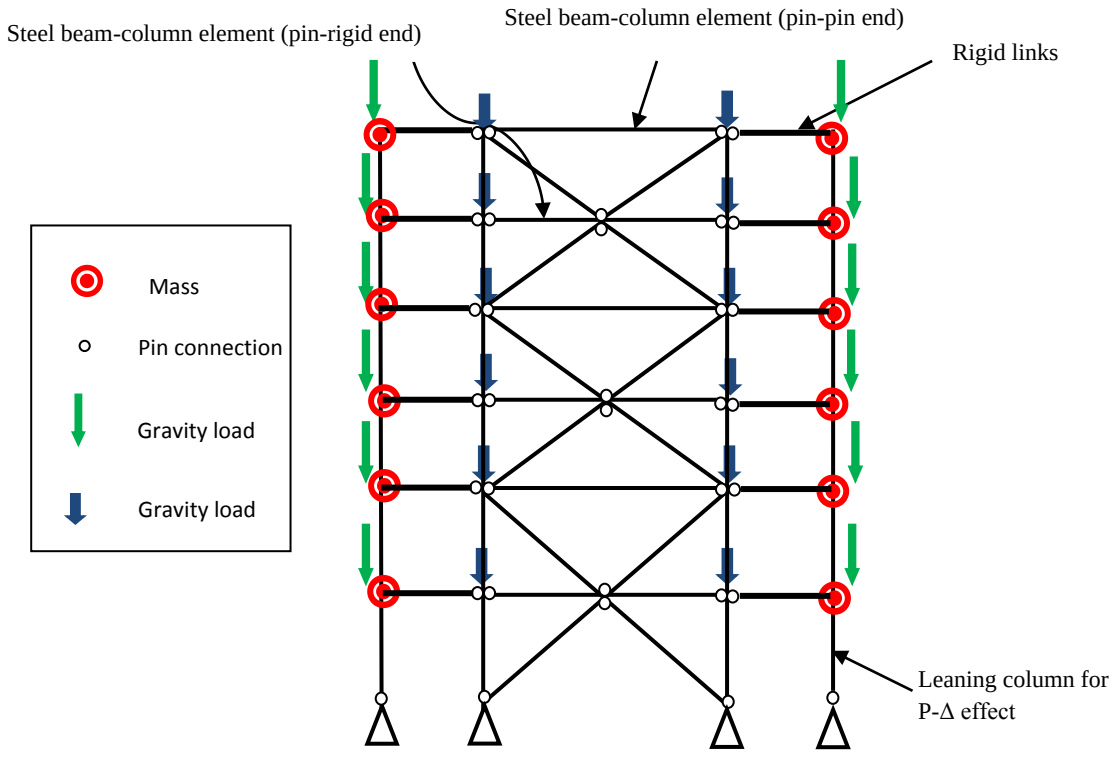

Figure 2.7. Analytical Model for two-story X-braced frames

2.4 Ground Motions

10 pairs of ground motions compatible with site class D in Los Angeles area were used in this study. Design spectrum parameters are S_{DS}=1.333(g), S_{D1}=1.000(g) and T_L=12.0 s. Ground motions were selected using PEER Ground motion database [18] with small mean squared error. The elastic response spectra of the ground motions and the target spectrum are illustrated in Figure 2.8. Each pair of ground motion is composed of two components, which are fault normal (FN) and fault parallel (FP) with the intention of avoiding event bias [4]. The detailed information on these ground motions are summarized in Table 2.4. Acceleration time histories of all ground motions are presented in Appendix A.

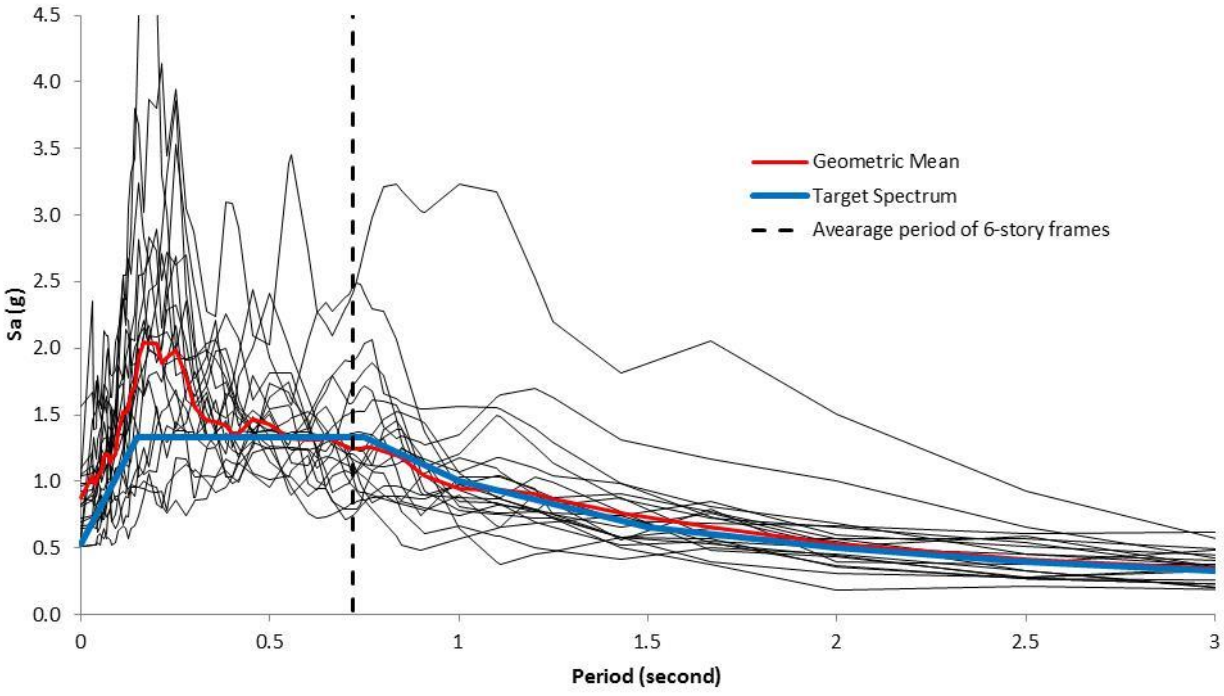

Figure 2.8. Response spectra of twenty ground motions used in the study

Table 2.4. Ground motions used in this study

ID No.	NGA#	Component	Scale Factor	Event	Year	Mag	Duration (seconds)	PGA (g)	PGV (inch/second)
GM1	1085	FN	1.1675	Northridge	1994	6.69	40	0.979	5.35
GM2		FP						0.578	3.60
GM3	1489	FN	2.8835	Chi-Chi-Taiwan	1999	7.62	90	0.810	5.08
GM4		FP						0.718	6.50
GM5	1515	FN	2.5841	Chi-Chi-Taiwan	1999	7.62	90	0.643	5.71
GM6		FP						0.513	5.02
GM7	1009	FN	3.8019	Northridge	1994	6.69	55.33	1.041	4.84
GM8		FP						0.985	3.68
GM9	726	FN	6.5733	Superstition Hills	1987	6.54	21.89	0.817	2.03
GM10		FP						1.059	4.61
GM11	179	FN	1.9573	Imperial Valley	1979	6.53	39	0.699	6.00
GM12		FP						0.929	3.09
GM13	802	FN	2.3023	Loma Prieta	1989	6.93	39.955	0.835	5.03
GM14		FP						0.866	3.92
GM15	779	FN	1.0816	Loma Prieta	1989	6.93	25.005	1.021	4.13
GM16		FP						0.581	3.07
GM17	722	FN	4.8465	Superstition Hills	1987	6.54	21.98	0.512	2.72
GM18		FP						0.669	6.31
GM19	1148	FN	7.2093	Kocaeli-Turkey	1999	7.51	30	1.566	5.72
GM20		FP						1.098	10.94

Note: NGA # - Sequential number in PEER Strong Ground Motion Database

CHAPTER III

SEISMIC RESPONSE OF THE FRAMES UNDER SELECTED GROUND MOTIONS

An ensemble of non-linear time history analyses has been carried out to assess seismic response of the brace-intersected beams as well as its interaction with overall response and seismic response of the other structural members. In this section, a detailed investigation is presented on the braces, the beams and the overall frame behaviors of Frames A and F under GMs 4 and 13. GM 11 was chosen to present the responses of Frame A and Frame E in order to investigate the effect of beam strength on seismic performance of frames in detail. It should be noted that all the data presented in Chapter IV were processed similar to those presented in this chapter. However, only the peak responses obtained from the non-linear time history analyses are presented in the next chapter to allow readers to notice the trend in the frame responses without difficulty.

Since the brace-intersected beams of Frames A and F have the same beam sizes, it would be expected that these two frames should exhibit similar behaviors under the same ground motion records. However, Frame A and Frame F exhibited an unanticipated behavior under GM4 and GM13. As can be seen from Figs. 3.1 and 3.2, both the peak story drift ratio and the peak brace ductility of Frame A are substantially larger than that of Frame F under GMs 4 and 13. Thus, it is decided to present the results of these two ground motions in detail. The details of the Frames A and E responses to GM11 are also presented to make a solid comparison between the frames in terms of the effect of the beam strength on seismic responses of the frames. It should be noted that Frame A has the strongest brace-intersected beams and the Frame E has the weakest brace-intersected beams. In Fig. 3.3 the peak results of Frame A and E in terms of story drift ratio, brace ductility and beam ductility can be seen. The reason for choosing GM 11 for

the comparison was that all the frames responded to GM11 consistent with their beam sizes as expected.

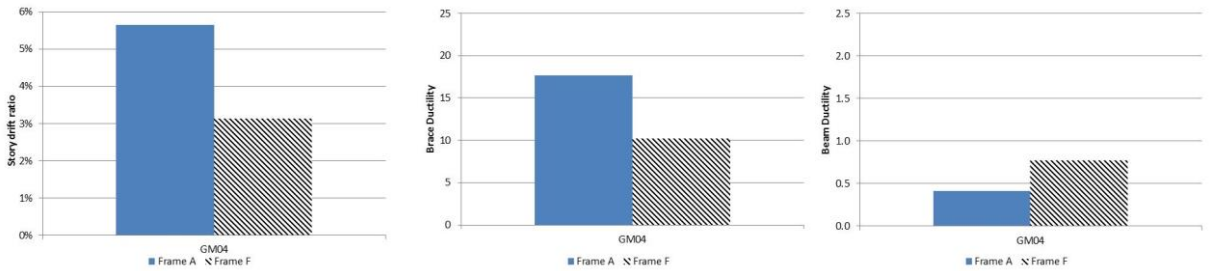

(a) The peak story drift ratio (b) The peak brace ductility (c) The peak beam ductility

Figure 3.1. Seismic response of Frames A and F under GM04

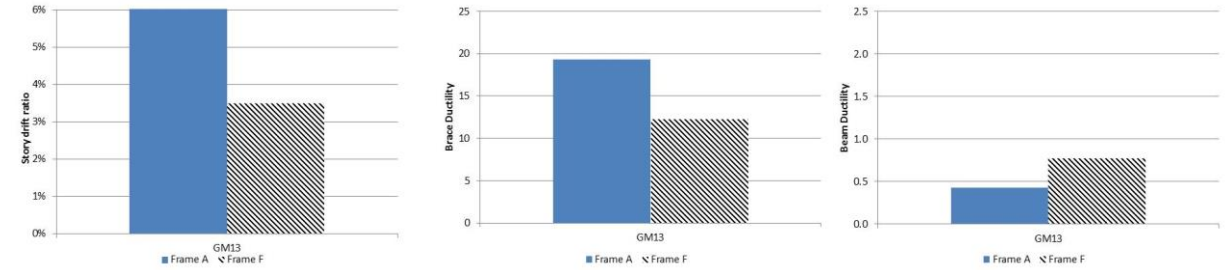

(a) The peak story drift ratio (b) The peak brace ductility (c) The peak beam ductility

Figure 3.2. Seismic response of Frames A and F under GM13

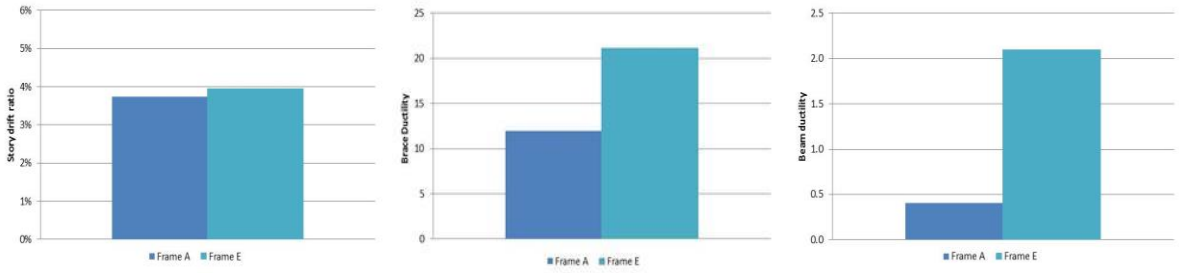

(a) The peak story drift ratio (b) The peak brace ductility (c) The peak beam ductility

Figure 3.3. Seismic response of Frames A and E under GM11

3.1 Seismic behavior of Frames A and F under GM4

3.1.1 Seismic response of Frame A under GM04

As can be seen in Table 2.4, GM4 is a ground motion with the peak ground acceleration of 0.718 g and the peak ground velocity of 6.50 in/s. The acceleration and velocity time history of GM4 is given in Figure 3.3a and b, respectively. The given velocity time history is derived by the integration of the acceleration time history of the ground motion.

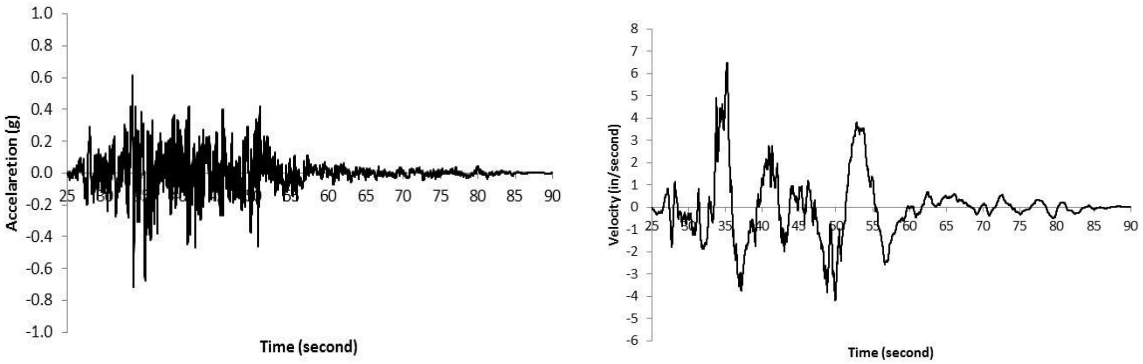

(a) Acceleration time history (b) Velocity time history

Figure 3.3. Acceleration and velocity time history of GM04

The first story drift ratio time history of Frame A represented in Figure 3.4. Since the peak story drift ratio has been obtained from the first story, the story drift ratio histories of the other stories are not included in this section. They can be found in Appendix B. It should also be noted that, even though story drift ratio is unitless, the positive story drift ratio values represent the relative displacement to the right direction and the negative values represent the relative displacement to the left direction with respect to the initial position. As can be seen from Figure 3.4, between 60th and 90th seconds of the record, the story drift ratio increased substantially and the peak story drift ratio has been obtained at the end of the ground motion record, which might have been due to the loss of overall structural stability.

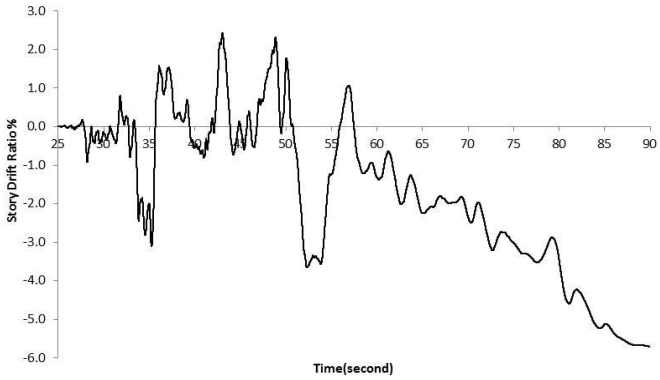

Figure 3.4. 1st story drift ratio time history under GM04

The peak brace ductility response obtained from Frame A under GM04 is given in the next section. However, the time history of normalized axial load of the braces below and above the first story brace-intersected beam need to be examined in detail to reveal the behavior of the braces during the ground motion. Normalized axial load time histories of the braces are given in Figures 3.5a, b, c and d. The response time histories were plotted from 25th second to 90th second, since the brace deformations were negligible during the first 25 seconds. The axial forces in tension and in compression are normalized by the initial yielding strength and the initial buckling strength, respectively. As detailed in Figures 3.5a, b, c and d, all the braces reached their axial load capacities between 25th and 40th seconds of the ground motion. It appears that the left brace below the beam reached both its yielding and buckling capacity while the right brace below the beam reached only its yielding capacity. Similarly, the right brace above the beam reached both its yielding and buckling capacity while the left brace above the beam reached only its yielding capacity during the excitation.

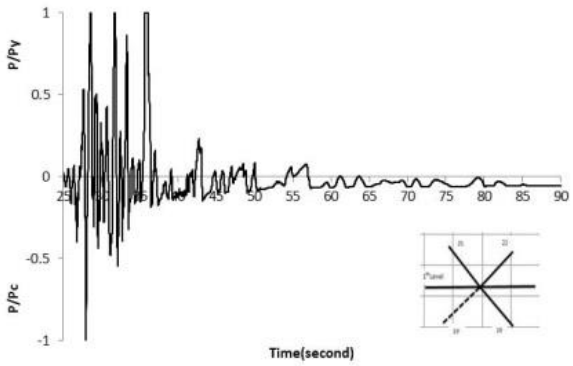

(a) The left brace below the beam

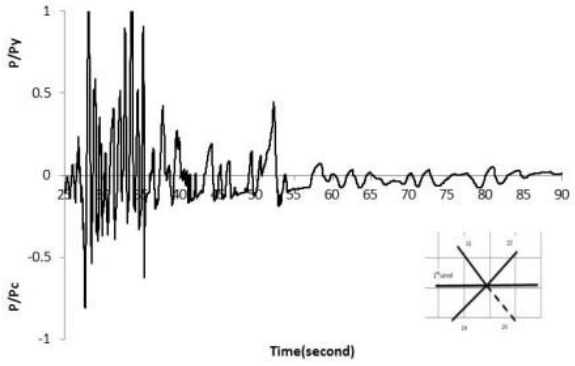

(b) The right brace below the beam

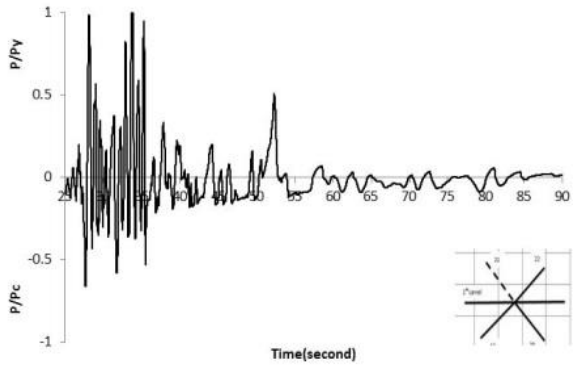

(c) The left brace above the beam

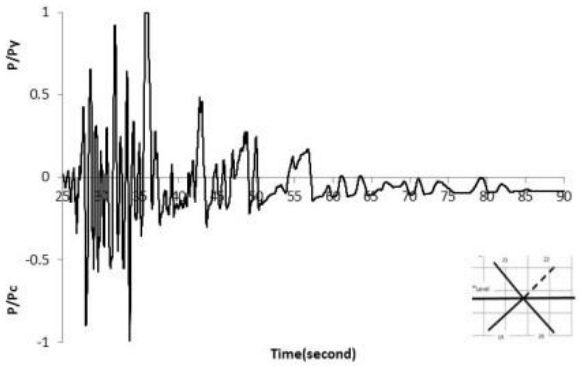

(d) The right brace above the beam

Figure 3.5. Normalized axial force histories of the braces above and below the first story beam

The hysteretic behavior of the braces under GM4 is also investigated. The hysteresis loops of the first level braces of Frame A can be seen in Figures 3.6a, b, c and d. It appears that the envelope of the hysteresis loops of the left brace below the beam is comparable to the right brace above the beam, since the brace-intersected beam remained elastic during the ground motion. Similarly, the envelope of the right brace below the beam and left brace above the beam hysteresis loops were similar to each other.

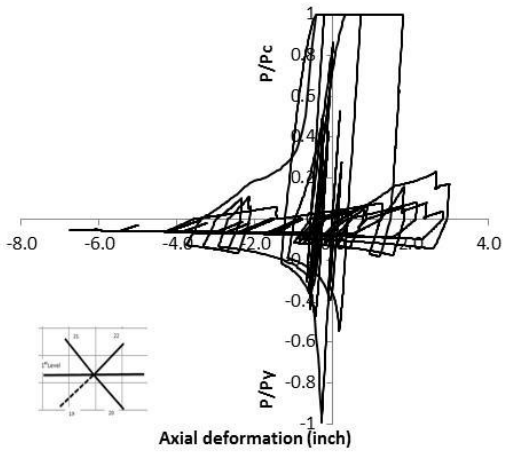

(a) The left brace below the beam

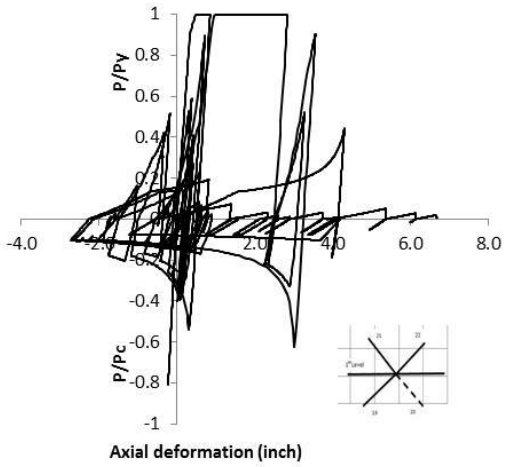

(b) The right brace below the beam

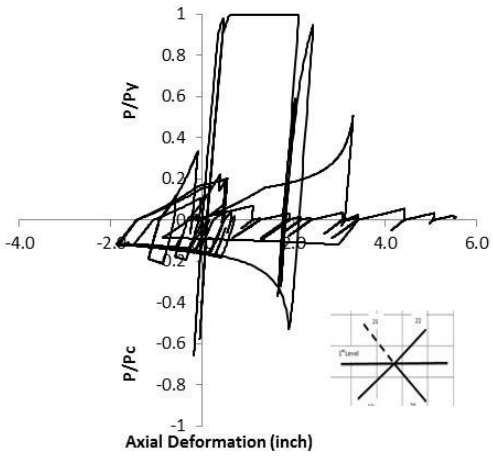

(c) The left brace above the beam

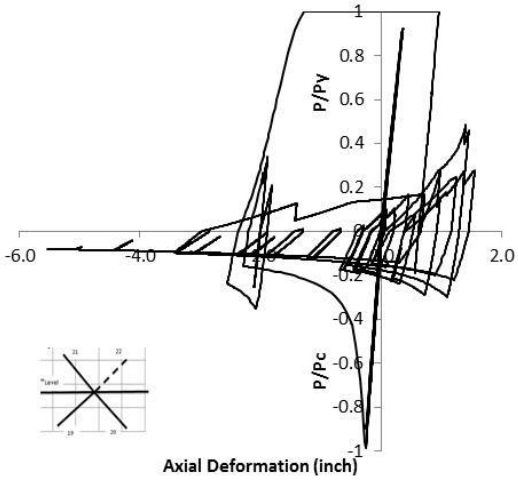

(d) The right brace above the beam

Figure 3.6. Hysteretic responses of the braces above and below the first story beam of Frame A

Since the peak beam ductility is obtained from the first story brace-intersected beam, only the first story beam ductility time history is given in Figure 3.7. As can be seen in Figure 3.7, the first floor brace-intersected beam remained elastic during the ground motion and the peak ductility ratio was around 0.4.

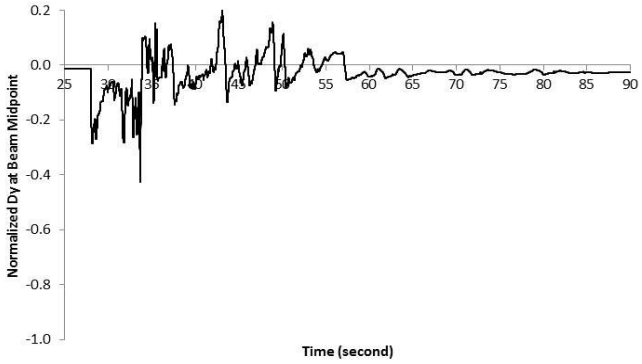

Figure 3.7. Beam ductility time history of the first floor brace-intersected beam under GM04

The seismic response of the overall structure in terms of story drift ratio, brace ductility and beam ductility of Frame A is investigated. It is clear that additional examination is required to understand the reasons for loss of structural stability (Fig. 3.4), which led the story drift ratio to increase rapidly. Therefore, it is decided to review the response of the columns in terms of combined strength ratio, which is the summation of axial force divided by the nominal axial force capacity of the column and bending moment divided by the nominal bending moment capacity of the column. Note that normalized axial force time history and normalized bending moment time history of each story column can be found in Appendix B.

The combined strength ratio ($P/P_c+M/M_c$) of each column under GM04 are given in Figure 3.8a, b, c, d, e and f. It seems that the first story column reached its capacity around 35th second of the ground motion (Fig. 3.8a), which must have been an explanation to the rapid increase in the story drift ratio response.

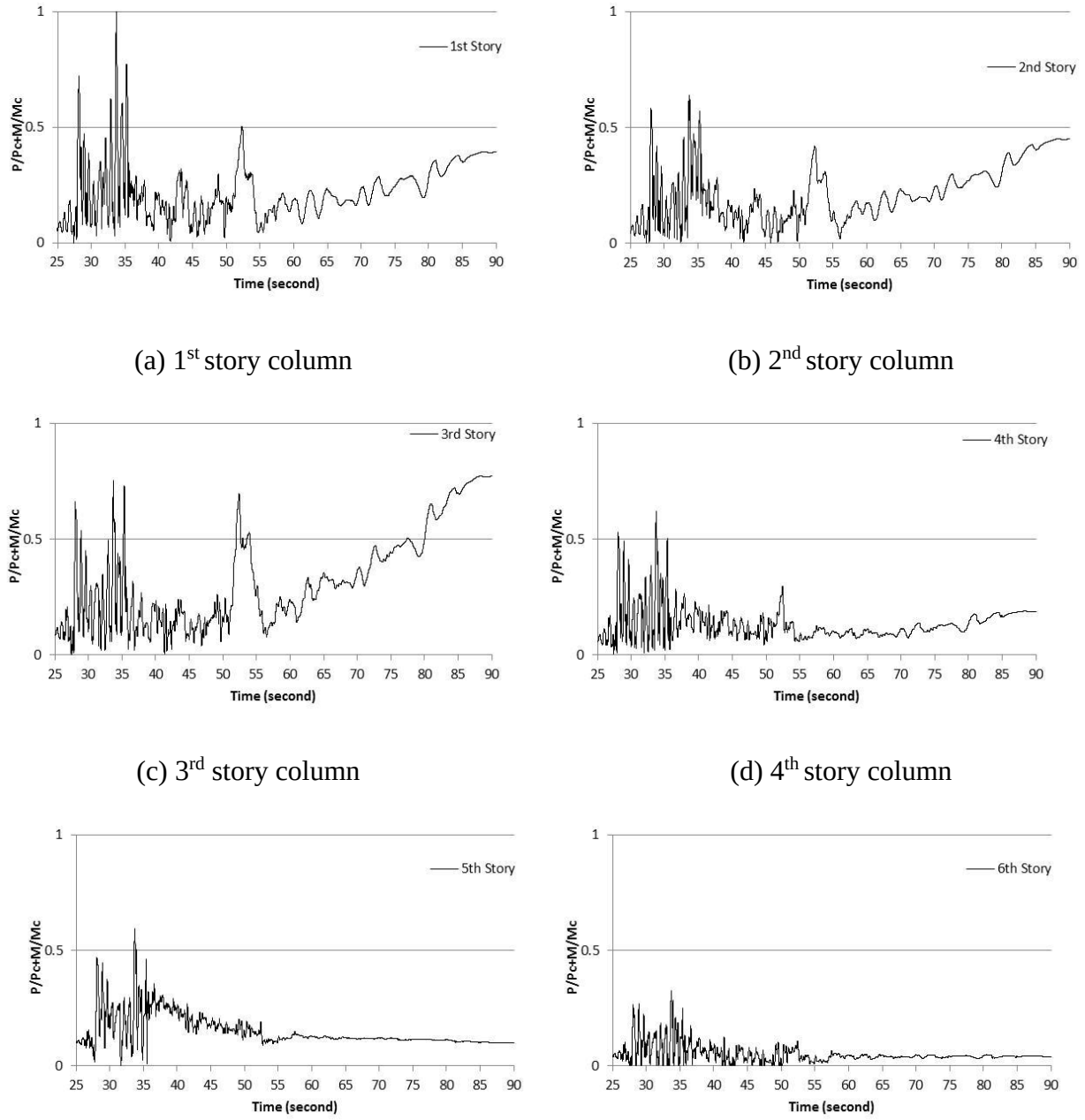

(a) 1st story column (b) 2nd story column

(c) 3rd story column (d) 4th story column

(e) 5th story column (f) 6th story column

Figure 3.8. Combined strength ratio history of all columns of Frame A under GM4

3.1.2 Seismic response of Frame F under GM04

As can be seen from Fig. 3.9, the peak first story drift ratio was about 3.5%. Comparing Figs. 3.4 and 3.9 shows that the story drift ratio time histories of Frame A and F are similar until

60th second of the ground motion. However, unlike Frame F, the story drift ratio response of Frame A increased dramatically due to yielding of the first story column.

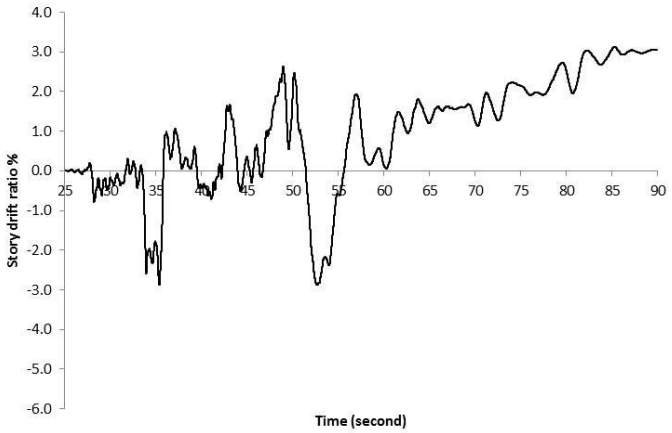

Figure 3.9. 1st story drift ratio time history of Frame F under GM04

Time histories of brace ductility of the first floor braces can be found in Figure 3.10a, b, c and d. Data in Fig. 3.10 suggests that the normalized axial force time histories of the left brace below and above the beam were similar. Also, it is noticed that the axial force response of the right brace above and below the beam were almost identical.

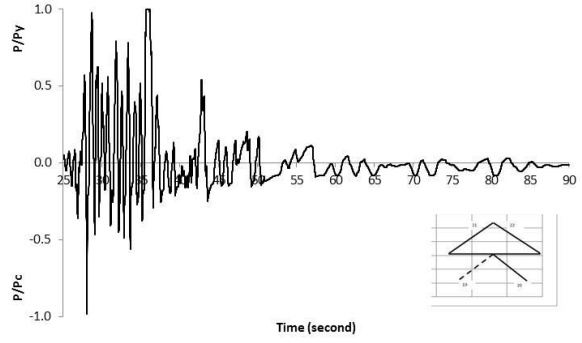

(a) The left brace below the beam

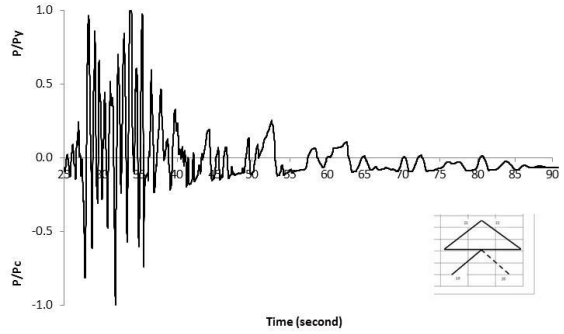

(b) The right brace below the beam

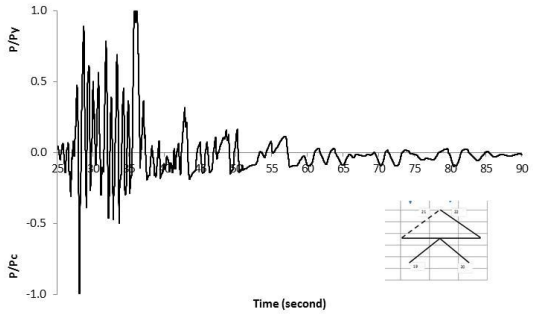

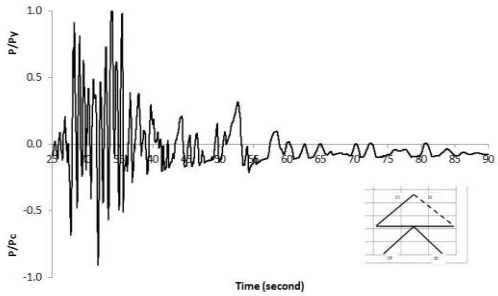

(c) The left brace above the beam (d) The right brace above the beam

Figure 3.10. Normalized axial force histories of the braces above and below the first story beam

The hysteresis loops of the braces above and below the first story beam displayed in Figs. 3.11a, b, c and d. Similar to the axial force time histories of the braces, the hysteretic behavior of the braces are consistent with each other.

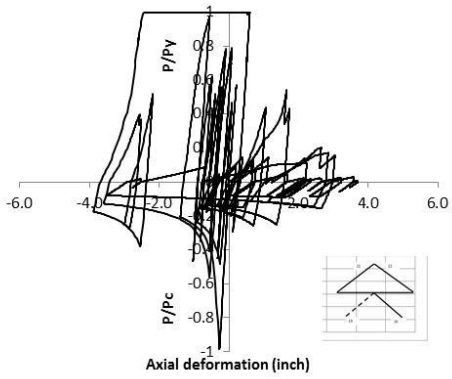

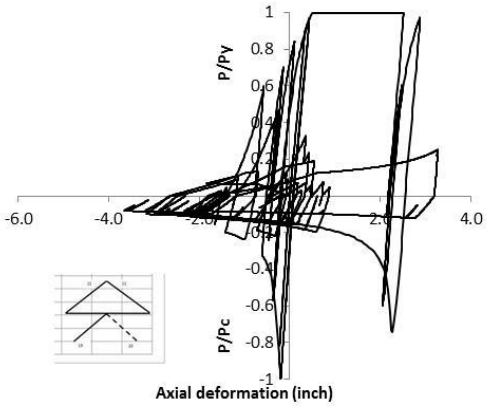

(a) The left brace below the beam (b) The right brace below the beam

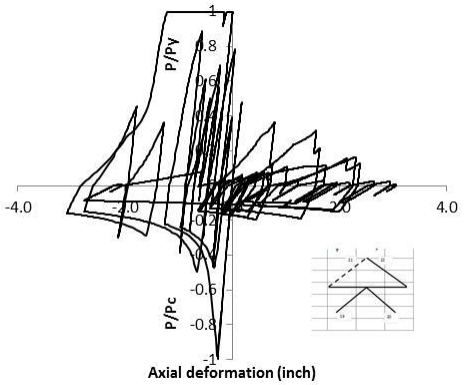

(c) The left brace above the beam

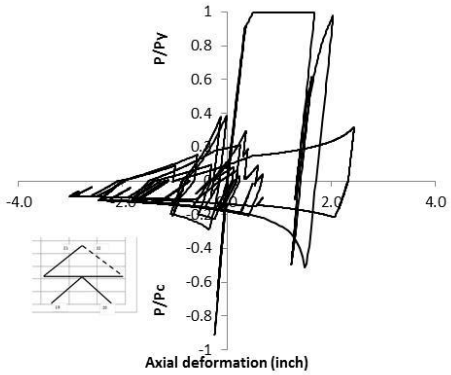

(d) The right brace above the beam

Figure 3.11. Hysteretic responses of the braces above and below the first story beam of Frame F

The peak beam ductility demand observed at the first floor of Frame F under GM4. Fig.3.12 illustrates that the first floor beam of Frame F remained elastic during the ground motion and the peak beam ductility was about 0.6.

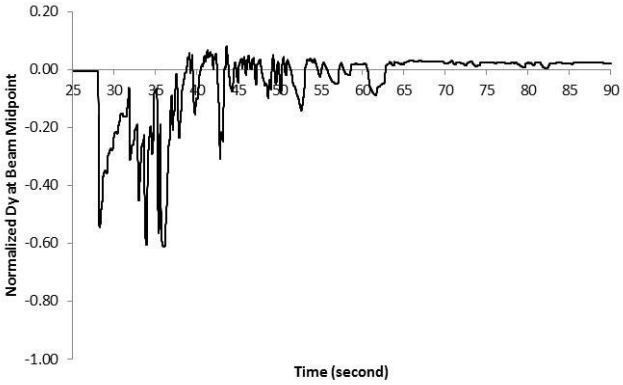

Figure 3.12. Beam ductility of the first story beam

The combined strength ratio time history of each column is presented in Figure 3.13a, b, c, d, e and f. The maximum combined strength ratio of columns was about 0.7, which means the columns remained elastic during the ground motion.

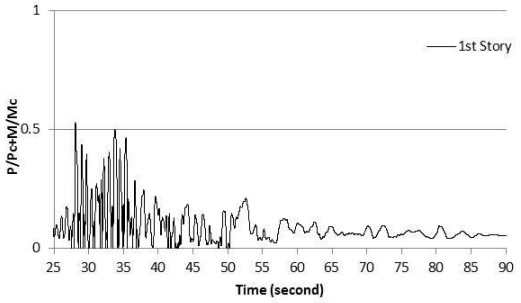

(a) 1st story column

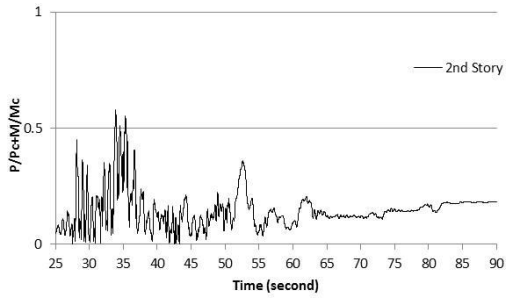

(b) 2nd story column

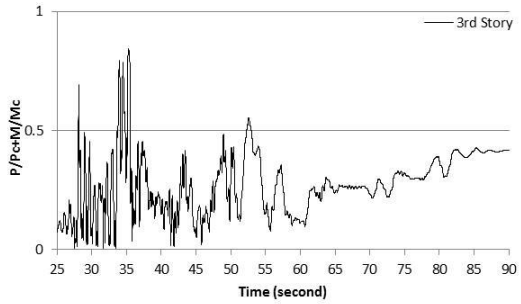

(c) 3rd story column

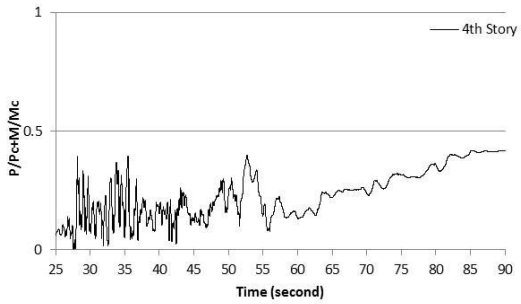

(d) 4th story column

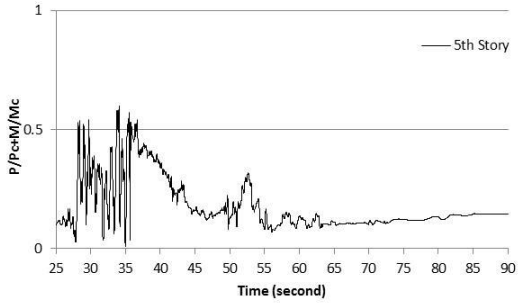

(e) 1st story column

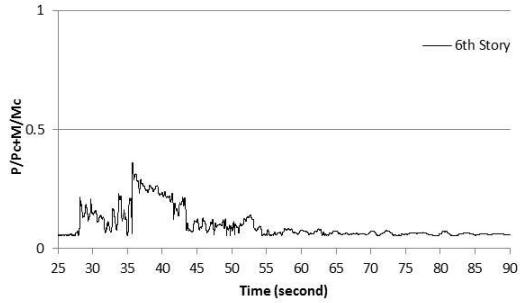

(f) 2nd story column

Figure 3.13 Combined strength ratio of all level columns of Frame F under GM4

3.1.3 Observations on the behavior of Frames A and F under GM04

- The story drift ratio responses of Frames A and F were significantly different. The peak story drift ratio of Frame A was 5.6% while the peak story drift ratio of Frame F was around 3%.

- From beam ductility perspective, the first story brace-intersected beam of Frame A reached its capacity while the beams of Frame F remained elastic.
- The most remarkable difference between the frames was the column behavior. The first story columns of Frame A yielded. On the other hand, the columns of Frame F remained elastic.

3.2 Seismic behavior of Frames A and F under GM13

3.2.1 Seismic response of Frame A under GM13

Acceleration time history of ground motion 13 with the peak ground acceleration of 0.835g can be seen in Fig. 3.14a. Velocity time history of GM13 with the peak ground velocity of 5.03 in/s is given in Fig.3.14b.

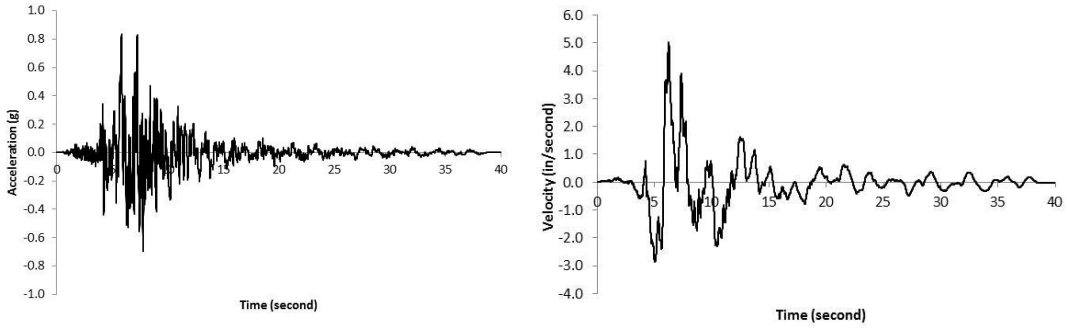

(a) Acceleration time history (b) Velocity time history

Figure 3.14. Acceleration and velocity time history of GM13

The first story drift ratio time history of Frame A under GM13 is illustrated in Fig. 3.15. The peak story drift ratio of the first level was larger than 6%. Inspection of Fig.3.15 indicates that the story drift ratio increased substantially after 20th second of the ground motion. The other stories' drift ratio time histories can be found in Appendix B.

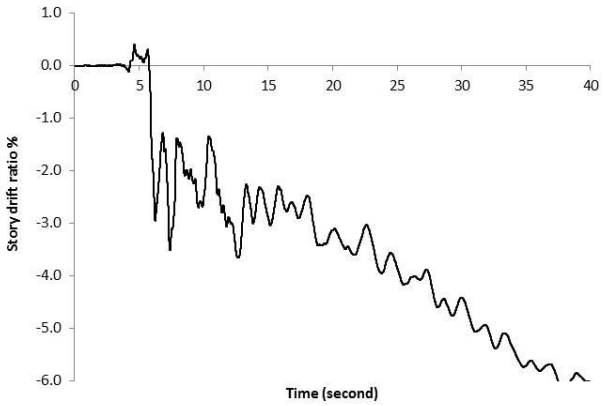

Figure 3.15. First story drift ratio time history of Frame A under GM13.

Normalized axial force time histories of the braces above and below the first story brace-intersected beam of Frame A are given in Figure 3.16. It can be observed from the Fig 3.16a, b, c and d that the braces reached their yielding and buckling capacities except for the left brace above the beam.

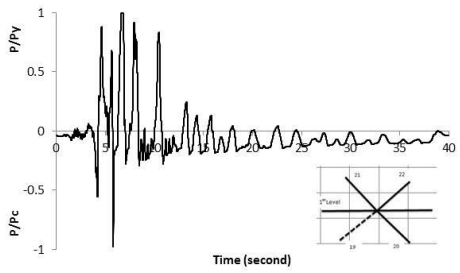

(a) The left brace below the beam

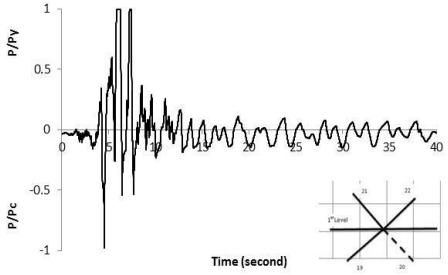

(b) The right brace below the beam

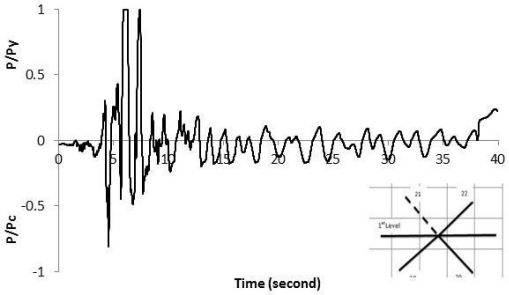

(c) The left brace above the beam

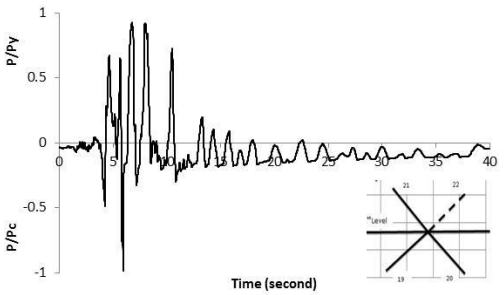

(d) The right brace above the beam

Figure 3.16. Normalized axial force histories of the braces above and below the first story beam

As illustrated in Fig.3.17a, b, c and d, the response of the left brace above the beam (Fig. 3.17c) and the right brace below the beam (Fig. 3.17b) were tension-dominated. On the other hand, the response of the right brace above the beam (Fig. 3.17d) and the left brace below the beam (Fig. 3.17a) were compression-dominated.

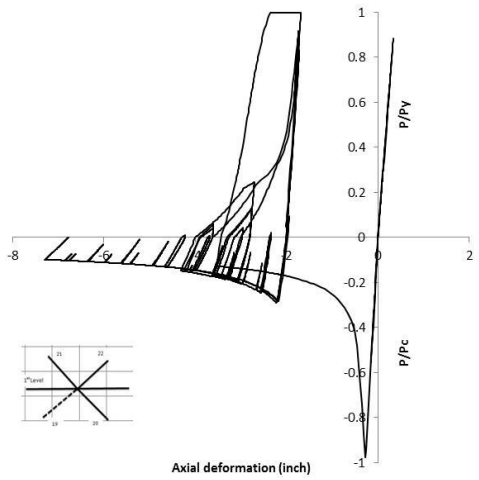

(a) The left brace below the beam

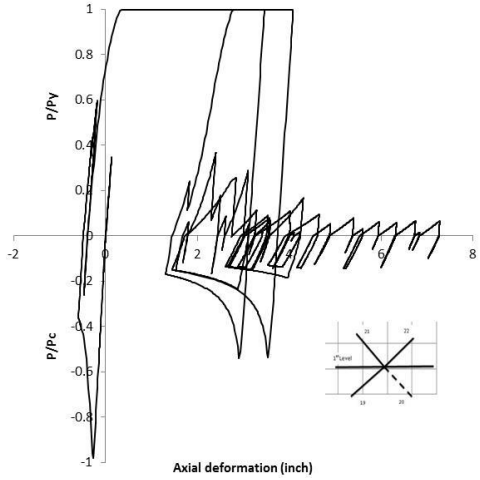

(b) The right brace below the beam

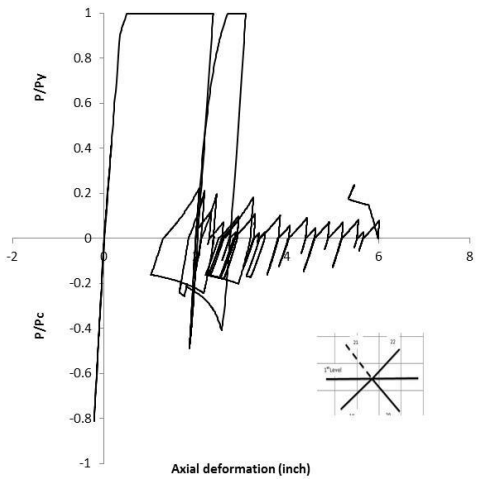

(c) The left brace above the beam

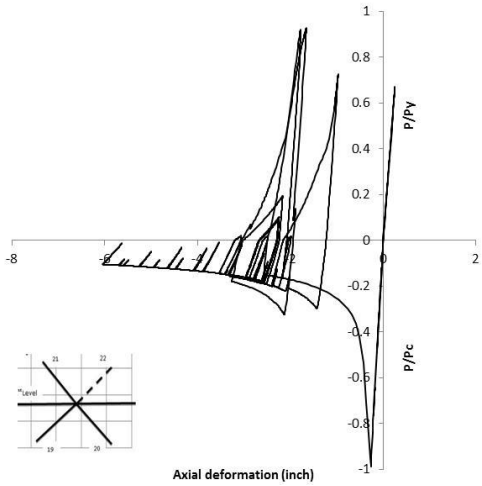

(d) The right brace above the beam

Figure 3.17. Hysteretic responses of the braces above and below the first story beam

Beam ductility of the first story brace-intersected beam can be seen in Figure 3.18. The brace-intersected beam remained elastic during the ground motion. The peak beam ductility of 0.40 was observed around 7th second.

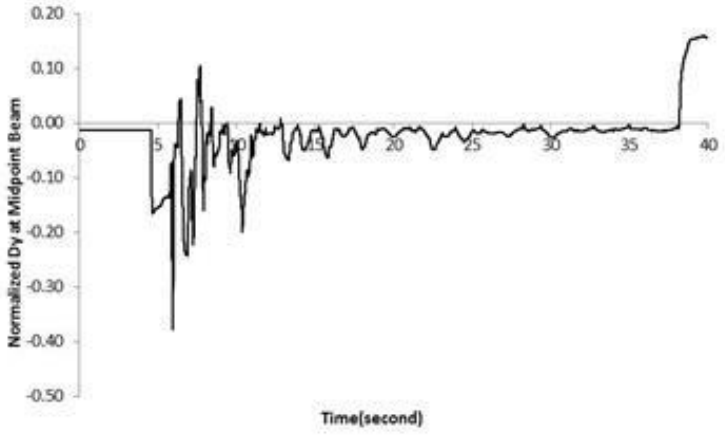

Figure 3.18. Beam ductility of the first story brace-intersected beam

Combined strength ratio of the columns of Frame A can be seen in Fig. 3.19. It is noticed that the first, third, fourth and fifth story columns almost reached their capacities with around a peak combined strength ratio of 0.9. Although the columns did not experience inelastic deformation, it seems that the stress levels of the columns were higher than expected. It should be noted that the largest contribution to the combined strength ratio was from bending moment. The details of the normalized axial load time histories and normalized bending moment time histories of each stories' columns can be found in Appendix B.

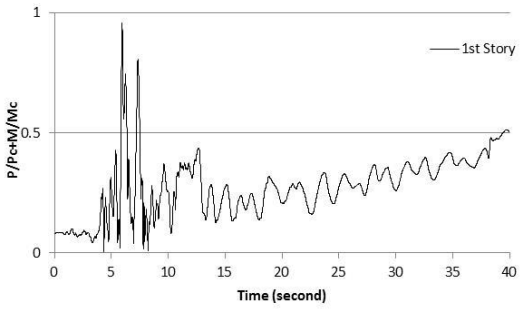

(a) 1st story column

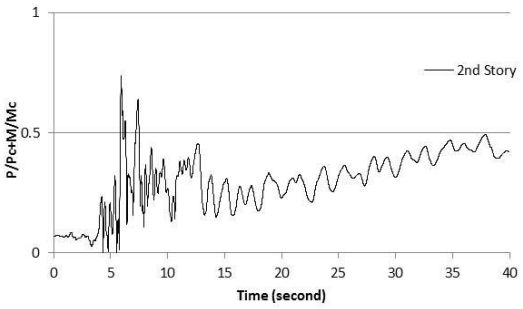

(b) 2nd story column

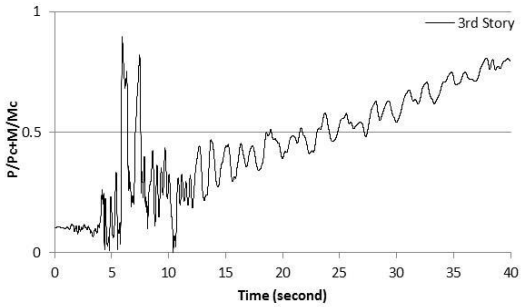

(c) 3rd story column

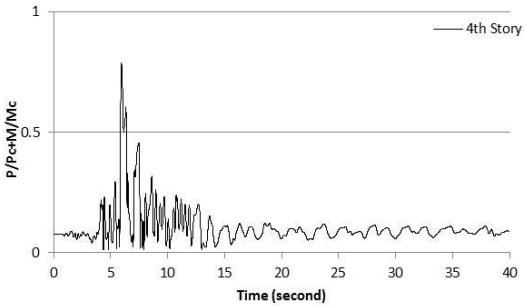

(d) 4th story column

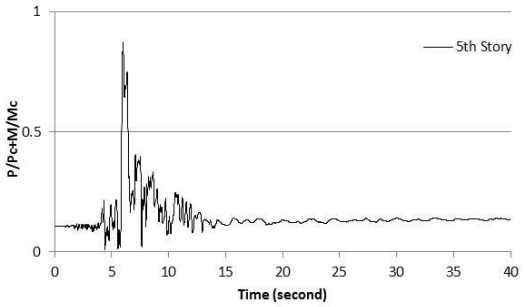

(e) 5th story column

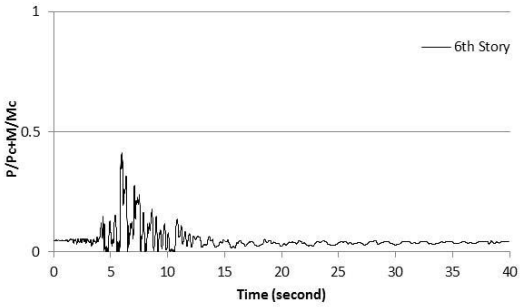

(f) 6th story column

Figure 3.19. Combined strength ratio time history of columns of Frame A

3.2.2 Seismic response of Frame F under GM13

First story drift ratio time history of Frame F under GM13 is given in Fig.3.20. The peak story drift ratio was around 3% and occurred between the 5th and 10th seconds. The other stories' drift ratio time histories can be found in Appendix B.

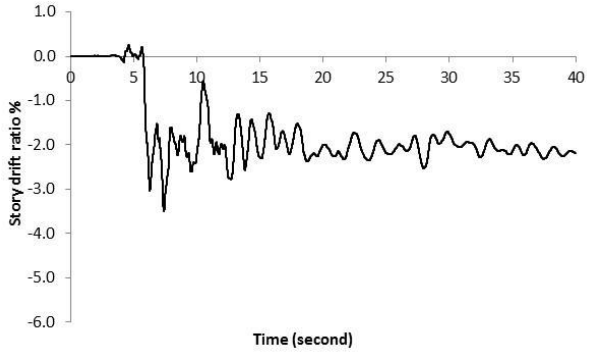

Figure 3.20. The first story drift ratio time history of Frame F under GM13.

Normalized brace ductilities of the braces above and below the first story beam are given in Fig. 3.21. As can be seen in Fig.3.21, the braces reached their yielding strength in tension and buckling strength in compression except for the right brace above the beam. The right brace above the beam did not reach its buckling capacity.

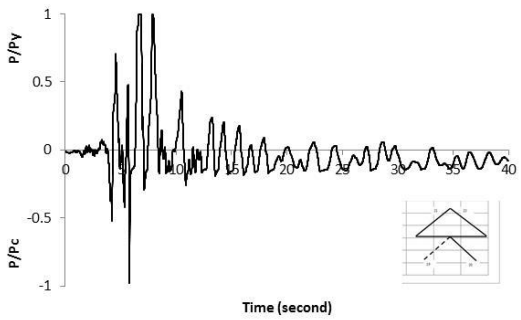

(a) The left brace below the beam

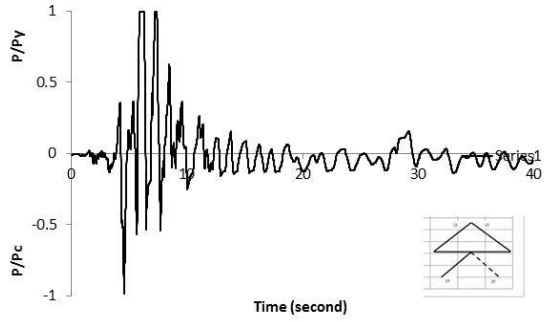

(b) The right brace below the beam

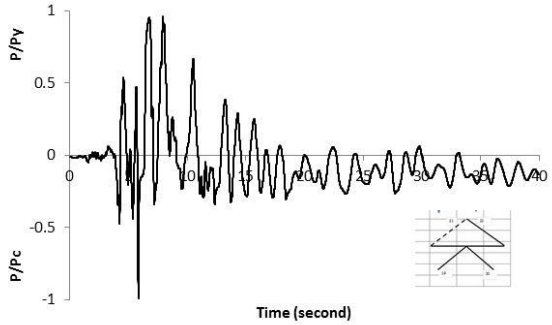

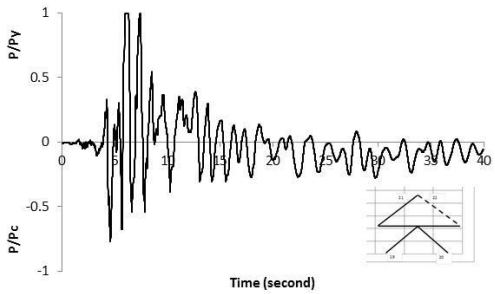

(c) The left brace above the beam (d) The right brace above the beam

Figure 3.21. Normalized axial force histories of the braces above and below the first story beam

The hysteresis loops of the braces above and below the first level brace-intersected beams are given in Fig.3.22. As indicated in Fig.3.22, the hysteretic responses of the left brace above and below the beam were compression-dominated (Figs. 3.22a and c) while the responses of the right brace above and below the beam were tension-dominated (Figs. 3.22b and d).

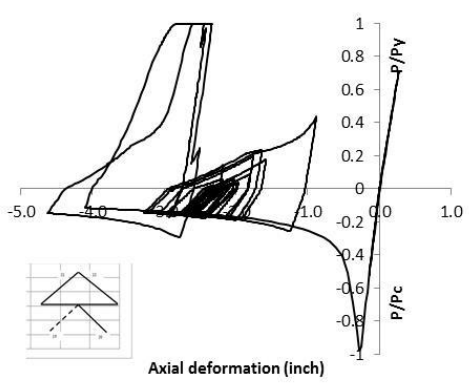

(a) The left brace below the beam

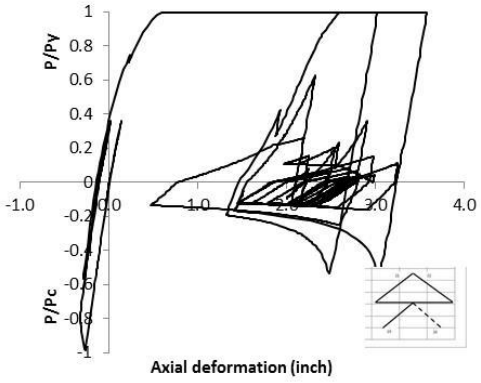

(b) The right brace below the beam

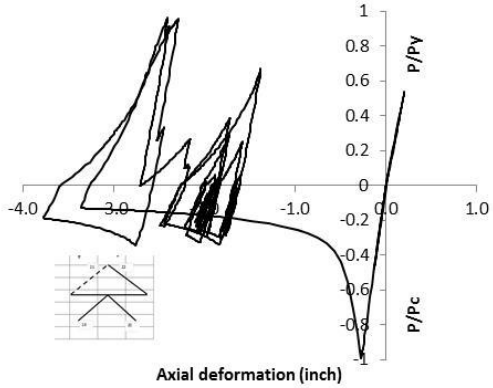

(c) The left brace above the beam

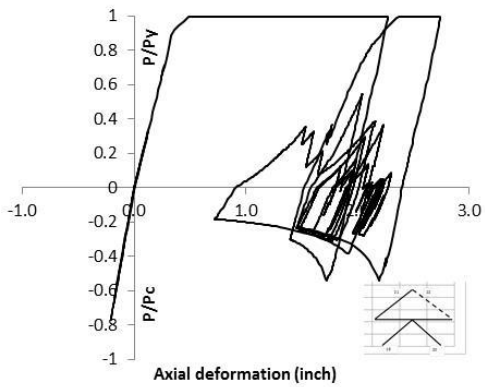

(d) The right brace above the beam

Figure 3.22. Hysteresis loops of the braces above and below the first story beam of Frame F

Beam ductility time history of the first story beam of Frame F under GM13 is displayed in Fig. 3.23. The peak beam ductility was around 0.6 and occurred between 5th and 10th second of the ground motion.

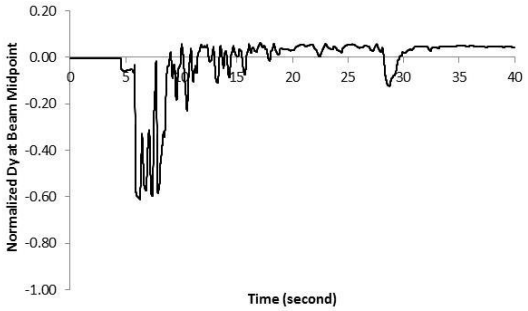

Figure 3.23. Beam ductility time history of the first story beam

Combined strength ratio of each level columns time histories can be seen from Fig.3.24. The first, third and fifth story columns remained elastic with a maximum combined strength ratio of 0.7. Normalized axial force and normalized bending moment time histories can be found in Appendix B.

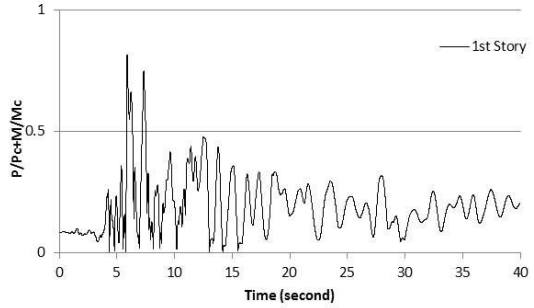

(a) 1st story column

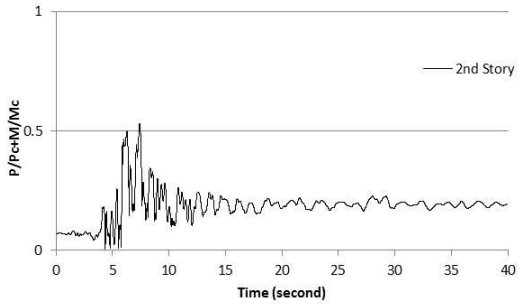

(b) 2nd story column

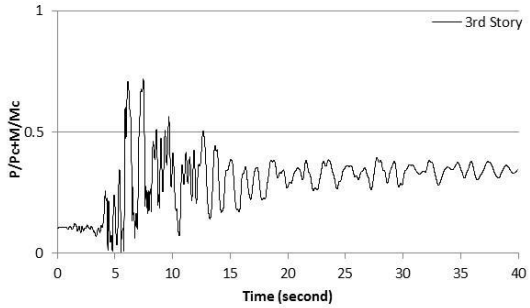

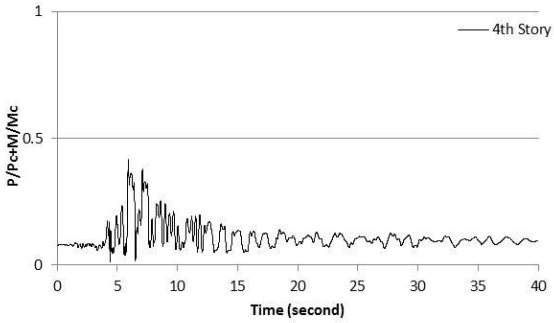

(c) 3rd story column

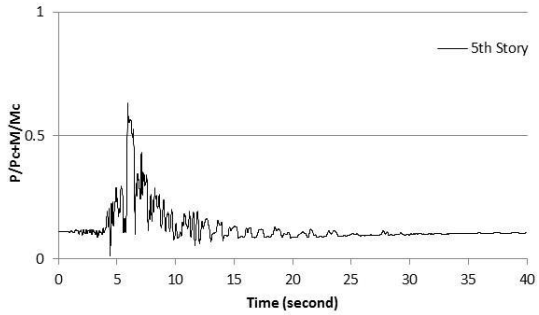

(d) 4th story column

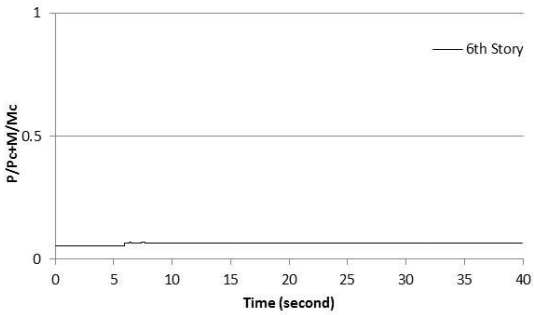

(e) 5th story column

(f) 6th story column

Figure 3.24. Combined strength ratio time history of columns of Frame F under GM13

3.2.3 Observations on the behavior of Frame A and F under GM13

- Over a peak story drift ratio of 6% and about a peak story drift ratio of 3.2% were obtained from Frame A and F, respectively.
- The beams of both frames remained elastic. The peak beam ductility of Frame A occurred at the first story brace-intersected beam and was around 0.4 while the peak beam ductility of Frame F was around 0.6.
- In terms of column behavior, most of the columns of Frame A reached very high stress levels. It is observed that the peak combined strength ratio of the first, third, fourth and fifth story columns of Frame A were around 0.96, 0.90, 0.80 and 0.90, respectively. On the other hand, the columns of Frame F remained elastic with about a maximum combined strength ratio of 0.6.

3.3 Seismic response of Frames A and E under GM11

Since the responses of frames under GM11 presented the trend coherent with the beam sizes, seismic response of Frame A and E under GM11 were illustrated in this section for comparison. Acceleration and velocity time history of GM11 can be found in Fig. 3.25.

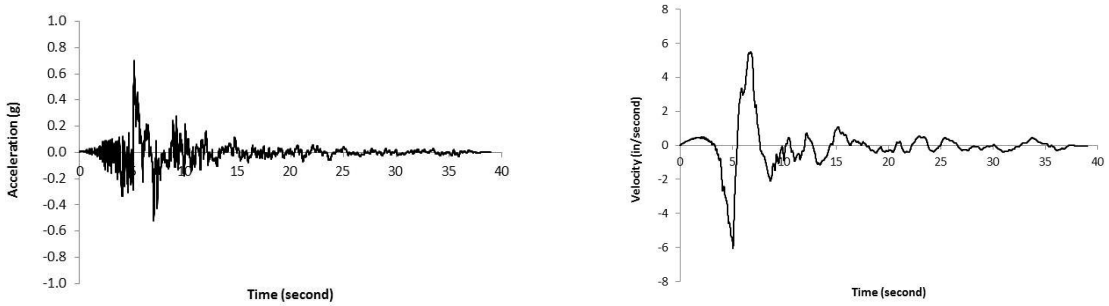

(a) Acceleration time history (b) Velocity time history

Figure 3.25 Acceleration and velocity time history of GM11

It should be noted that Frame A has the strongest brace-intersected beams and Frame E has the weakest brace-intersected beams. In this section, it was decided to present the results of Frame A and E for comparison in order to investigate the differences between the seismic responses of frames due to the beam strength. That is why, Frame A and E have been chosen for the comparison .The first story drift ratio time history of Frame A and Frame E displayed in Fig. 3.26. The peak story drift ratio has been occurred between the 5^{th} and 10^{th} second and was around 4% for both frames. It is obvious that both frames showed very similar responses under GM11 in terms of story drift ratio.

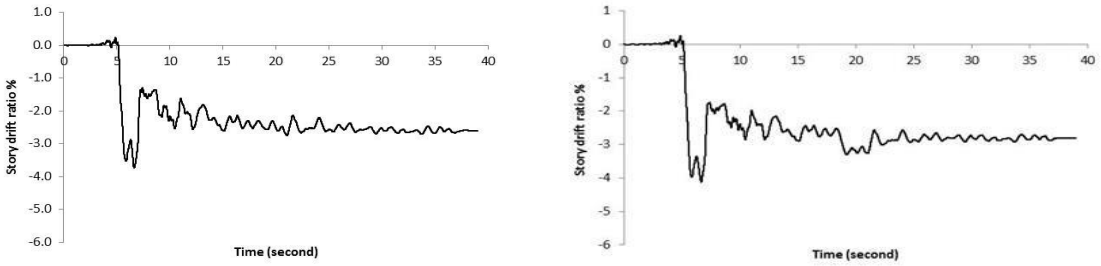

(a) Frame A (b) Frame E

Figure 3.26. The first story drift ratio time histories of Frames A and E under GM11

Normalized axial force time histories of braces above and below the first story beam of Frames A and E are displayed in Fig. 3.27 and Fig.3.28, respectively. Comparing Fig. 3.27 and Fig.3.28 shows that the normalized axial force time histories of the braces of Frames A and E did not differ substantially from each other. Note that the peak brace ductility of Frame A was 13 while Frame E peak brace ductility was 21.

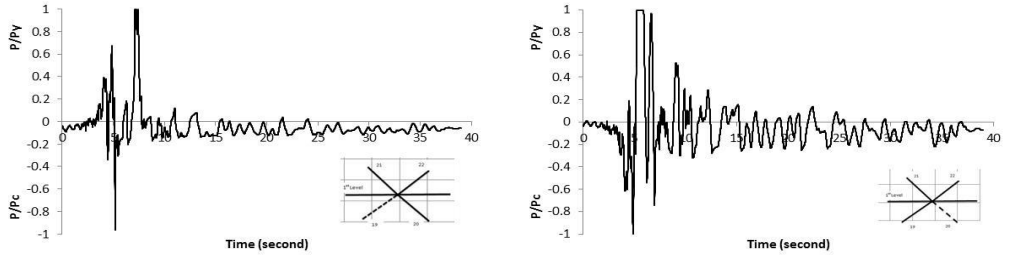

(a) The left brace below the beam (b) The right brace below the beam

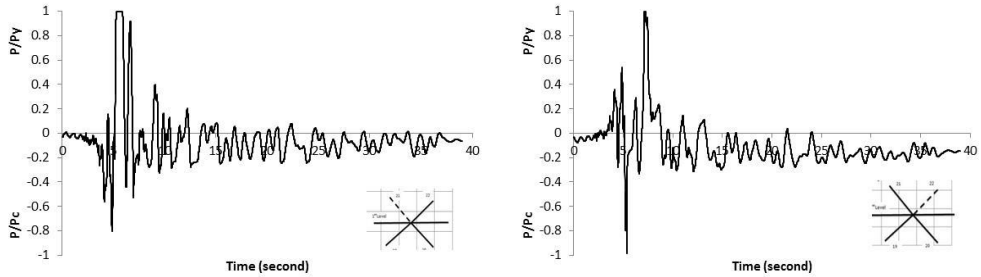

(c) The left brace above the beam (d) The right brace above the beam

Figure 3.27. Normalized axial force time histories of the braces above and below the first story beam of Frame A

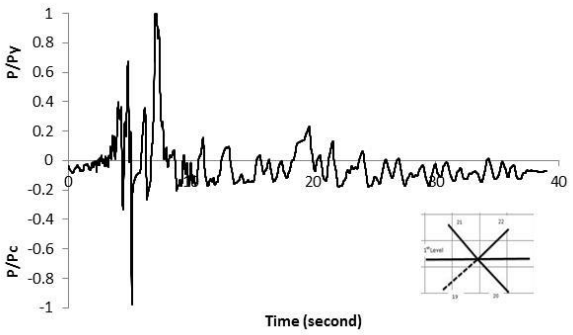

(a) The left brace below the beam

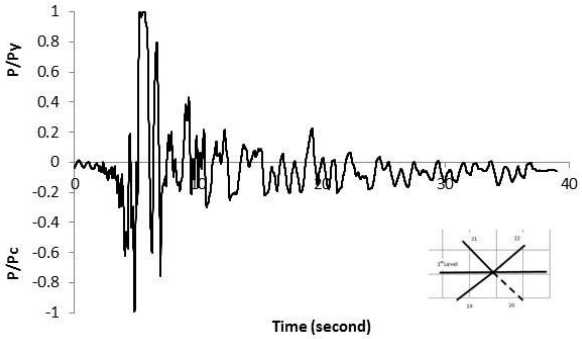

(b) The right brace below the beam

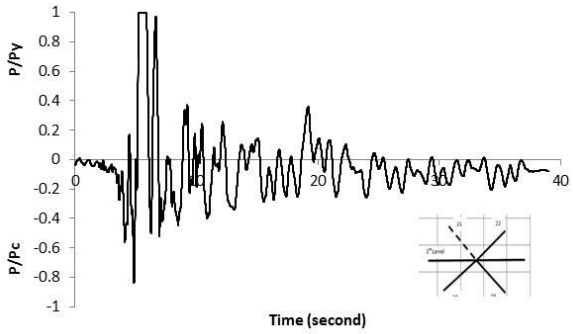

(c) The left brace above the beam

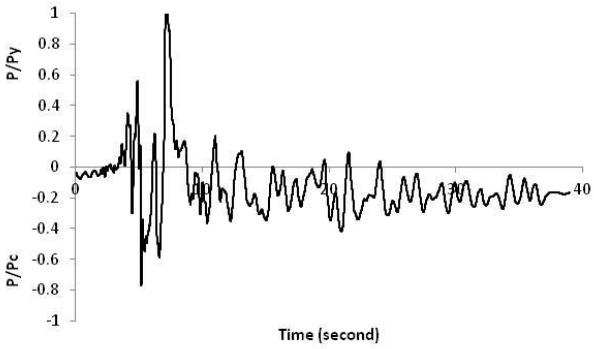

(d) The right brace above the beam

Figure 3.28. Normalized axial force time histories of the braces above and below the first story beam of Frame E

As shown in Fig. 3.29, the first story beam of the Frame A remained elastic during the ground motion with about a peak beam ductility responses of 0.4 while the first story beam of the Frame E showed inelastic deformation. From the story drift perspective, the Frames A and E showed very similar behavior. On the other hand, a significant difference was observed between the frames in terms of brace ductility and beam ductility.

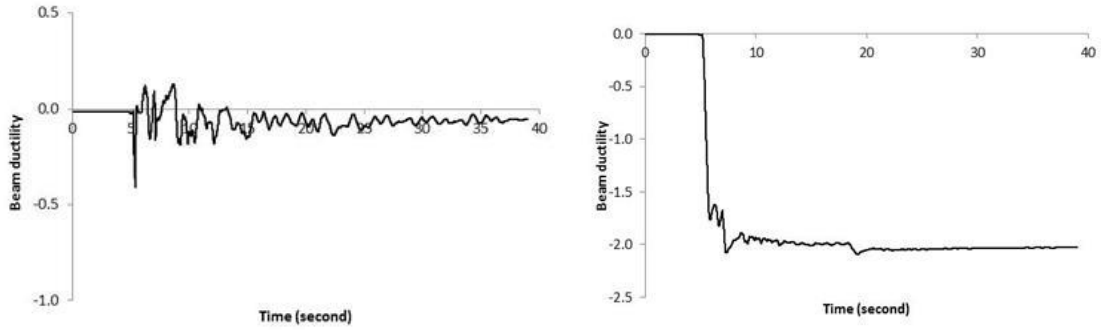

(a) Frame A (b) Frame F

Figure 3.29. Beam ductility time history of the first level brace-intersected beam of Frames A and E

CHAPTER IV

SEISMIC BEHAVIOR OF THE FRAMES UNDER THE TWENTY GROUND MOTIONS

4.1 Overview

In this chapter, the seismic response of the 6-story TSXBFs is presented. The braced frames were subjected to twenty ground motions. Results of the non-linear time history analyses are presented and discussed in terms of story drift ratio, normalized beam deflection (beam ductility) and brace ductility demand. As mentioned in the literature review, inelastic behavior of the brace-intercepted beams in two-story X-braced frames (TSXBFs) has not been extensively studied. The primary purpose of this study is to assess the inelastic behavior of brace–intersected beams under seismic loads, and its impact on seismic performance of the TSXBFs.

Traditionally, story drift ratio is used as a damage index to measure seismic response of seismic force resisting systems, such as moment frames and TSXBFs. Although using story drift ratio to measure seismic response of moment frames is adequate, it might be an issue for TSXBFs due to their complicated inelastic behavior. Unfortunately, previous studies on TSXBFs do not provide any information on the beam behavior [11, 19]. In this study, in addition to peak story drift ratios of the frames, seismic responses of the frames were evaluated through the seismic demands on the critical members of the frames. Thus, seismic response of braces and beams were also included in terms of ductility demands.

Twenty ground motions used in the study divided into three groups based on the peak story drift ratio response of the frames during the excitations for the sake of the discussion. By dividing the ground motions into three groups, it was possible to evaluate the similar ground motion intensities based on the frame responses separately. As indicated in Fig. 4.1, the global

seismic response of frames varies from about a story drift ratio of 0.5% to over a story drift ratio of 6%. The mean value of the responses of Frame A through F has been used for determination of the groups. Ground motion group I consists of ground motions that developed less than 2% story drift ratio response in the frame. Ground motion group II consists of ground motions that developed a story drift ratio response between 2% and 4%. Ground motion group III is composed of ground motions that developed larger than 4% story drift ratio response in the frame. The ground motions of each group are as follows:

- Ground Motion Group I (GMG1): 10 ground motions out of 20 ground motions. (SDR ≤ 0.02) GM 1, GM5, GM8, GM9, GM10, GM14, GM15, GM16, GM17, GM19.
- Ground Motion Group II (GMG2): 7 ground motions out of 20 ground motions. (0.02≤SDR≤0.04) GM2, GM4, GM6, GM7, GM11, GM12, GM18, GM20.
- Ground Motion Group III (GMG3): 3 ground motions out of 20 ground motions. (SDR> 0.04) GM3, GM13.

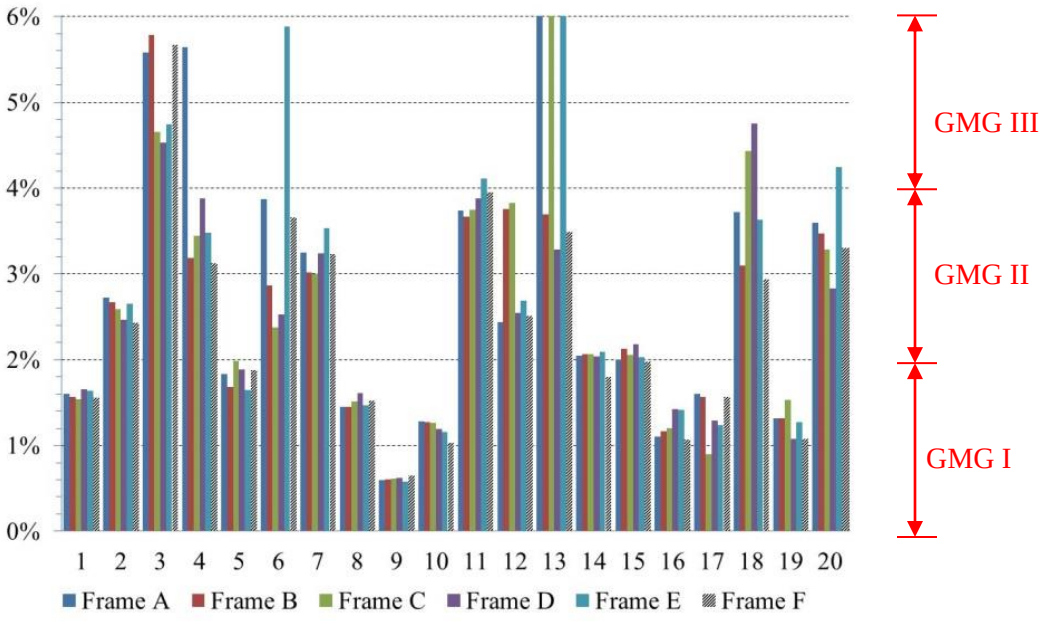

Figure 4.1. Peak story drift ratio distribution of the frames under 20 GMs

4.2 Seismic response of the frames in terms of story drift ratio

Fig. 4.2 illustrates the peak story drift ratio of each frame during the ground motions and the horizontal lines in the figure represent the mean value of each frame's response to the GMG I. As can be seen in Fig. 4.2, all the frames subjected to the ground motions of GMG I exhibited similar responses.

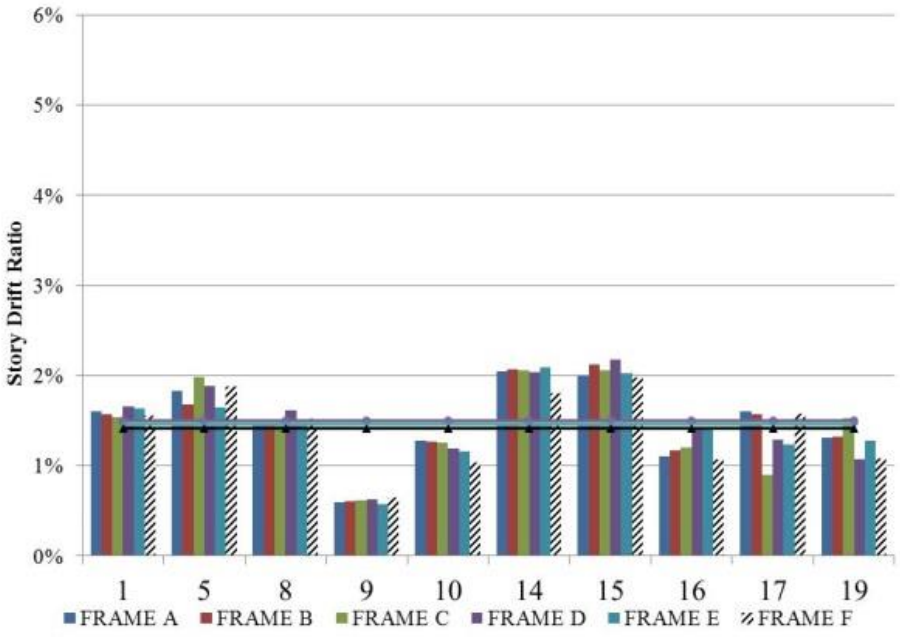

Figure 4.2. Peak story drift ratio responses of the frames under GMG I

Based on the results of the analyses, following observations can be made:

- It appears that all frames had virtually the same mean story drift ratio (~ 1.6%), which is smaller than the design story drift ratio (2%).
- The responses in Frame A and F, which are the frames that having the same beam sizes (strongest beams) but different bracing configurations were almost identical to each other under all ground motions of GMG I.
- The difference between the peak story drift ratios obtained from the analyses of the frames under GMs 1, 8, 9, 14 and 15 were negligible while the variation in the peak story

drift ratios under GMs 5, 16, 17 and 19 was more noticeable. Furthermore, it is noticed that there is a good correlation between the brace-intersected beam sizes and the peak story drift ratio of the frames under GM 16.

The peak story drift ratio responses of the frames under eight ground motions of GMG II are shown in Fig. 4.3. The following can be observed from the figure:

- It seems that the distinction between the mean responses (the horizontal lines in the figure) of the frames was more substantial compared to the observed responses of GMGI.
- The impact of the beam size on the frame responses in terms of story drift ratio was significant, since the other structural members of the frames were identical.
- The peak story drift ratios obtained from the Frames A and F were quite similar to each other when the frames subjected to all the ground motions except for GM4, which is investigated thoroughly in the previous section. The peak response of the Frame A was almost two times the peak response of Frame F when subjected to GM4.
- It is apparent that Frames A through F exhibited a consistent behavior with their beam sizes under both GMs 7 and 11. On the other hand, the frame responses to the rest of the ground motions of GMG II were arbitrary owing to the complexity of the deformation patterns in inelastic stage.

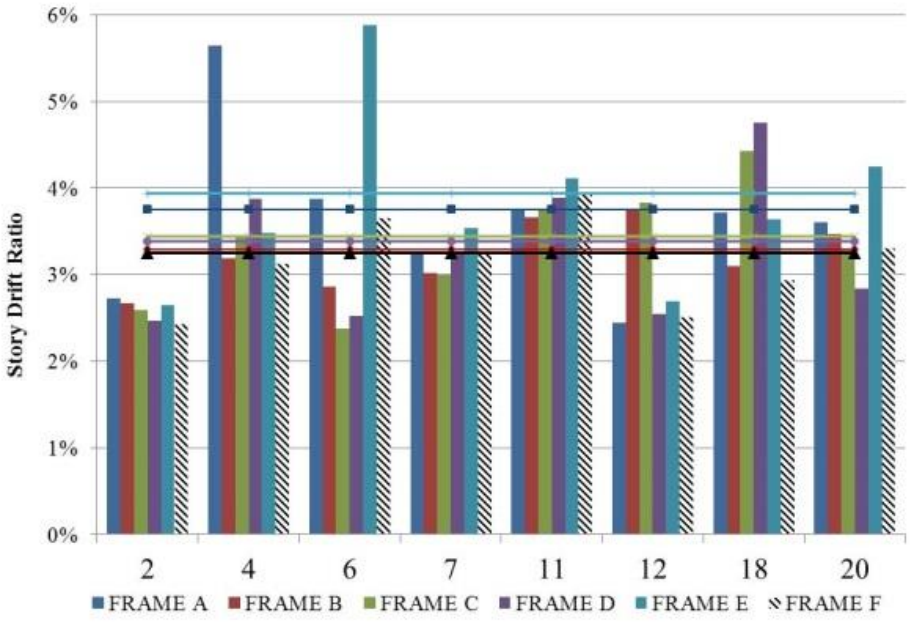

Figure 4.3 Peak story drift ratio responses of the frames under GMG II

Fig. 4.4 plots the responses to the ground motions of GMG III in terms of the peak story drift ratios. The mean frame responses were larger than 6% when the frames subjected to GMs 3 and 13. The results of Frame A, B and F were quite similar in terms of story drift ratio under GM3 while Frame C, D and E showed virtually the same response with relatively smaller results compared to the Frames A, B and F.

Comparing the results of Frames A and F under GM 13 shows that the bracing configuration has an impact on the inelastic behavior of braced frames, since the frames were designed to have the same member sizes. Also, it is noticed that there was no correlation between the member sizes and the peak story drift ratios. Thus, in addition to the frame behavior under GM4, the behavior of the frames under GM 13 is also carefully inspected in the previous section of the study.

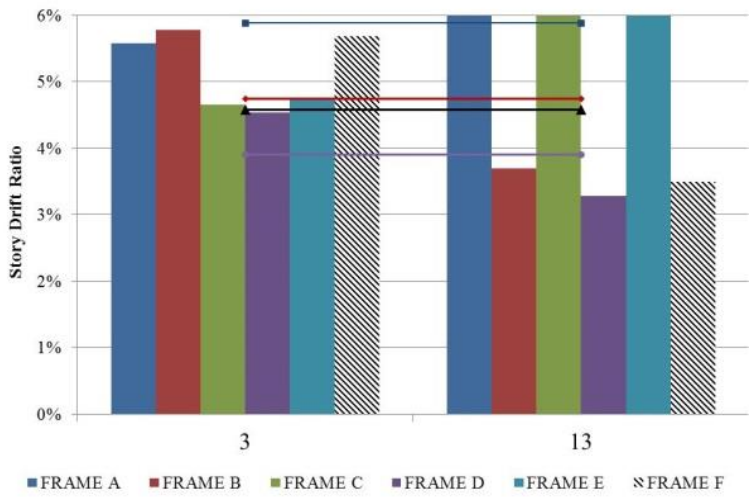

Figure 4.4. Peak story drift ratio responses of the frames under GMG III

As can be intrepreted from Fig. 4.5, similar behavior was observed in terms of the mean value of the peak story drift ratios when the frames subjected to the ground motions of GMG I. Data of Group II in Fig. 4.5 suggests that the responses of Frames A and E, which are the frames having the strongest and the weakest beams were similar and larger than that of the other three frames including Frame F. The mean value of the group III displays that Frames A and E experienced more severe inelastic deformations in terms of story drift ratio than Frames B, D and F.

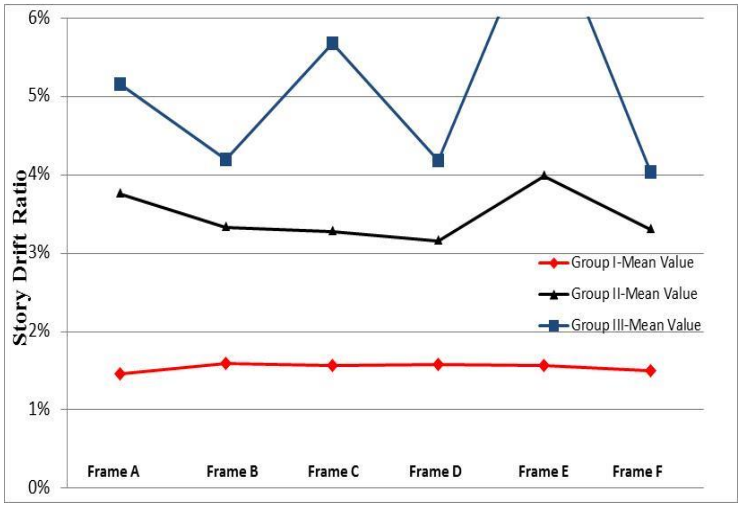

Figure 4.5. The mean responses of the frames subjected to GMGs

4.3 Seismic response of the frames in terms of brace ductility

The peak ductility response of the braces, which is the largest of the peak axial deformation in tension divided by the axial deformation corresponding to yielding and the peak axial deformation in compression divided by the deformation corresponding to buckling is presented in this section. Braces are the key components of a TSXBFs in terms of energy dissipation capacity, since the other structural members of TSXBFs (e.g. beams) are designed to remain elastic. It is generally accepted that the brace response can be associated with the overall response in terms of story drift ratio. In order to examine adequacy of this assumption, the ductility response of the braces are investigated. Fig. 4.6 shows the peak brace ductility response in the frames. As can be seen from the figure, the ductility response in the braces varies from 2.5 to over 25.

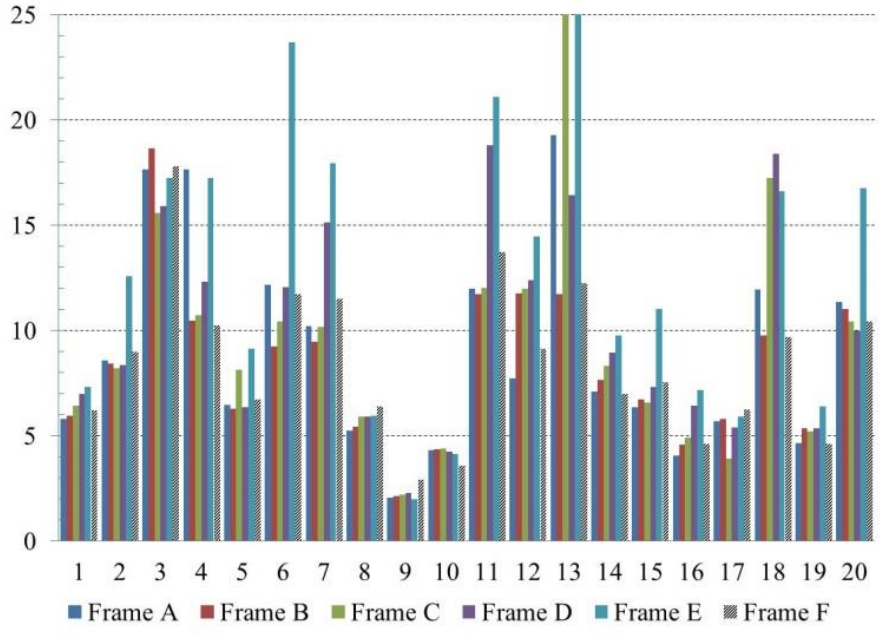

Figure 4.6. Peak brace ductility distribution of the frames under 20 GMs

Fig. 4.7 displays the peak brace ductilities in the frames responding to GMG I. The observations on the brace ductility can be summarized as follows:

- Overall, the difference between the frames in terms of brace ductility was substantially larger than the difference between the frames in terms of story drift ratio.
- It seems that the ductility response in Frame E, which is the frame with the weakest beams was higher than that in the other frames in general. Moreover, the largest brace ductility response obtained from Frame E under GM 15 while the peak story drift ratio responses of the frames were almost identical when the frames subjected to the same ground motion.
- The brace ductility responses in the frames responding to GMs 1, 8, 14, 15, 16 and 19 were consistent with their beam sizes. In other words, the demand on the braces increased as the brace-intersected beam sizes reduced.

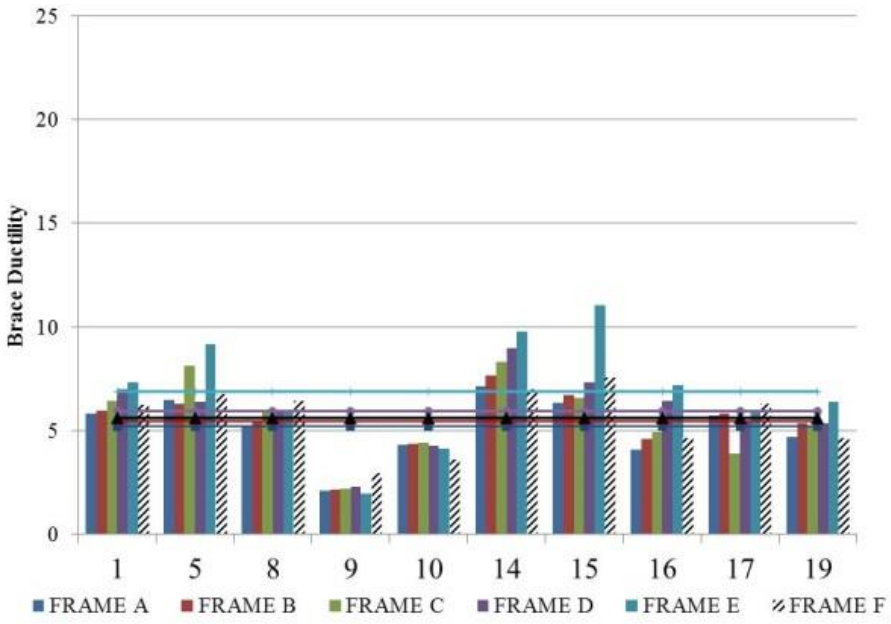

Figure 4.7. Peak brace ductility distribution of the frames under GMG I

Fig. 4.8 presents the peak brace ductility response in the frames responding to GMGII. The ductility response differed from 8 to 23 when the frames subjected to the ground motions of GMG II. The observations on the results can be summed up as follows:

- The demand on the braces varies significantly among the frames responding to the same ground motions. The mean value of (the horizontal lines in the figure) Frame E was about 50% larger than that of Frames A, B and F.
- In most cases, the peak responses in the frames with the strongest beams (Frames A and F) were close to each other.
- Comparing Figures 4.3 and 4.8 shows that there is a significant disagreement between the peak story drift ratio and the peak brace ductility values. For instance, the overall structural responses of all frames are essentially the same under GMs 2, 7 and 11, while the brace ductilities of Frames D and E were substantially larger than that of the other frames.

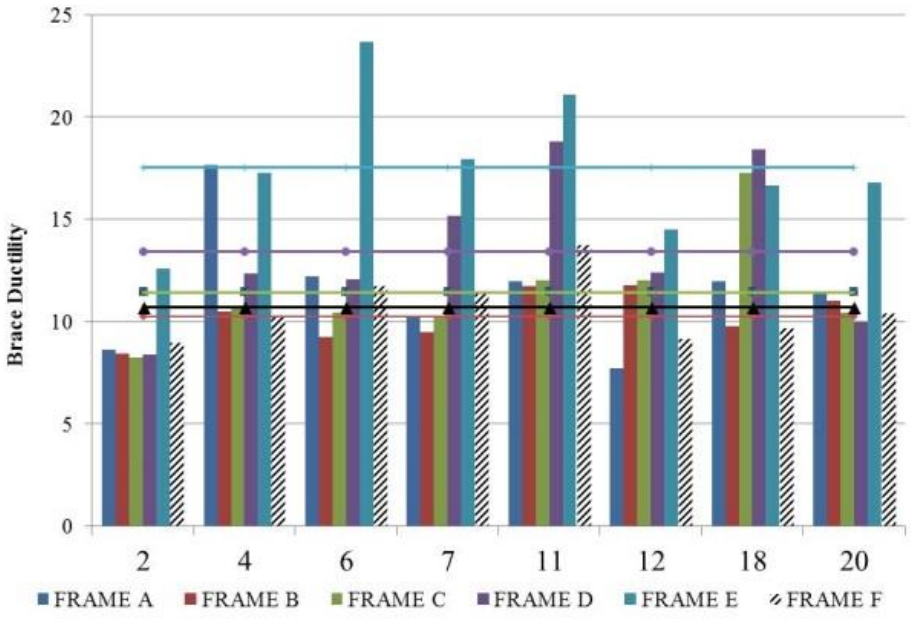

Figure 4.8. Peak brace ductility distribution of the frames under GMG II

Similar to the overall responses of the frames (Fig. 4.4), the brace ductility response in the frames responding to GM 13 was completely distinct from that in the frames responding to GM 3, as indicated in Fig 4.9. The brace ductility responses in Frame A through F were between 15 and 20 under GM 3. Furthermore, the brace ductility response of the frames follows the same trend as in the peak story drift ratio response when the frames subjected to GM 3. Unlike the response to GM 3, the brace ductility response of the frames under GM 13 was not in general agreement with the overall response in terms of story drift ratio.

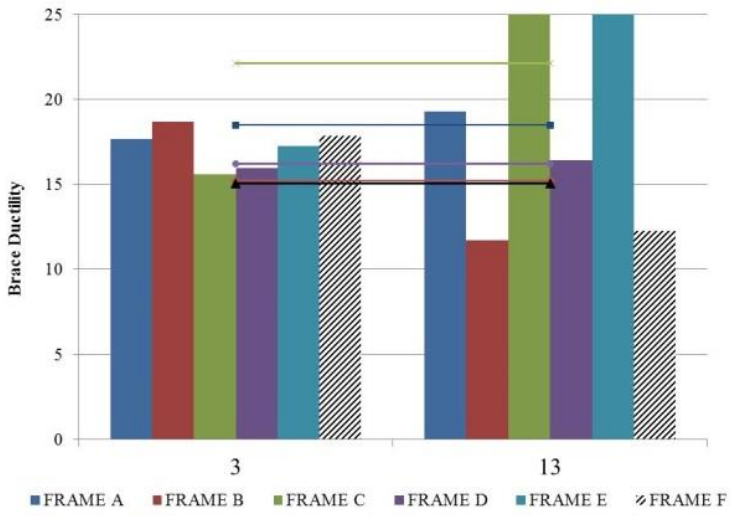

Figure 4.9. Peak brace ductility distribution of the frames under GMG III

According to Fig. 4.10, the demand on the braces tends to increase as the brace-intersected beam sizes reduce. It is recognized that the difference among the frame responses in terms of brace ductility demand is more substantial in the frames responding to GMG II than that in the frames responding to GMG I. It seems likely that the correlation between the ductility demand on braces and the beam sizes becomes more visible as the intensity of the demand increases. However, it is evident from the mean value of the frame responses to GMG III that the

relation between the beam sizes and the brace ductility might not be proportional to each other due to the complexity of the possible mechanisms in inelastic stage.

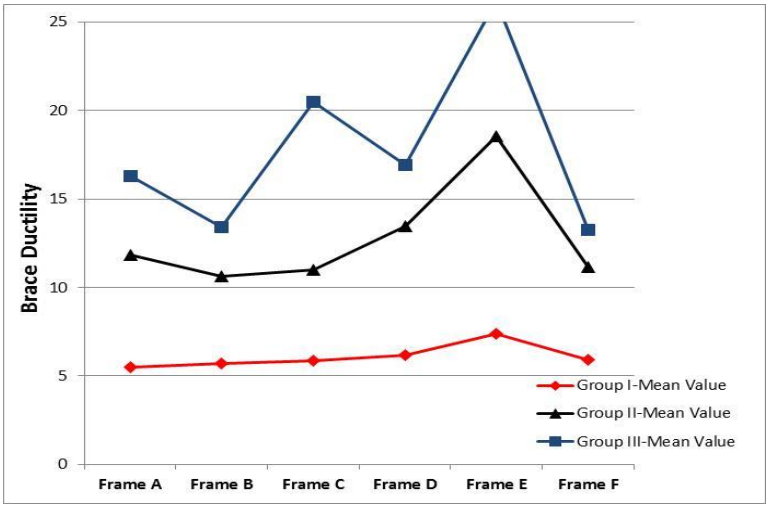

Figure 4.10. The mean responses of the frames subjected to GMGs

4.4 Seismic response of the frames in terms of beam ductility

Seismic response of the beams in terms of ductility response is summarized in Fig. 4.11. Since ductility accounts for the ratio between the maximum deformation and the yielding deformation, the beams with a ductility response of one or larger than one experienced vertical inelastic deformations during the earthquake ground motions. As detailed in Fig. 4.11, the beams did not remain elastic in some cases, which might be an explanation for the previously mentioned inconsistency between the brace ductility and story drift ratio responses. It should, however, be noted that according to AISC 341 (2010) [2] beams shall be designed to remain elastic.

The maximum vertical deflection within the beam span is divided by the yielding deformation of the beams to determine the ductility response on each beam. The yielding deformation is determined based on the plastic moment capacity, M_p, of each beam. The vertical

displacement acting on the brace intercepting point of the beam to produce M_p is found to be $\Delta_y=(F_yZ_x)L^2/(12EI_x)$, where F_y= nominal yield stress of steel, Z_x=plastic section modulus of the beam, I_x=moment of inertia of the beam about x-axis, L=span length of the beam and E is the elastic modulus of steel.

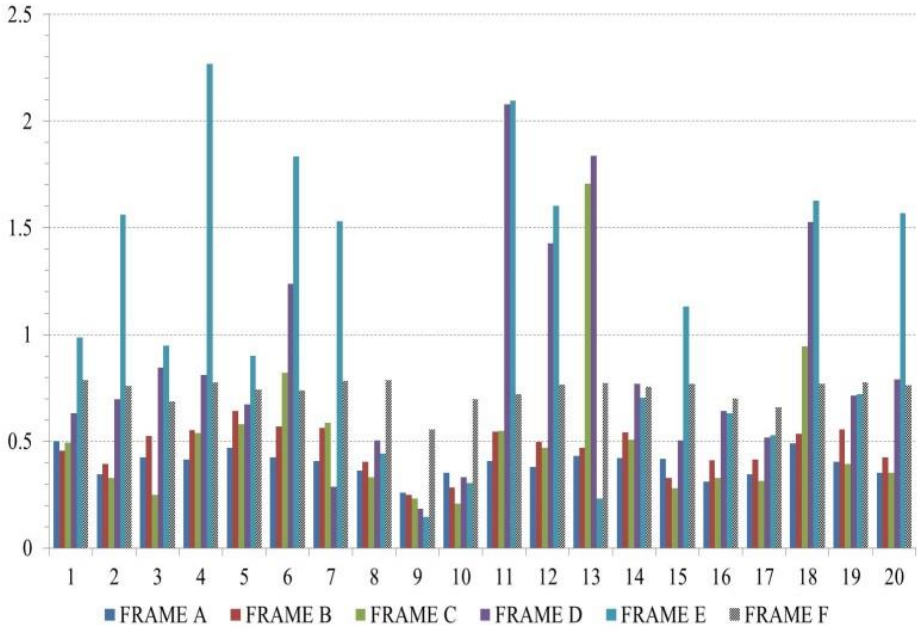

Figure 4.11. Peak beam ductility distribution of the frames under 20 GMs

As illustrated by Fig. 4.12, the peak ductility response of the brace-intersected beams was less than 1.0 in all frames except for Frame E under GM 15. It is believed that the largest brace ductility response obtained from Frame E might be due to yielding of the beam, since the peak story drift ratio values were virtually the same for all frames under GM 15. It is obvious that, in all ground motions of GMG I, there is a dramatic difference between Frames A and F in terms of beam deflections, which might be due to the brace configuration. The demand on the beams (unbalanced force imposed by the braces) of Frame A would have been mitigated by the braces above the brace-intersected beams when the inelastic response dominated by first mode shape.

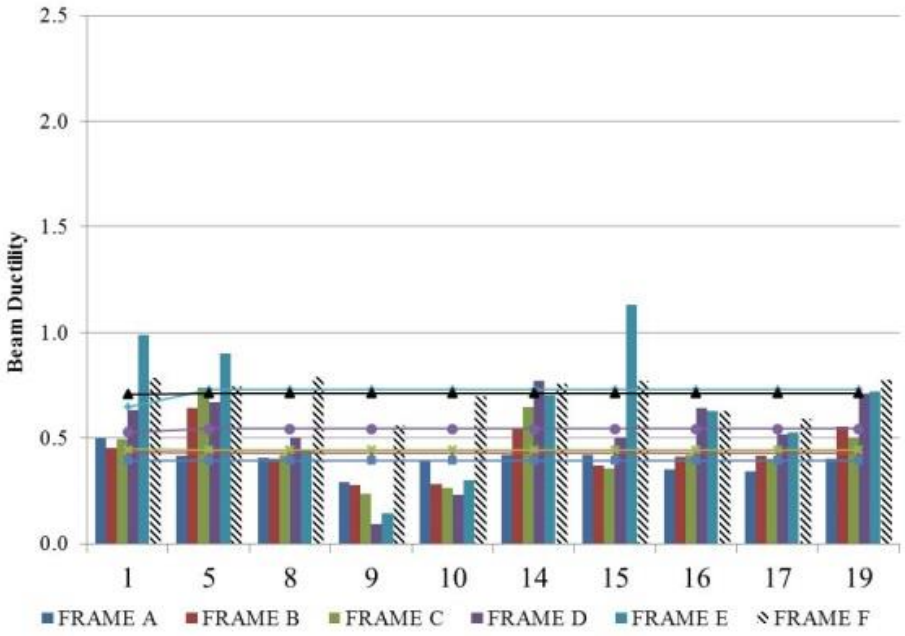

Figure 4.12. Peak beam ductility distribution of the frames under GMG I

It appears that the seismic demand on the brace-intersected beams of the frames responding to GMG II is considerably higher than than of the frames responding to GMG I. In most cases, the brace-intersected beams of the frames with weaker beams (Frames D and E) reached their capacities. Besides, the beam sizes and the seismic response of the beams are in an excellent agreement with each other. It is also noticed that the inelastic deformation of the brace-intersected beams intensifies the discrepancy between the story drift ratio and the brace ductility response of the frames responding to GMG II (Figs. 4.3 and 4.8).

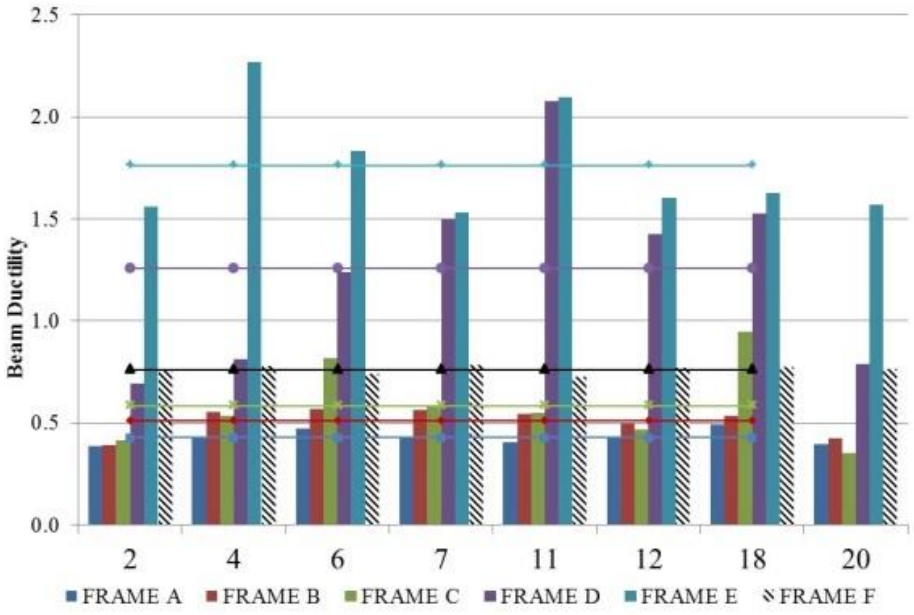

Figure 4.13. Peak beam ductility distribution of the frames under GMG II

Even though seismic response of the frames were severe when subjected to GM 3, the beam ductilities of all frames were under 1.0, which clarifies the consistency between the brace ductility and the story drift ratio values. Comparing Figs. 4.4, 4.9 and 4.14 indicates that the ductility response of the braces is not significantly affected by the vertical displacement of the brace-intersected beams, since the beams remained elastic during GM 3. As can be observed in Fig. 4.14, the beams of Frame E (the frame with the weakest beam) remained elastic under GM 13 while the beams of the frames with relatively heavier sizes (Frames C and D) exceeded the elastic limit.

Fig. 4.15 shows the mean beam responses of the frames. Apparently, the brace intersected beams of Frames A, B, C and F tend to remain elastic. However, the beams of frames with relatively weaker beams (Frames D and E) experienced inelastic deformations when subjected to GMG II. It is also observed that the trend in the beam responses to GMG II is

inverse proportional to beam sizes. It seems highly probable that the unbalanced force acting on the brace-intersected beams of Frame A must have been reduced by the braces above the beams, since the peak vertical beam deflection of Frame F was larger than that of Frame A in all cases.

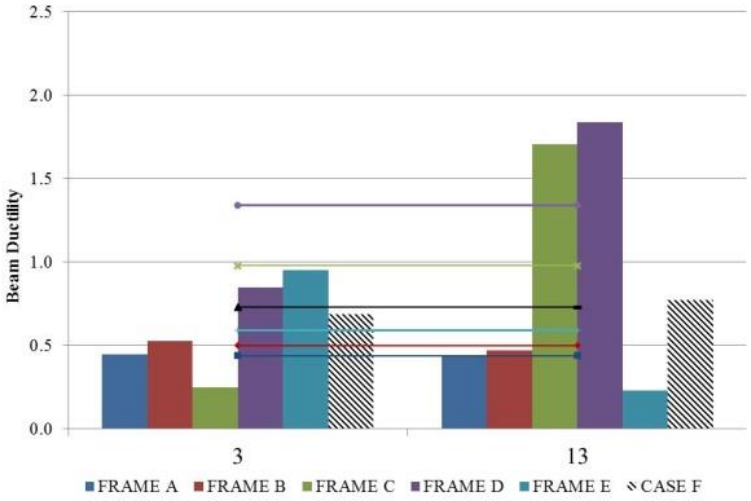

Figure 4.14. Peak beam ductility distribution of the frames under GMG III

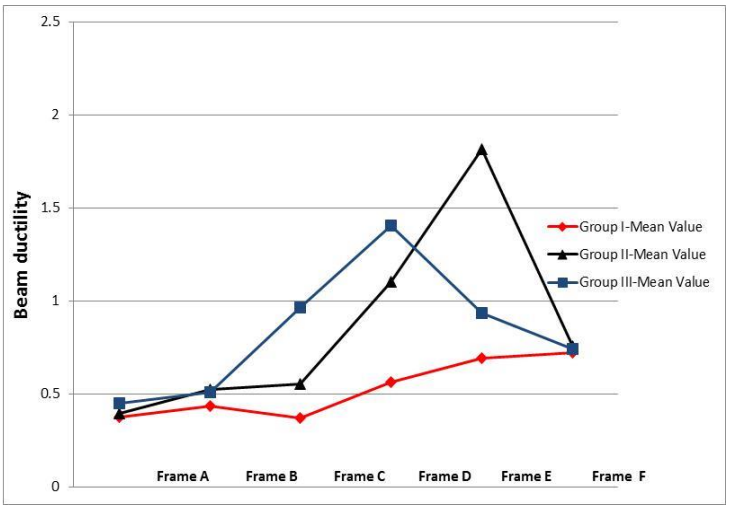

Figure 4.15. The mean responses of the brace-intersected beams subjected to GMGs

CHAPTER V

SUMMARY AND CONCLUSIONS

5.1 Introduction

A brief summary of the design and the non-linear time history analyses as well as the observations on the results is presented in this chapter. The conclusions based on the analyses results presented in Chapter III and IV are also discussed and the recommendations for future work is presented.

5.2 Summary

A total of hundred and twenty non-linear time history analyses have been carried out on five TSXBFs (Frame A through E) and one chevron braced frame (Frame F) which were designed based on the seismic design requirements for SCBFs stipulated in ASCE 7 (2010) [1] and AISC 341 (2010) [2]. The brace, beam and column sections were selected considering the strength, slenderness and compactness (width-to-thickness ratio) requirements specified in AISC 341 (2010) [2]. The brace-intersected beams of each TSXBF were designed based on the contribution of the V braces above in order to evaluate the beam responses as well as its influence on the performance of the other structural members in the seismic force resisting system. Thus, Frames A, B, C, D and E were designed considering 0%, 25%, 50%, 75% and 100% of the expected strength of the V braces above the brace-intersected beams, respectively. The frame with inverted V type bracing configuration (Frame F) was designed to make a solid comparison between the seismic behavior of the TSXBFs and the inverted V-braced frame.

Finite element modeling of the frames have been performed using two dimensional inelastic dynamic analysis program RUAMOKO 2D [15]. Since it is crucial to simulate hysteretic behavior of bracing members properly for an accurate frame modeling, two steel

column specimens tested by other researchers [5, 16] were simulated and satisfactory results obtained. 10 pairs of ground motions based on the design spectrum were selected using PEER Ground Motion Database [18]. The twenty ground motions divided into three groups based on the story drift responses of the frames and the analyses results were presented based on the ground motion groups. Then, seismic response of Frames A and F under GMs 4, 11 and 13 were presented in detail so as to elaborate on the unexpected frame responses to GMs 4 and 13. Finally, seismic responses of the frames were evaluated and discussed in terms of story drift ratio, brace ductility and beam ductility.

5.3 Conclusions and Recommendations

A study on seismic response of the brace-intersected beams in TSXBFs and its impact on the overall response is presented. Considering the analyses results and observations on the numerical study, the following conclusions can be drawn:

(1) Brace-intersected beams in TSXBFs designed with the current seismic design provisions (Frame E) would undergo significant vertical inelastic deformation when the frames experience expected story drift ratio.

(2) The vertical inelastic deformation of the beam results in a substantial increase in ductility demand on the braces, and such increase cannot be detected by using story drift response alone.

(3) Higher beam strengths (used in frames A, B, C and D) beyond the minimum required by the design provisions tend to reduce the brace ductility demands with moderately increased beam sizes, which indicates that there exists a range of optimal beam design

strength to achieve much enhanced seismic performance with moderately increased beam sizes.

(4) Ductility demand on the braces might increase significantly when the vertical inelastic deformation at the brace-intercepting point of the beam takes place.

(5) Using story drift response alone for seismic performance evaluation of TSXBFs would underestimate the demand on braces, which are prone to fracture when yielding of the brace-intersected beams in TSXBFs occurs.

(6) Yielding of the brace-intersected beams lead the beams to deform vertically within their spans, which would result in much more complicated deformation patterns than the first-mode mechanism anticipated by AISC.

(7) Based on the detailed investigation of Frames A and F, hysteretic behavior of braces during an earthquake excitation and the interaction between the internal forces, which produces the unbalanced forces acting on the brace-intersected beams might be more complicated than the simplified brace model specified by AISC for the design of girders and columns.

(8) In some cases, it is observed that columns reached their capacities.

(9) It is found that even mid-rise frames studied in this work were affected by higher modes. Future work should therefore aim to investigate the impact of the beam responses on brace ductility response as well as overall seismic response of high-rise TSXBFs.

(10) Even though the results presented in this study are encouraging, further work is needed to propose a design recommendation for TSXBFs.

REFERENCES

1. ASCE 7. Minimum Design Loads for Buildings and Other Structures, ASCE 7-10. Virginia: American Society of Civil Engineers; 2010.
2. American Institute of Steel Construction (AISC). Seismic provisions for structural steel buildings (ANSI/AISC 341-10), Chicago; 2010.
3. AISC. Seismic Design Manual. 2nd ed. Chicago, U.S.A.: American Institute of Steel Construction, Inc.; 2012
4. Jay Shen, Rou Wen, Bulent Akbas, Bilge Doran, Eren Uckan, "Seismic demand on brace-intersected beams in two-story X-braced frames." Engineering Structures 76 (2014) 295–312.
5. Fell BV, Kanvinde AM, Deierlein GG, Myers AT., "Experimental investigation of inelastic cyclic buckling and fracture of steel braces." J. Struct. Eng. (2009) ;135:19–32.
6. Tremblay, R., "Inelastic Seismic Response of Steel Bracing Members," Journal of Constructional Steel Research, Vol. 58, No. 5-8, 2002, pp. 665-701.
7. Tremblay, R., "Influence of Brace Slenderness on the Fracture Life of Rectangular Tubular Steel Bracing Members Subjected to Seismic Inelastic Loading," Proceedings of ASCE Structures Congress, Vancouver, 2008.
8. Uriz P., Mahin S.A., Toward Earthquake-Resistant Design of Concentrically Braced Steel-Frame Structures .PEER 2008/08.November 2008.
9. Astaneh ASL A. Seismic behavior and design gusset plates. Steel Tips. 1998.
10. Stoakes S.D., Fahnestock L. A., Cyclic flexural analysis and behavior of beam-column connections with gusset plates. Journal of Constructional Steel Research 72 (2012) 227–239.
11. Yoo H.J., Roeder C. W., Lehman D.E. Simulated behavior of multi-story X-braced frames. Engineering Structures 31 (2009) 182_197.
12. Hsiao P., Lehman D.E., Roeder C.W. Improved analytical model for special concentrically braced frames. Journal of Constructional Steel Research 73 (2012) 80–94.
13. Black, R. Gary; Wenger, W. A.; Popov, Egor P. Inelastic buckling of steel struts under cyclic load reversals, rep no. UCB/EERC-80/40. Dept. of Civil Engineering, University of California, Berkeley, California; 1988.
14. Khatib I, Mahin SA, Karl SP. Seismic behavior of concentrically braced steel frames, rep no. UCB/EERC 88-01. Dept. of Civil Engineering, University of California, Berkeley, California; 1988.
15. Carr AJ. RUAUMOKO manual, vols. 1 and 2. Christchurch, New Zealand: University of Canterbury; 2004.
16. Nip K.V, Gardner L.V., Elghazouli A.Y. Cyclic testing and numerical modeling of carbon steel and stainless steel tubular bracing members. Engineering Structures 32 (2010) 424_441.
17. AISC 360-10. Seismic design manual, 2nd ed. American Institute of Steel Construction Inc., Chicago; 2010.
18. PEER. Peer.berkeley.edu/peer_ground_motion_database. Pacific Earthquake Engineering Research Center, 325 Davis Hall, University of California, Berkeley, CA 94720.
19. Hsiao P-C, Yoo, Lehman DE, Roeder CW. Evaluation of the response modification coefficient and collapse potential of special concentrically braced frames. Earthq. Eng. Struct. Dynam. 2013;42:1547–64.

APPENDIX A. ACCELARATION TIMES HISTORIES OF THE GROUND MOTIONS

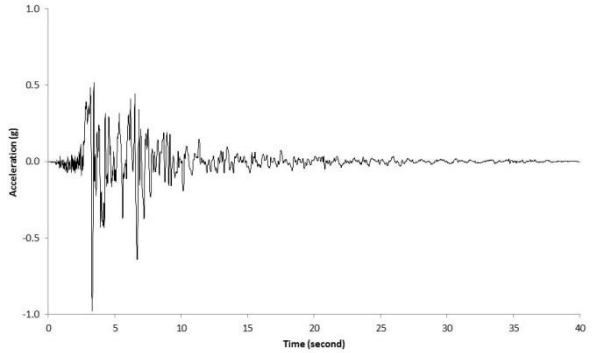

Fig. A1. Acceleration time history of GM1

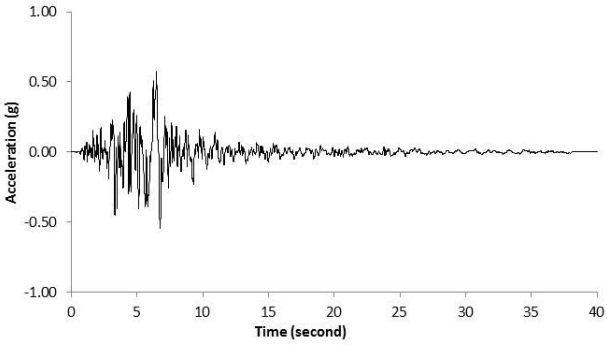

Fig. A2. Acceleration time history of GM2

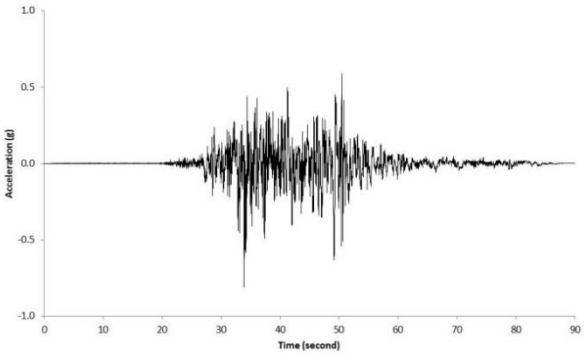

Fig. A3. Acceleration time history of GM3

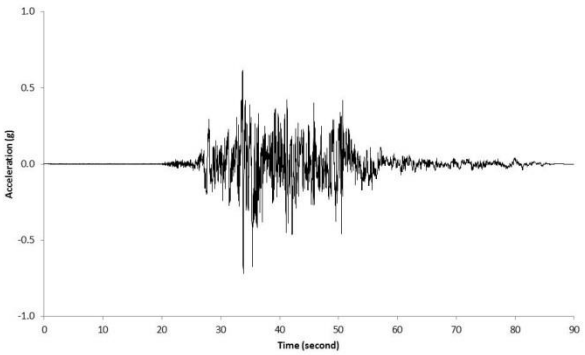

Fig. A4. Acceleration time history of GM4

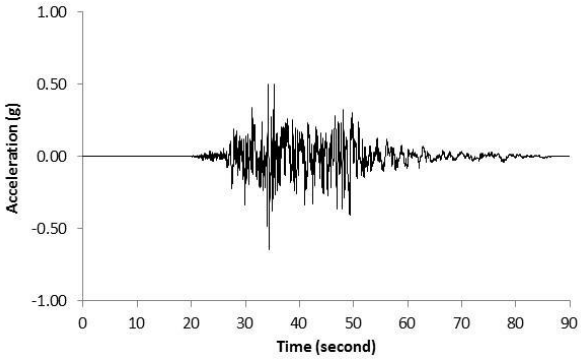

Fig. A5. Acceleration time history of GM5

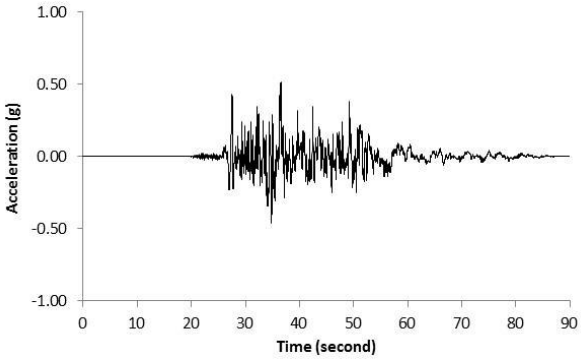

Fig. A6. Acceleration time history of GM6

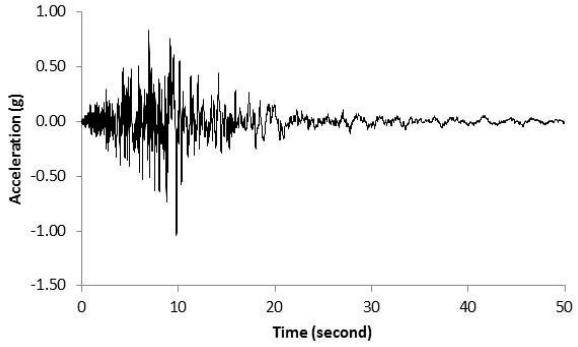

Fig. A7. Acceleration time history of GM7

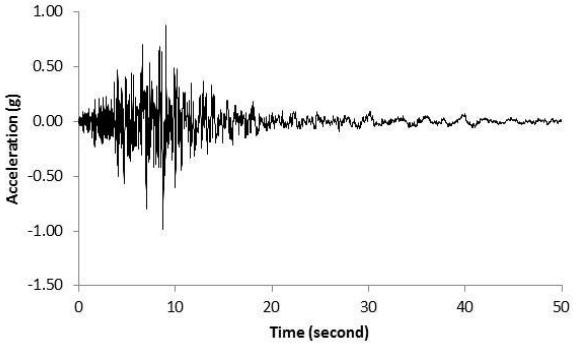

Fig. A8. Acceleration time history of GM8

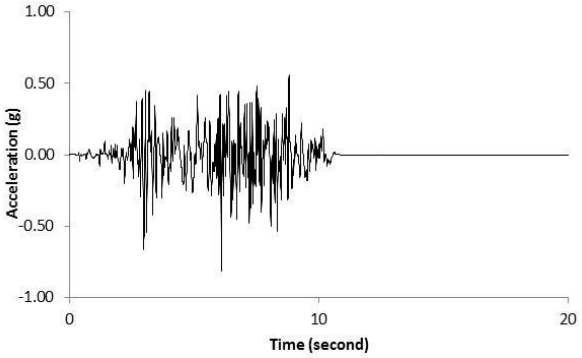

Fig. A9. Acceleration time history of GM9

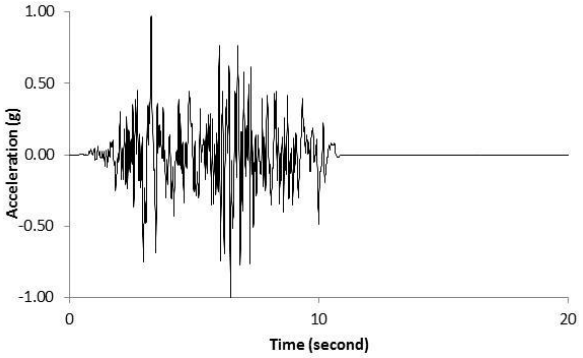

Fig. A10. Acceleration time history of GM10

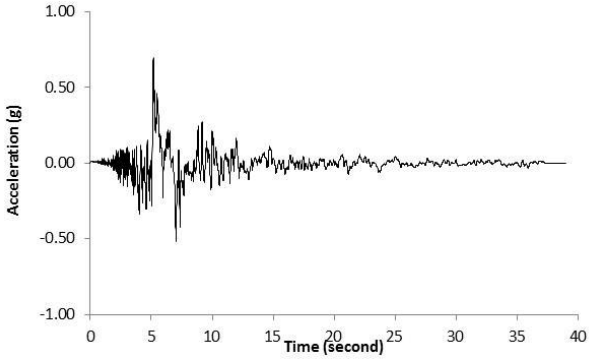

Fig. A11. Acceleration time history of GM11

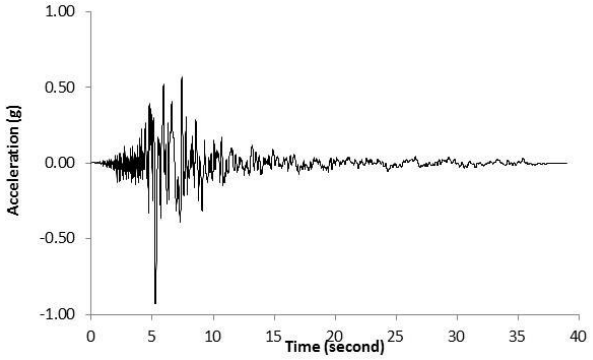

Fig. A12. Acceleration time history of GM12

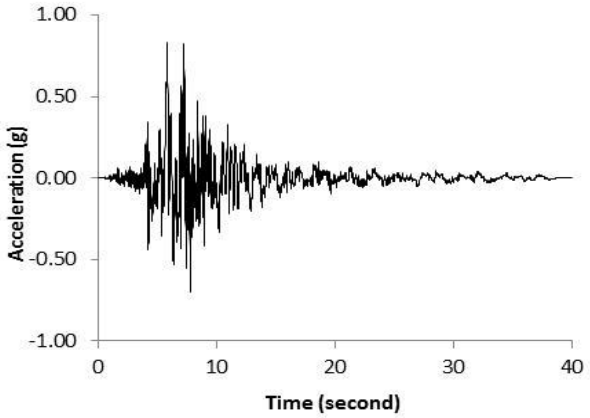

Fig. A13. Acceleration time history of GM13

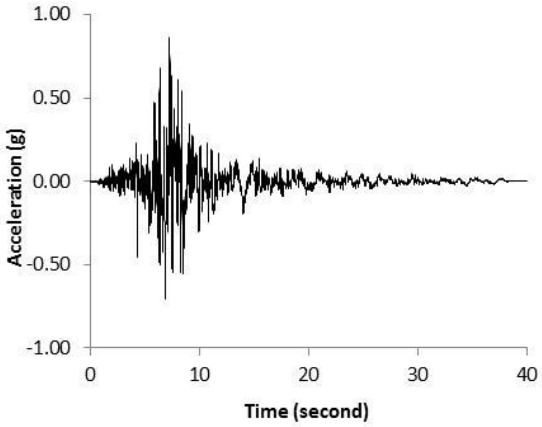

Fig. A14. Acceleration time history of GM14

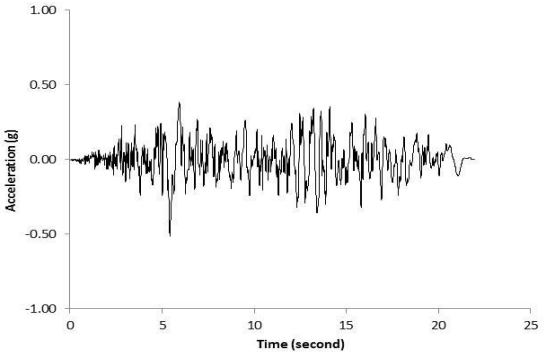

Fig. A15. Acceleration time history of GM15

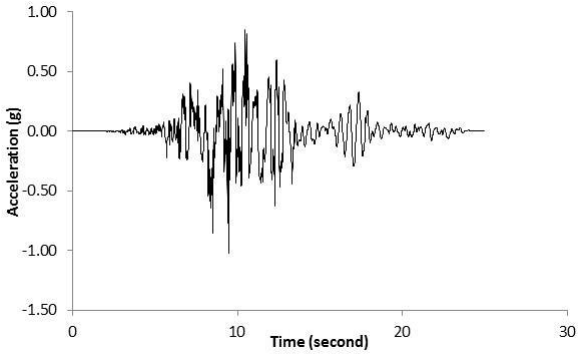

Fig. A16. Acceleration time history of GM16

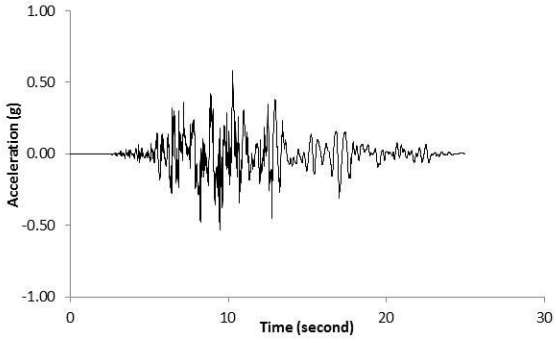

Fig. A17. Acceleration time history of GM17

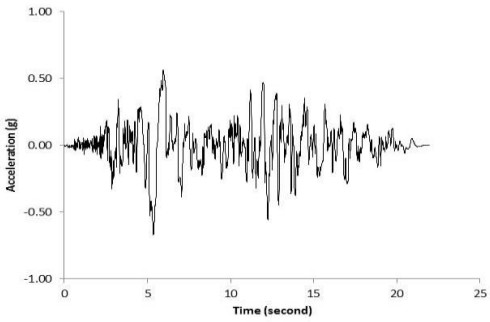

Fig. A18. Acceleration time history of GM18

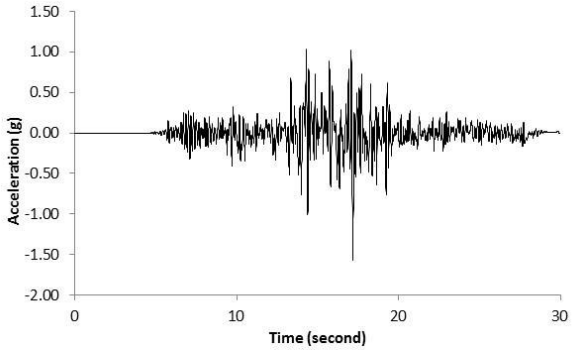

Fig. A19. Acceleration time history of GM19

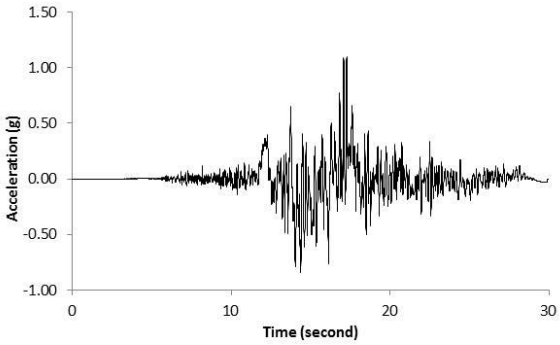

Fig. A20. Acceleration time history of GM20

APPENDIX B. TIME HISTORY OF FRAME RESPONSES TO SELECTED GMs

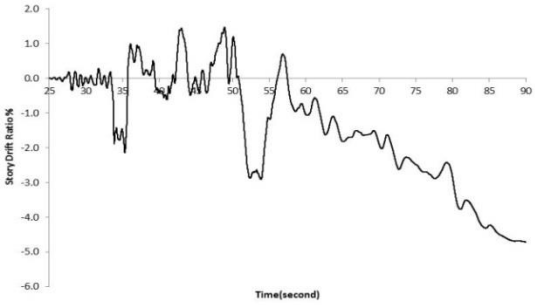

(a) 2nd story

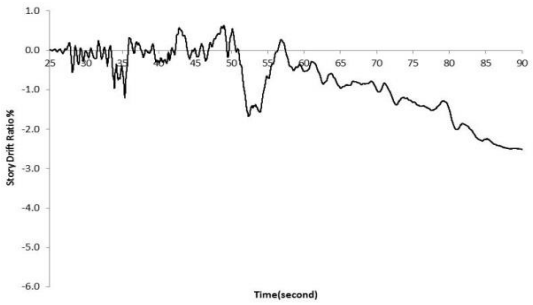

(b) 3rd story

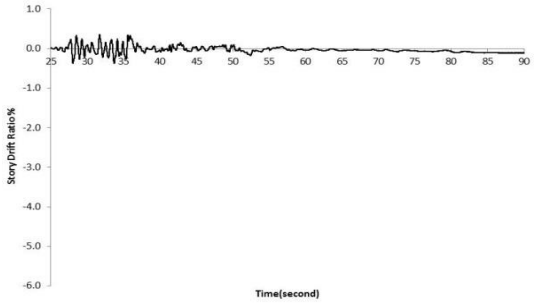

(c) 4th story

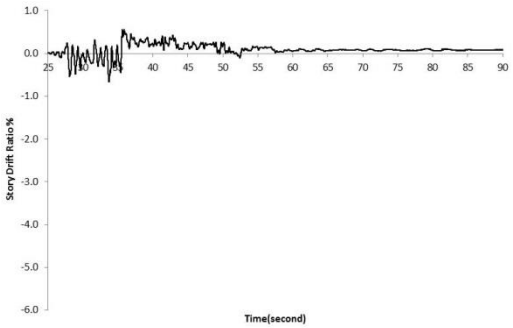

(d) 5th story

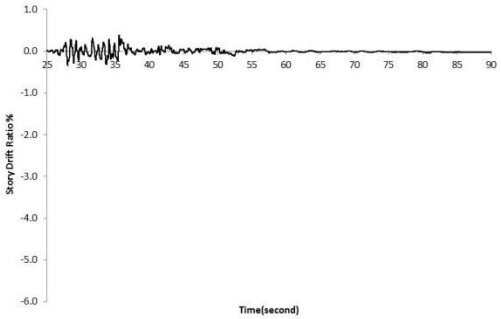

(c) 6th story

Fig. B1. Story drift ratio time history of Frame A under GM4.

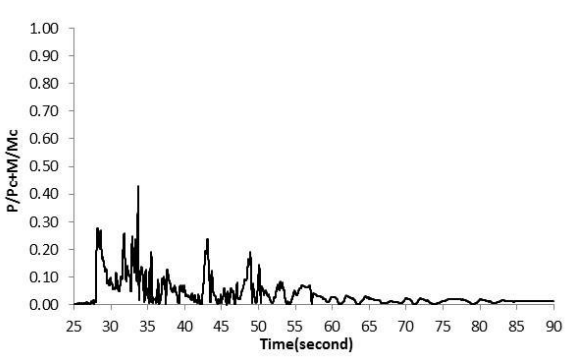

(a) 1st story

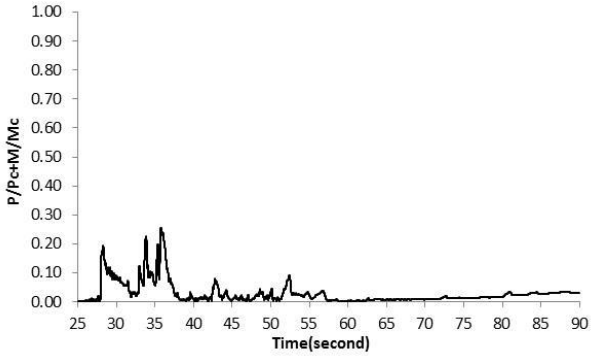

(b) 2nd story

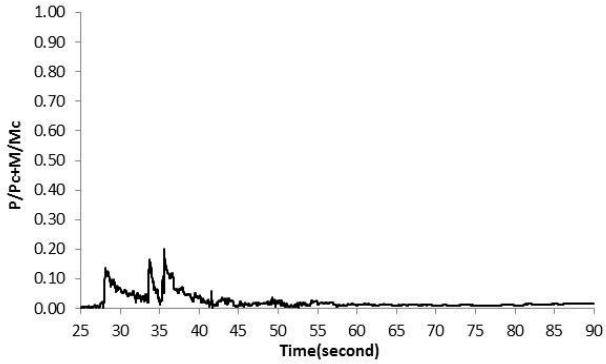

(c) 3rd story

Fig. B2. Combined strength ratio time history of brace-intersected beams of Frame A under GM4

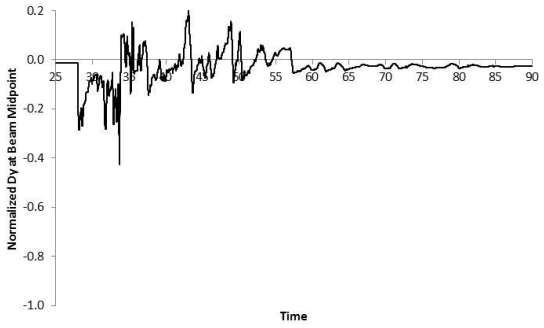

(a) 1st story

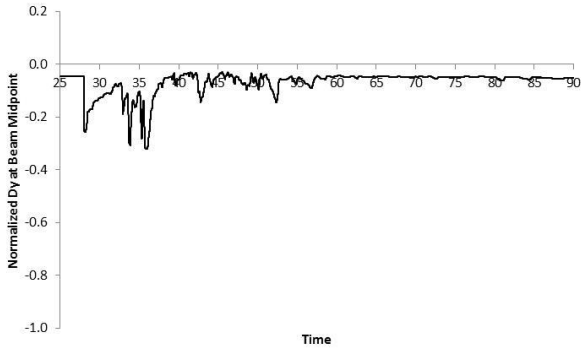

(b) 3rd story

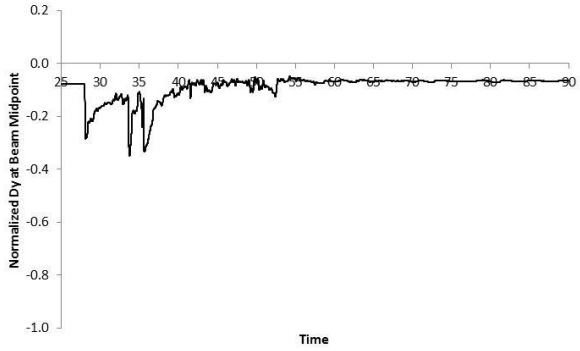

(c) 5th story

Fig. B3. Beam ductility history of brace-intersected beams of Frame A under GM4

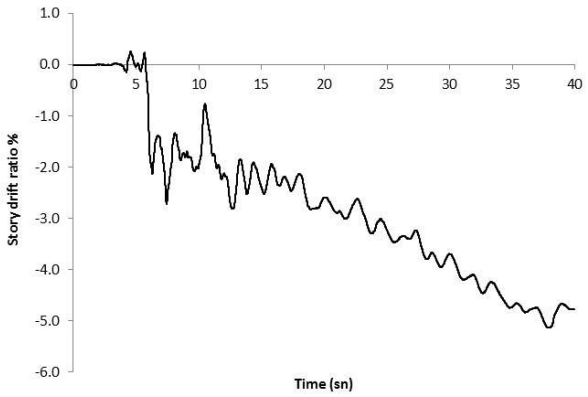

(a) 2nd story

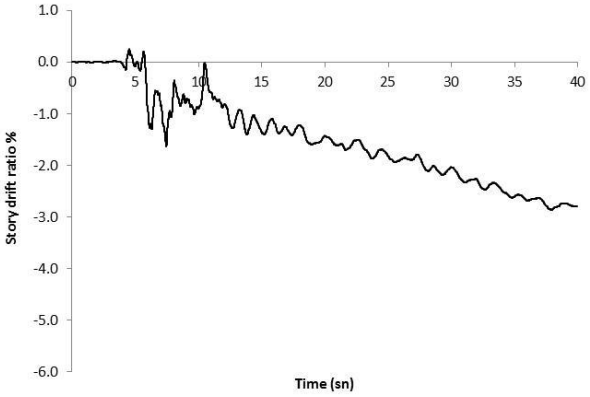

(b) 3rd story

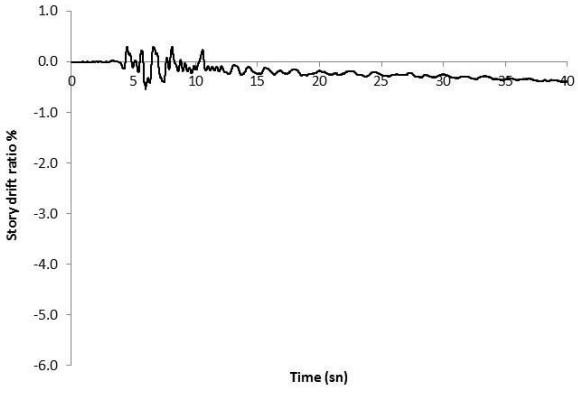

(c) 4th story

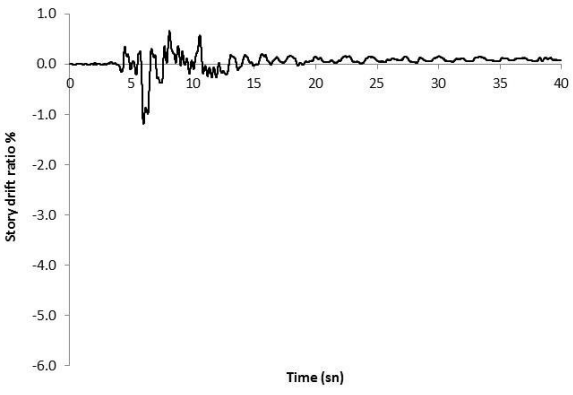

(d) 5th story

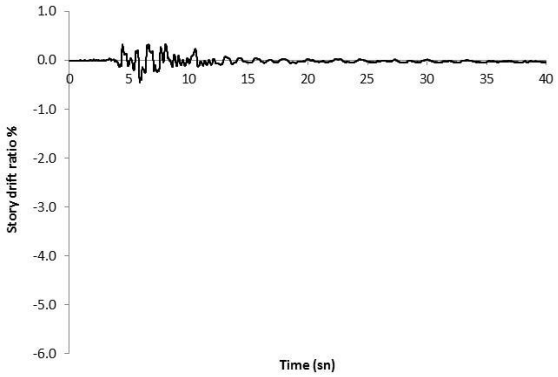

(c) 6th story

Fig. B4. Story drift ratio time history of Frame A under GM13.

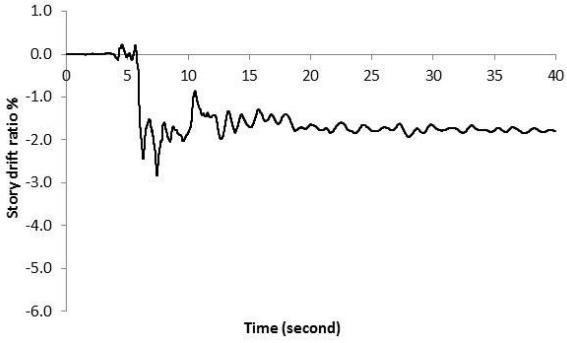

(a) 2nd story

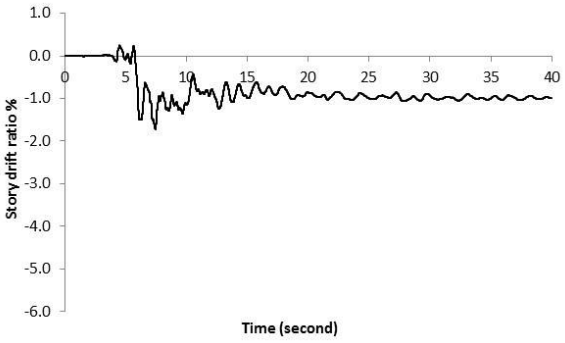

(b) 3rd story

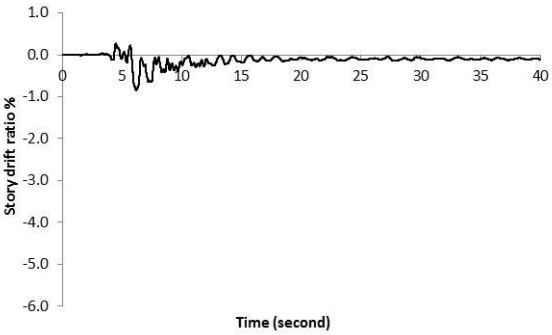

(c) 4th story

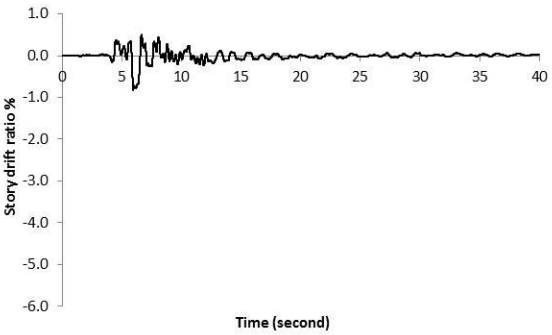

(d) 5th story

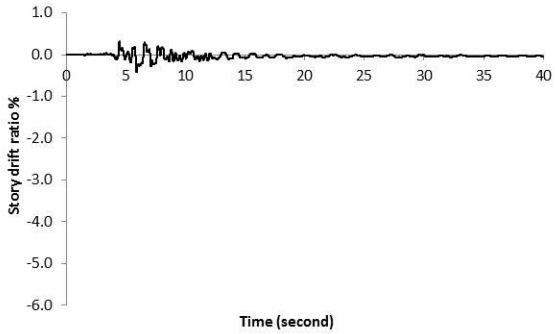

(c) 6th story

Fig. B5. Story drift ratio time history of Frame F under GM13.

APPENDIX C. PEAK FRAME RESPONSES TO THE GROUND MOTIONS

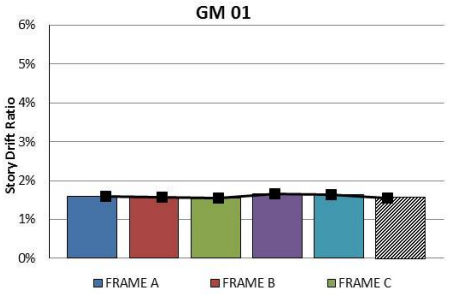

(a) Story drift ratio

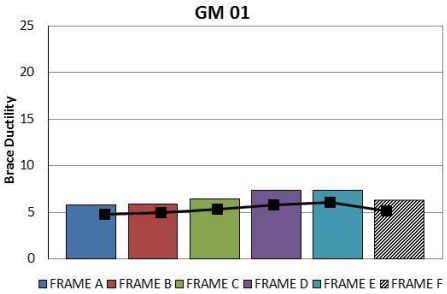

(b)Brace ductility

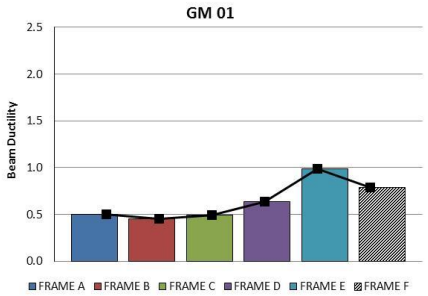

(c) Combined strength ratio

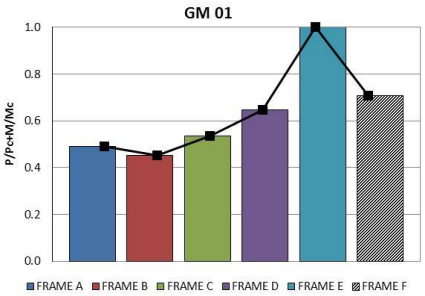

(d)Beam ductility

Fig. C1. Frame responses under GM01

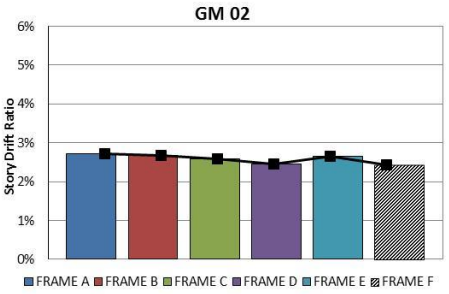

(a) Story drift ratio

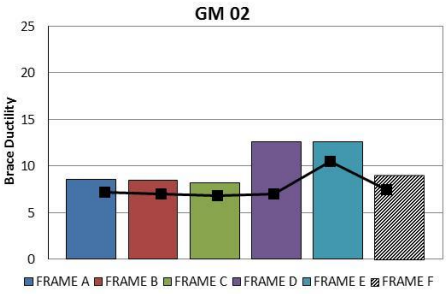

(b)Brace ductility

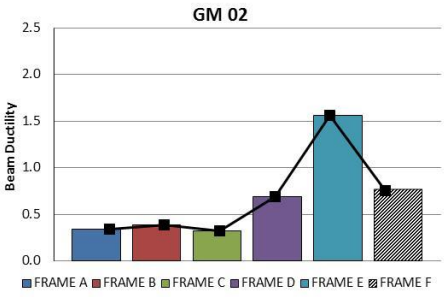

(c) Combined strength ratio

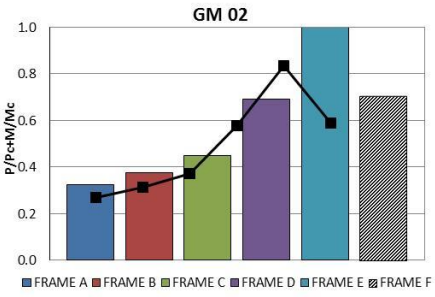

(d)Beam ductility

Fig. C2. Frame responses under GM02

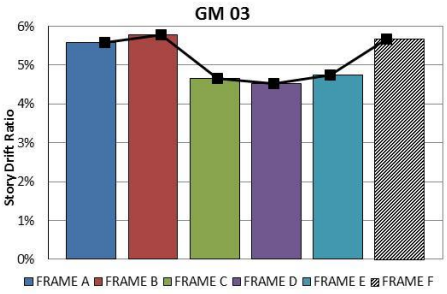

(a) Story drift ratio

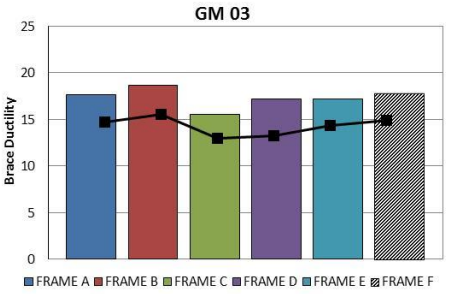

(b)Brace ductility

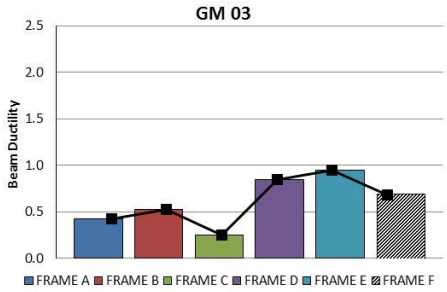

(c) Combined strength ratio

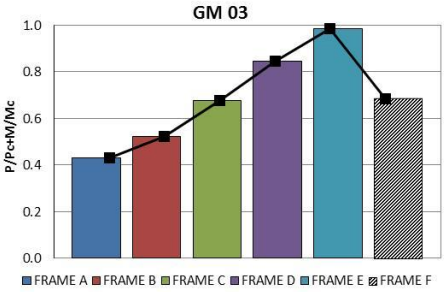

(d)Beam ductility

Fig. C3. Frame responses under GM03

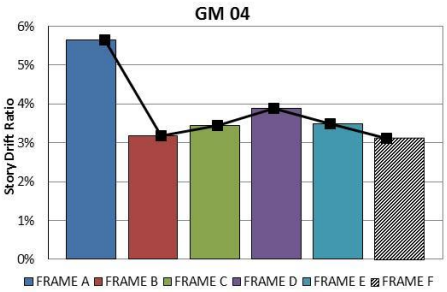

(a) Story drift ratio

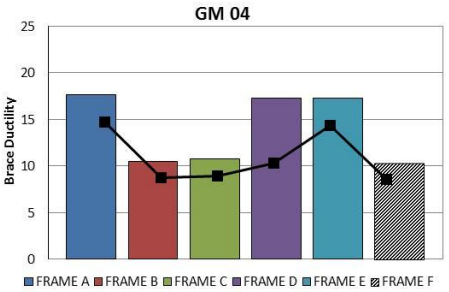

(b)Brace ductility

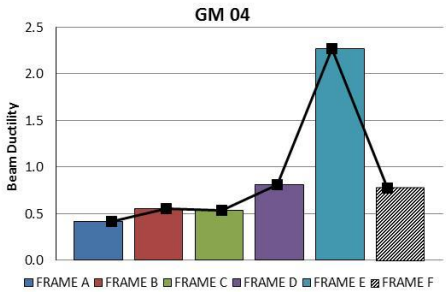

(c) Combined strength ratio

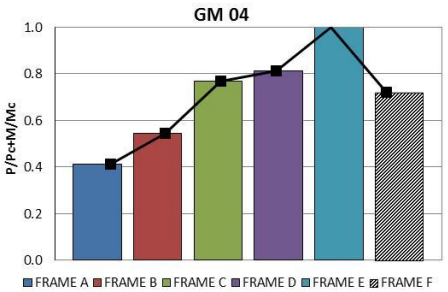

(d)Beam ductility

Fig. C4. Frame responses under GM04

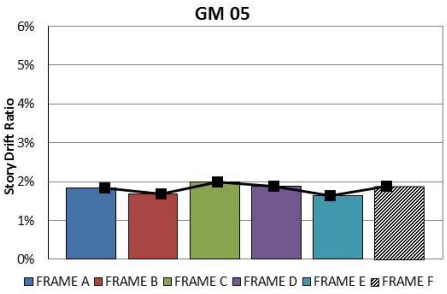

(a) Story drift ratio

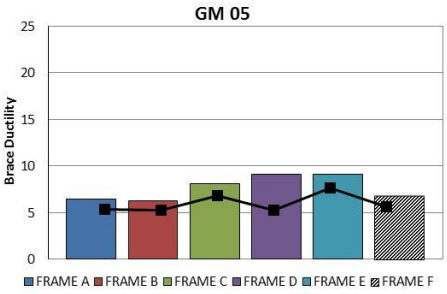

(b)Brace ductility

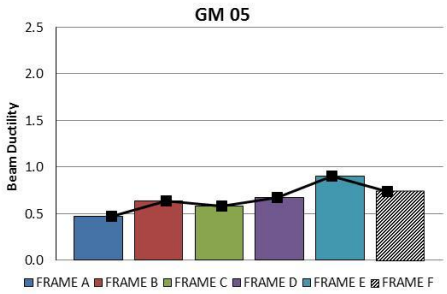

(c) Combined strength ratio

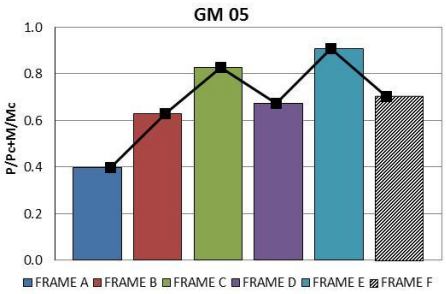

(d)Beam ductility

Fig. C5. Frame responses under GM05

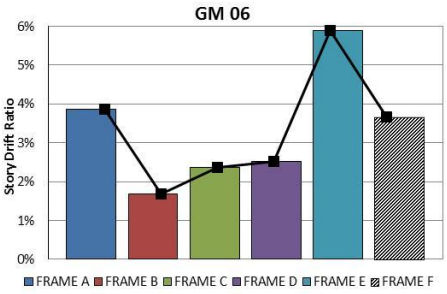

(a) Story drift ratio

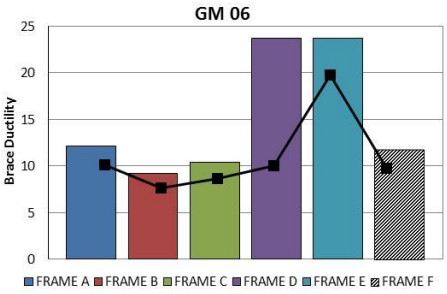

(b)Brace ductility

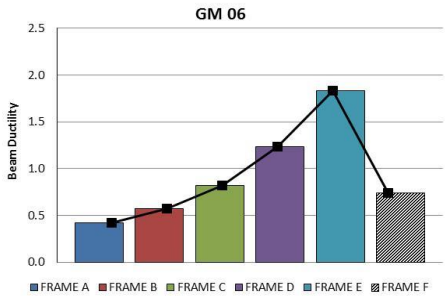

(c) Combined strength ratio

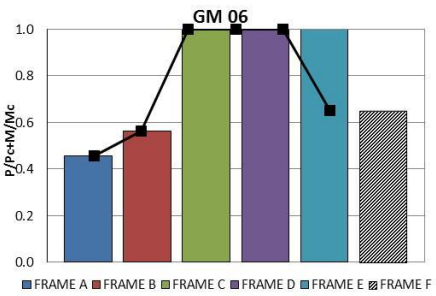

(d)Beam ductility

Fig. C6. Frame responses under GM06

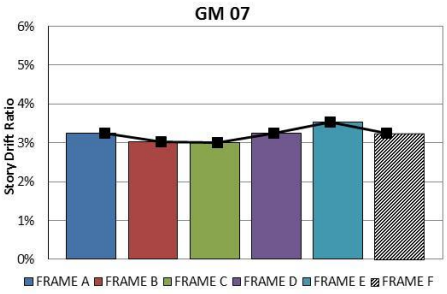

(a) Story drift ratio

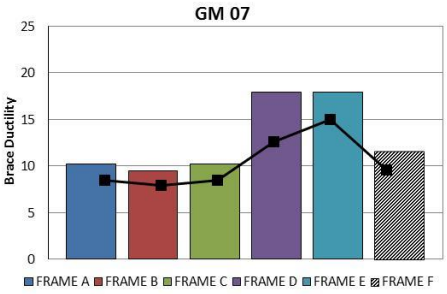

(b)Brace ductility

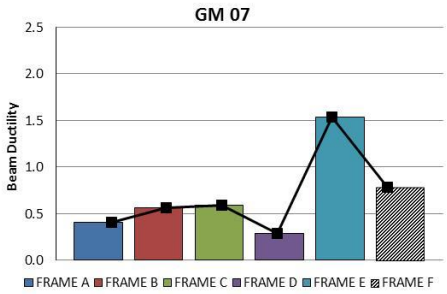

(c) Combined strength ratio

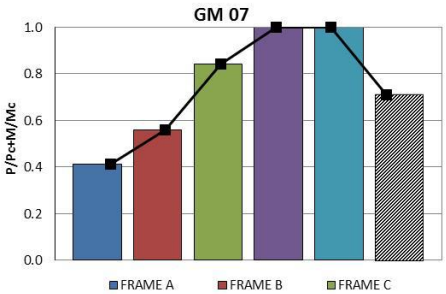

(d)Beam ductility

Fig. C7. Frame responses under GM07

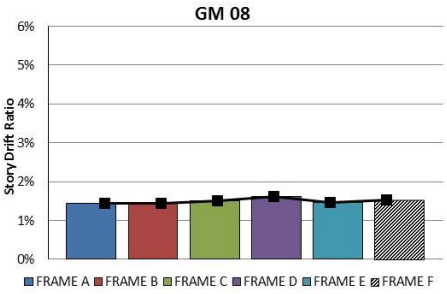

(a) Story drift ratio

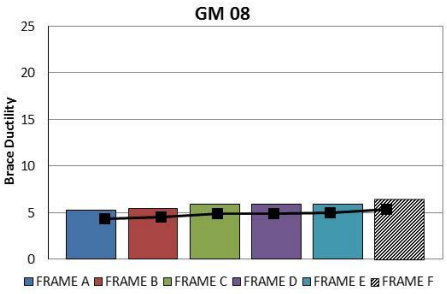

(b)Brace ductility

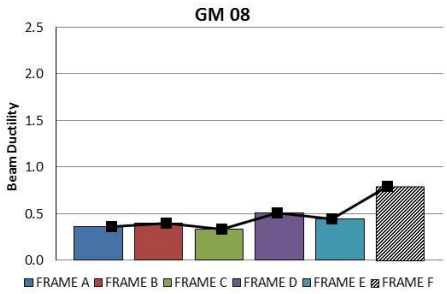

(c) Combined strength ratio

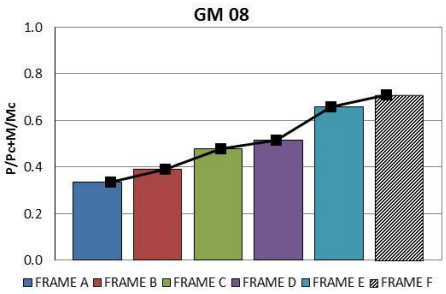

(d)Beam ductility

Fig. C8. Frame responses under GM08

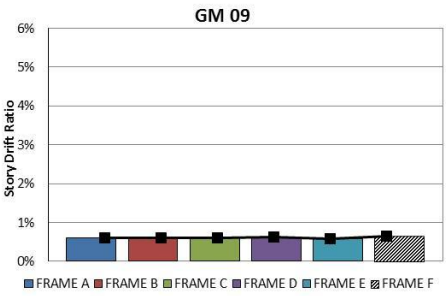

(a) Story drift ratio

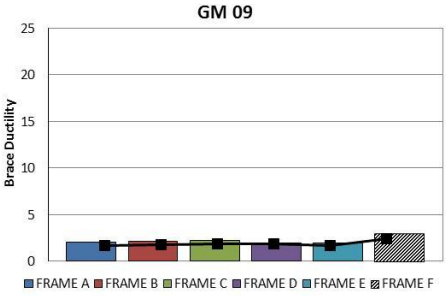

(b)Brace ductility

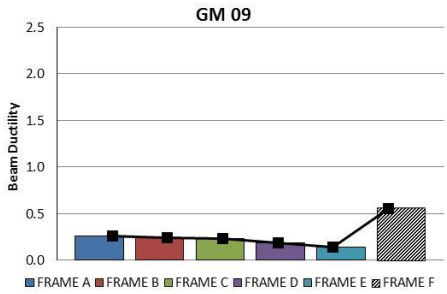

(c) Combined strength ratio

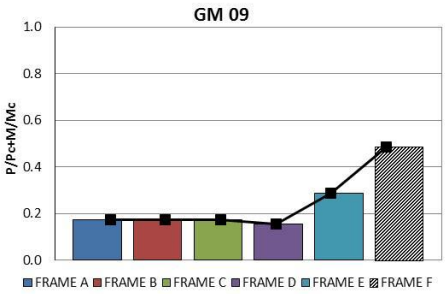

(d)Beam ductility

Fig. C9. Frame responses under GM09

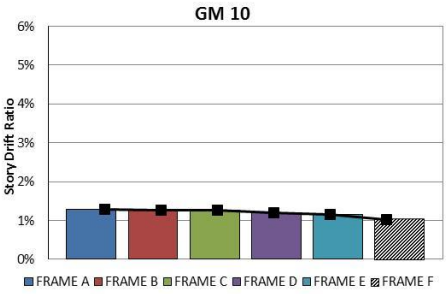

(a) Story drift ratio

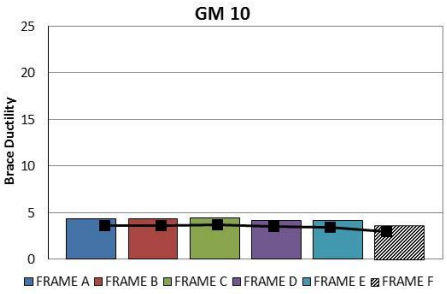

(b)Brace ductility

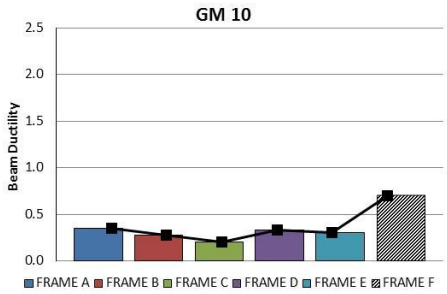

(c) Combined strength ratio

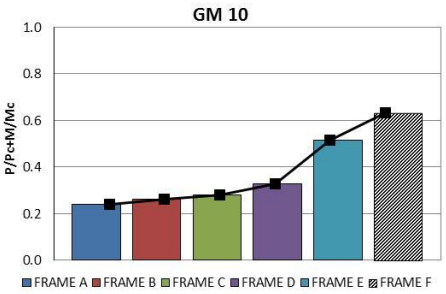

(d)Beam ductility

Fig. C10. Frame responses under GM10

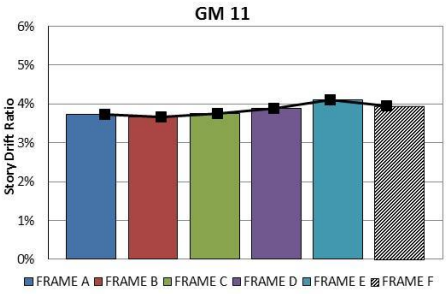

(a) Story drift ratio

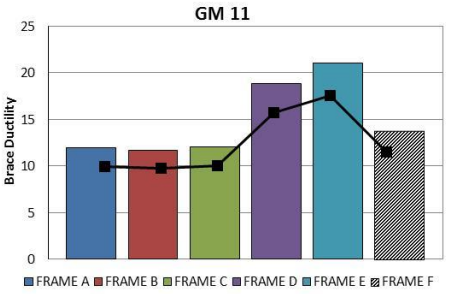

(b)Brace ductility

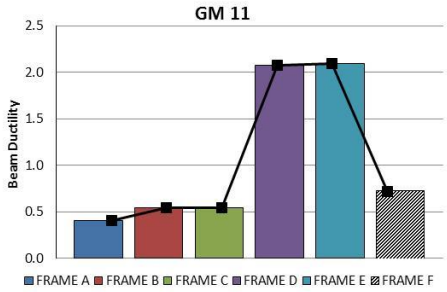

(c) Combined strength ratio

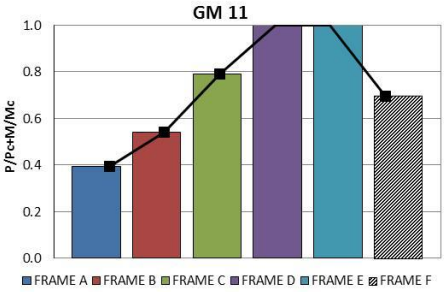

(d)Beam ductility

Fig. C11. Frame responses under GM11

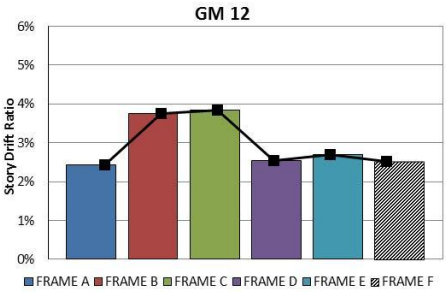

(a) Story drift ratio

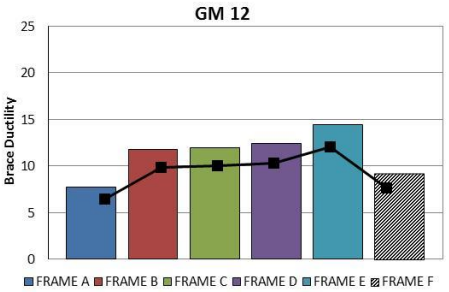

(b)Brace ductility

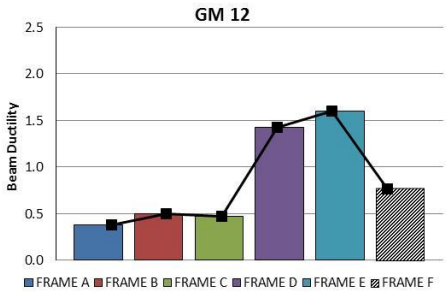

(c) Combined strength ratio

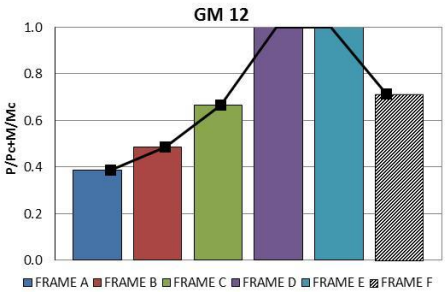

(d)Beam ductility

Fig. C12. Frame responses under GM12

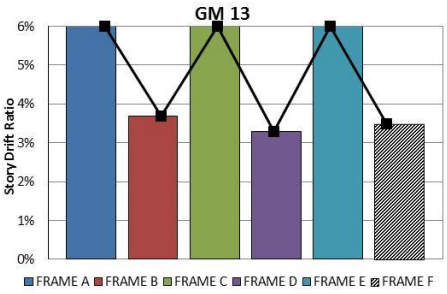

(a) Story drift ratio

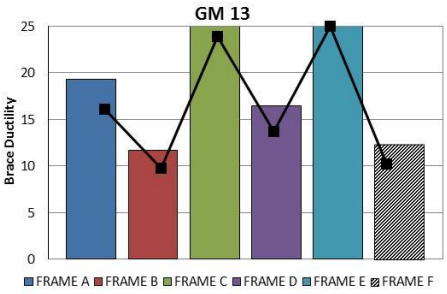

(b)Brace ductility

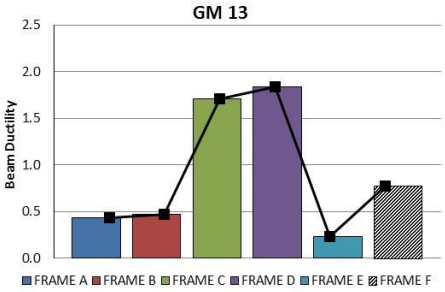

(c) Combined strength ratio

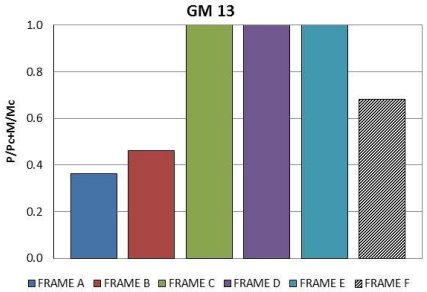

(d)Beam ductility

Fig. C13. Frame responses under GM13

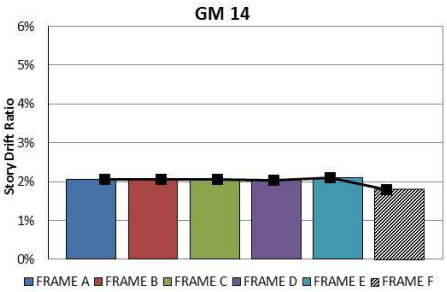

(a) Story drift ratio

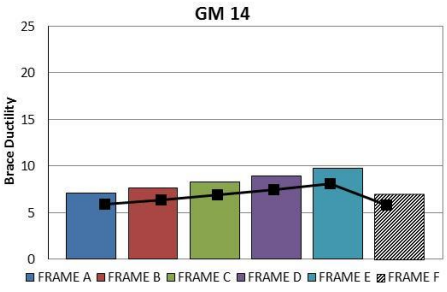

(b)Brace ductility

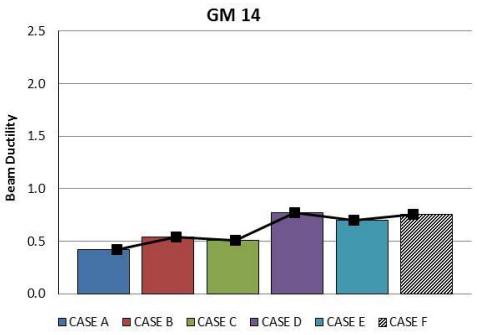

(c) Combined strength ratio

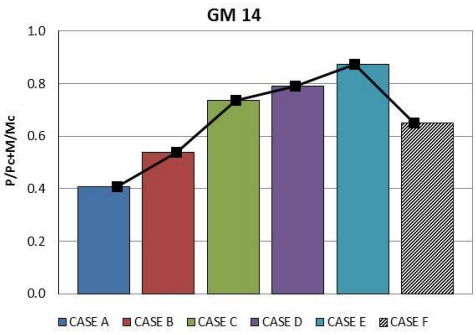

(d)Beam ductility

Fig. C14. Frame responses under GM14

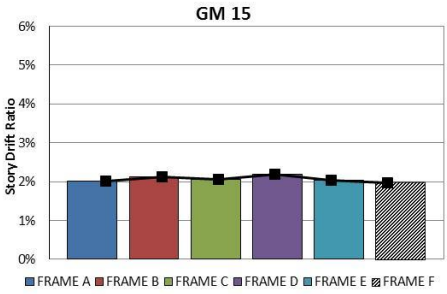

(a) Story drift ratio

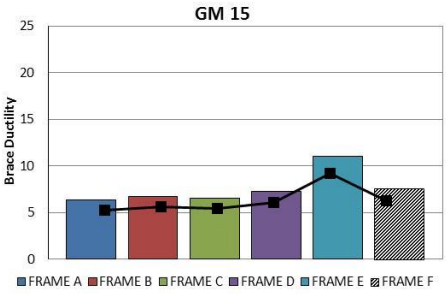

(b)Brace ductility

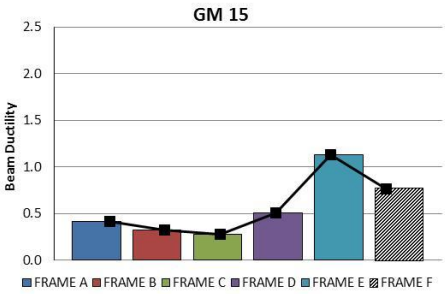

(c) Combined strength ratio

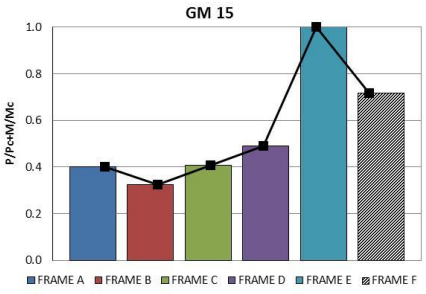

(d)Beam ductility

Fig. C15. Frame responses under GM15

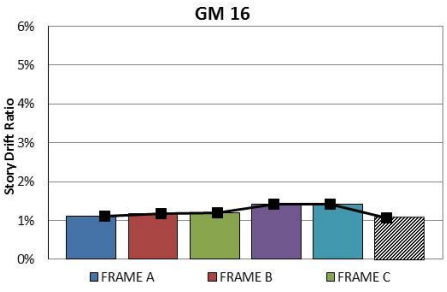

(a) Story drift ratio

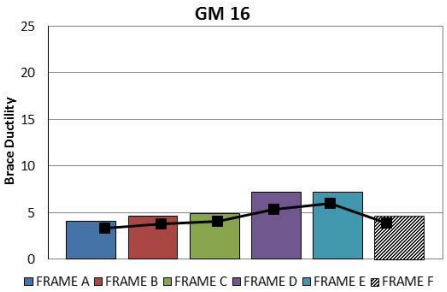

(b)Brace ductility

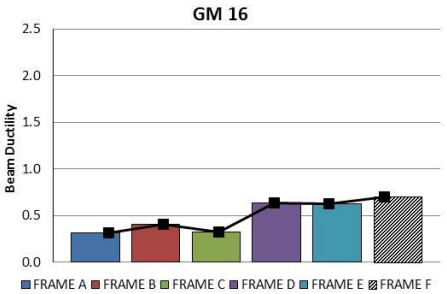

(c) Combined strength ratio

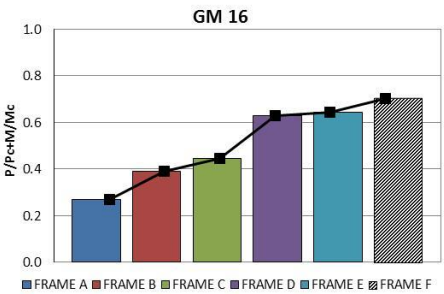

(d)Beam ductility

Fig. C16. Frame responses under GM16

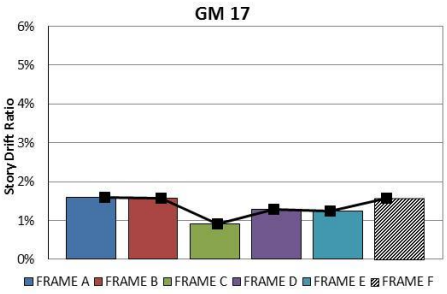

(a) Story drift ratio

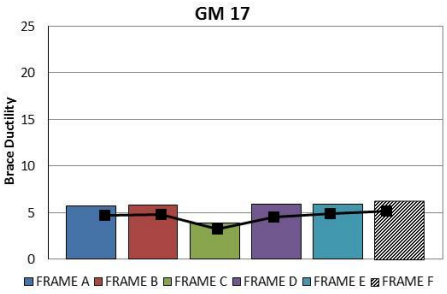

(b)Brace ductility

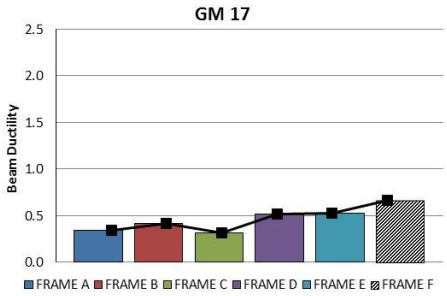

(c) Combined strength ratio

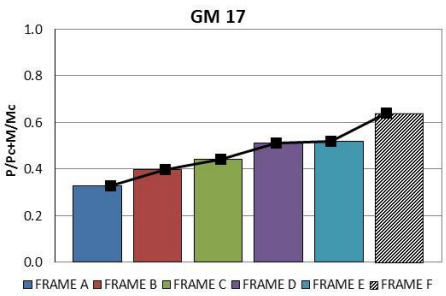

(d)Beam ductility

Fig. C17. Frame responses under GM17

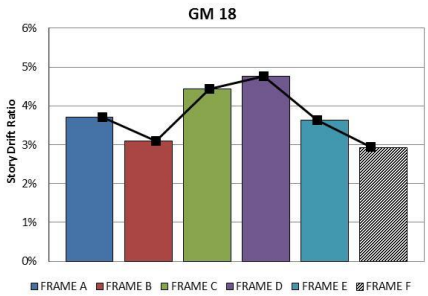

(a) Story drift ratio

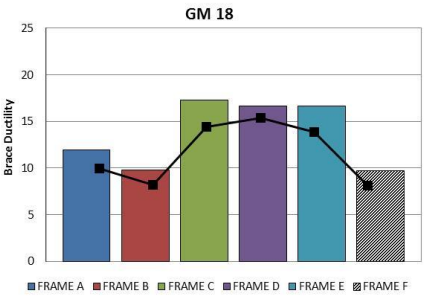

(b)Brace ductility

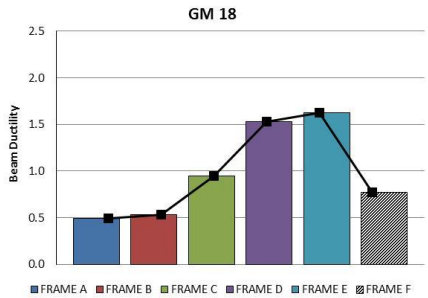

(c) Combined strength ratio

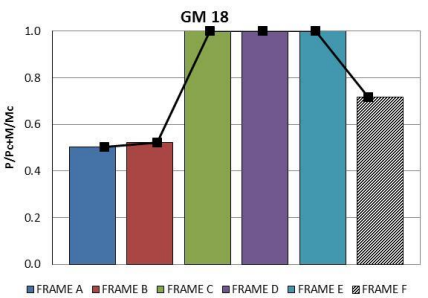

(d)Beam ductility

Fig. C18. Frame responses under GM18

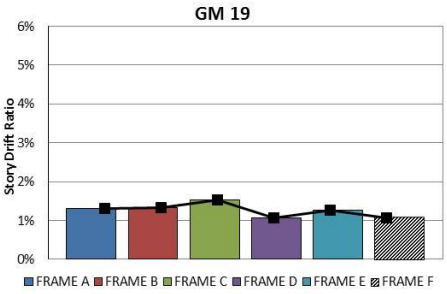

(a) Story drift ratio

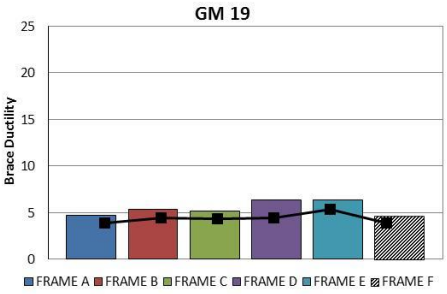

(b)Brace ductility

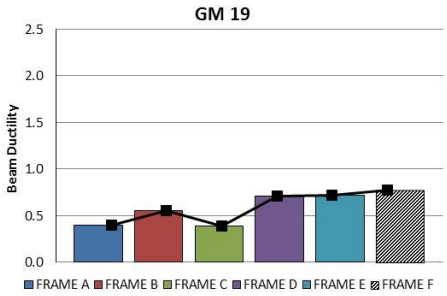

(c) Combined strength ratio

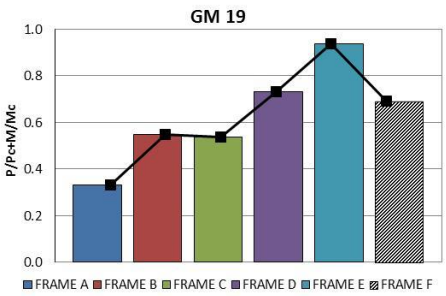

(d)Beam ductility

Fig. C19. Frame responses under GM19

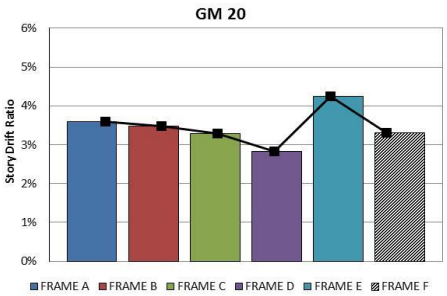

(a) Story drift ratio

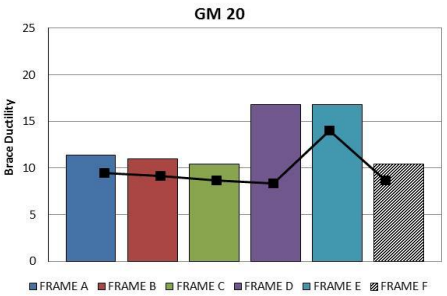

(b)Brace ductility

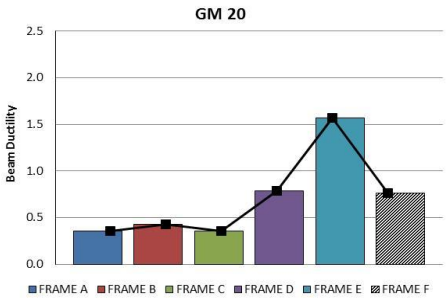

(c) Combined strength ratio

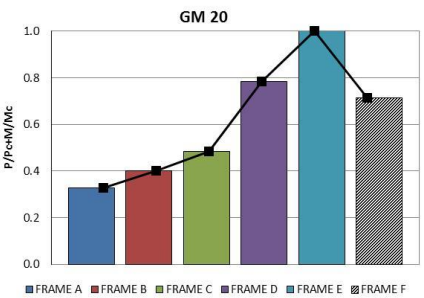

(d)Beam ductility

Fig. C20. Frame responses under GM20